

**SSC-251**

**A STUDY OF SUBCRITICAL CRACK GROWTH  
IN SHIP STEELS**

**This document has been approved for  
public release and sale; its  
distribution is unlimited.**

**SHIP STRUCTURE COMMITTEE**

**1975**

## **SHIP STRUCTURE COMMITTEE**

AN INTERAGENCY ADVISORY  
COMMITTEE DEDICATED TO IMPROVING  
THE STRUCTURE OF SHIPS

### MEMBER AGENCIES:

United States Coast Guard  
Naval Sea Systems Command  
Military Sealift Command  
Maritime Administration  
American Bureau of Shipping

### ADDRESS CORRESPONDENCE TO:

Secretary  
Ship Structure Committee  
U.S. Coast Guard Headquarters  
Washington, D.C. 20590

SR-209

Small discontinuities exist in any complex structure. These discontinuities may grow by fatigue or stress corrosion to a critical size during the service life of the structure. This could result in ships leaking or even unstable crack propagation.

The Ship Structure Committee undertook a project to conduct a critical survey and analysis of those conditions under which pre-existing flaws may grow in high-strength ship steels and weldments when subjected to loading and environmental conditions of ship service.

The enclosed report contains the results of this study. Comments on this report or suggestions for other projects in the ship structure area will be welcomed.



W. M. Benkert  
Rear Admiral, U. S. Coast Guard  
Chairman, Ship Structure Committee

SSC-251

FINAL TECHNICAL REPORT

on

Project SR-209, "Subcritical Crack Growth"

A STUDY OF SUBCRITICAL CRACK GROWTH IN SHIP STEELS

by

P. H. Francis  
J. Lankford, Jr., and  
F. F. Lyle, Jr.

Southwest Research Institute

under

Department of the Navy  
Naval Ship Engineering Center  
Contract No. N00024-73-C-5199

*This document has been approved for public release  
and sale; its distribution is unlimited.*

U. S. Coast Guard Headquarters  
Washington, D.C.  
1975

## ABSTRACT

This report presents an evaluation of crack initiation and sub-critical crack growth in high-strength, low-alloy steels used in welded ship structure. An interpretive review of the state-of-the-art is given, emphasizing design tools that are available and their potential for use in fail safe or safe crack growth ship design philosophy. A crack initiation and crack growth criterion is presented, which permits welded ship structure to be designed with confidence that serious failures can be avoided, while at the same time full use of the attractive static properties of HSLA steels can be exploited. The report also includes a list of problem areas in need of further clarification in order to enhance confidence in the proposed criterion.

# CONTENTS

	<u>Page</u>
LIST OF ILLUSTRATIONS	v
LIST OF TABLES	x
NOMENCLATURE	xi
I. INTRODUCTION	
II. SUBCRITICAL CRACK GROWTH IN SHIP STEELS AND WELDMENTS	2
A. Crack Initiation in Ship Steels	2
1. Sources of Initiation	2
2. Influence of Surface and Flaw Geometry	4
3. Model for Crack Initiation	6
B. Crack Propagation in Ship Steels	7
1. Relation to Strength and Fracture Toughness	8
2. Influence of Microstructure	13
3. Crack Growth Theories	16
C. Crack Initiation in Welds and Heat Affected Zones	21
1. Sources of Initiation	22
2. Influence of Surface and Flaw Geometry	26
3. Models for Crack Initiation	29
D. Crack Propagation in Welds and Heat-Affected Zones	30
1. Factors Controlling Fatigue Crack Growth in Welds and Heat-Affected Zones	30
2. Crack Growth Theories	32
E. Fatigue Damage Estimation	38
1. Cumulative Damage Analysis	38
2. Frequency and Temperature Effects	40
3. Multiaxial Stress Fatigue	41
4. Random Loads	42
5. Equivalence Between Sinusoidal and Random Fatigue Damage	45
III. ENVIRONMENTAL TOPICS RELATED TO SUBCRITICAL CRACK GROWTH	47
A. Stress Corrosion Cracking	47
1. General Characteristics of SCC	47
2. Stress Corrosion Testing	47
3. SCC of Ship Steels in Marine Environments	47

TABLE OF CONTENTS (Cont'd)

	<u>Page</u>
B. Corrosion Fatigue	57
1. General Characteristics of Corrosion Fatigue	57
2. Analysis of Fatigue Crack Growth	58
3. Crack Propagation Behavior Above $K_{Isc}$	60
4. Crack Propagation Behavior Below $K_{Isc}$	64
5. Factors Affecting Corrosion Fatigue Crack Growth Rates	69
C. Control of Stress Corrosion Cracking and Corrosion Fatigue	76
IV. CRACK INITIATION AND SUBCRITICAL CRACK GROWTH CRITERION	83
A. General Principles Governing Ship Design with HSLA Steels	83
B. Purpose of the Criterion	84
C. Rationale for Criterion	85
1. Technical Basis	85
2. Implications	101
D. Tentative Criterion for Fatigue Resistant Design of Ships	103
E. Example	108
V. CONCLUSIONS AND RECOMMENDATIONS	111
A. Significance of Crack Initiation and Growth in HSLA Ship Steels	111
B. Priority Problem Areas	113
VI. REFERENCES	116
APPENDIX	127

## LIST OF ILLUSTRATIONS

<u>Figure</u>		<u>Page</u>
1	Schematic S-N curves of initiation, propagation, and total fatigue lives	3
2	Correlation of fatigue-crack-initiation life with the parameter $K_I/\sqrt{\rho}$ for HY-130 steel	5
3	Comparison of observed crack initiation in SAE 1015 mild steel notched plates with predicted values	7
4	Typical S-N fatigue curves for several ferrous and nonferrous high-strength alloys	8
5	Summary of fatigue-crack-growth data for ferrite-pearlite steels	9
6	Relationship between the index $n$ and yield stress	10
7	Relationship between $A$ (in equation $\frac{da}{dN} = A \Delta K^n$ ) and yield stress	10
8	Log-log plot of fatigue crack growth rate ( $da/dN$ ) vs stress-intensity factor range ( $\Delta K$ ) showing the scatterband limits for a broad sample of high-strength steels	12
9	Schematic illustration of the typical effect of fracture toughness on fatigue life in crack propagation	12
10	Schematic drawing showing relation of crack to oriented fibered structure	14
11	Effect of stress intensity factor range on fatigue crack propagation rate for banded Pearlite-ferrite microstructure	15
12	Effect of stress intensity factor range on fatigue crack propagation rate for banded Martensite-ferrite microstructure	15

LIST OF ILLUSTRATIONS (Cont'd)

<u>Figure</u>		<u>Page</u>
13	Log-log plot of fatigue crack growth rate $da/dN$ as a function of the stress-intensity factor range $\Delta K$ , under conditions of constant $K_{max}$	18
14	Schematic plot of crack growth rate per cycle ( $\Delta a/\Delta N$ ) with respect to log (stress intensity factor) showing the upper and lower limits of stress intensity factor, $K_c$ and $K_{th}$	18
15	Schematic illustration of failure by fatigue-crack propagation	21
16	Summary of results relating to the effect of lack of penetration on the fatigue strength of transverse butt welds in mild steel	23
17	Summary of results obtained for mild steel butt welds containing porosity tested under a tensile mean stress of 19 ksi	24
18	The effect of defect length on the fatigue strength, at $2 \times 10^6$ cycles under pulsating tension loading, of transverse butt welds containing slag inclusions	25
19	The relationship between reinforcement angle and fatigue strength of transverse butt welds	27
20	Parent metal specimens used to study the effect of 'weld' reinforcement shape	28
21	The effect of reinforcement shape found by Sanders, et al., in tests on parent metal specimens subjected to alternating loading	28
22	Variation in crack propagation rate and hardness along the fatigue crack path through a mild steel H.A.Z. at 75 deg to the tensile axis	32
23	Two models for flawed weldments	34
24	Types of flaws found in weldments	36

LIST OF ILLUSTRATIONS (Cont'd)

<u>Figure</u>		<u>Page</u>
25	Effect of initial flaw size on the crack propagation life of a flawed 1-in. -thick HY-130 weldment	37
26	Power spectral density plot	43
27	Stress equivalence factor	46
28	The three phases of structural failure by corrosion	48
29	Stress vs time-to-failure curves illustrating stress-corrosion cracking threshold stresses in an acidified 3.5% NaCl + saturated with H <sub>2</sub> S for an alloy steel heat treated to different hardness levels	49
30	Generalized stress-corrosion cracking resistance of high-strength steels (1-in. plates) in salt water	51
31	Stress intensity vs time-to-failure curve illustrating stress-corrosion cracking threshold level	52
32	Stress-corrosion behavior of HY-130(T) steel in laboratory studies	56
33	Effect of environment on fatigue properties of a 0.35% carbon steel	59
34	Fatigue crack growth behavior of hypothetical steels	61
35	Comparison between static and tension-tension fatigue crack growth rates as a function of the static and mean stress intensity levels	62
36	Above $K_{Isc}$ corrosion fatigue crack growth rate behavior of 4340 steel for fully reversed sinusoidal loading as a function of frequency	63
37	Air and salt water fatigue crack growth rate behavior of 9 Ni-4 Co-0.25 C steel	65
38	Air and salt water fatigue crack growth rate behavior of 13 Cr-8 Ni-2 Mo PH stainless steel	65

LIST OF ILLUSTRATIONS (Cont'd)

<u>Figure</u>		<u>Page</u>
39	Air and salt water fatigue crack growth rate behavior of 12 Ni (180) maraging steel	66
40	Below $K_{Isc}$ corrosion fatigue crack growth rate behavior as a function of frequency	66
41	Corrosion-fatigue crack-growth data as a function of test frequency	67
42	Fatigue-crack-growth rates in air and in 3% solution of sodium chloride below $K_{Isc}$ for various high-yield-strength steels	68
43	Relationship between $D(t)$ and cyclic-stress frequency in various steels subjected to sinusoidal loading in 3% solution of sodium chloride	70
44	Fatigue crack growth rates in air under sinusoidal, triangular, and square loads	71
45	Corrosion fatigue crack growth rates below $K_{Isc}$ under sinusoidal, triangular, and square loads	71
46	Relationship between $D(t)$ and cyclic stress frequency in 12Ni-5Cr-3Mo steel in 3% solution of sodium chloride under sinusoidal, triangular, and square loads	72
47	Corrosion fatigue crack growth rates in 12Ni-5Cr-3Mo steel in 3% solution of sodium chloride under various cyclic stress fluctuations with different stress-time profiles	72
48	Effect of potential on corrosion fatigue life, two stress levels	75
49	Various load-time profiles	75
50	Schematic illustration of the typical effect of stress-ratio on fatigue-crack propagation	77

LIST OF ILLUSTRATIONS (Cont'd)

<u>Figure</u>		<u>Page</u>
51	Effect of removal of weld reinforcement on axial-load fatigue strength of transversely butt-welded 1/4-in. -thick constructional alloy steel plates (R = -1)	77
52	Typical $\Delta\sigma$ - $N_f$ curves for structural weldment	87
53	Typical crack growth data for welded steel plate	90
54	$\Delta\sigma$ - $N_f$ curves for Type 1 weldments	94
55	$\Delta\sigma$ - $N_f$ curves for Type 2 weldments	95
56	$\Delta\sigma$ - $N_f$ curves for Type 3 weldments	96
57	$\Delta\sigma$ - $N_f$ curves for Type 4 weldments	97
58a	$\Delta\sigma$ - $N_f$ curves for Type 5 weldments	98
58b	Common geometries for Type 5 weldments	99
59	$\Delta\sigma$ - $N_f$ curves for Type 6 weldments	100
60	Gamma function	104
61	Crack initiation period, in service years, for typical weldments	106
62	Crack propagation period, in service years, for various initial flaw sizes	107

LIST OF TABLES

<u>Table</u>		<u>Page</u>
1	Material Properties	16
2	Results of Smooth Surface SCC Tests on Low Alloy Steels in Marine Atmospheres 80-ft Lot, Kure Beach, N. C.	54
3	Results of Smooth Surface SCC Tests on Low Alloy Steels in Seawater	54
4	Coatings Tested	80
5	Effect of Protective Coatings on Stress Corrosion of Aircraft Alloys	81
6	Bent-Beam Stress-Corrosion Tests for Coatings Evaluation	82
7	<u>Wolverine State</u> Load Spectral Data Used in Criterion	101
8	Design Endurance Limits for Structural Weldments	104

## NOMENCLATURE

A	Constant
a	Crack length
$a_o$	Initial crack length
$a_{cr}$	Critical crack length
b	Constant
c	Constant
E	Elastic modulus
e	Strain
f	Frequency
K	Stress intensity factor
$\Delta K$	Cyclic range of K
$K_c$	Critical value of K, corresponding to fracture
$K_{Ic}$	Plane strain fracture toughness
$K_f$	Fatigue concentration factor
$K_{max}$	Maximum cyclic value of K
$K_{Isc}$	Threshold value of K, below which SCC will not occur
$\Delta K_T$	Value of $\Delta K$ for transition to accelerated crack growth rate
$K_t$	Elastic stress concentration factor
$\Delta K_{th}$	Lower threshold value of $\Delta K$ needed for subcritical crack growth
$K_{tha}$	$K_{th}$ as measured in aggressive environment
$K_{thi}$	$K_{th}$ as measured in inert environment
k	Stress equivalence factor Also, constant
N	Number of fatigue cycles
$N_f$	Number of cycles to failure

## NOMENCLATURE (Cont'd)

$N_i$	Number of cycles to initiate crack Also, number of cycles to failure at i-th stress level
$N_p$	Number of cycles (beyond initiation) to failure
$n$	Constant
$n_i$	Number of cycles applied at i-th stress level
$R$	Stress ratio: $\sigma_{\min} / \sigma_{\max}$ Also, Boltzmann gas constant  Also, maximum dimension of plastic zone
$S$	Stress
$T$	Temperature
$t$	Time
$U$	Activation energy
$\alpha$	Constant
$\beta$	Constant
$\Gamma ( )$	Gamma function
$\epsilon$	Strain
$\epsilon_e$	Effective strain
$\epsilon_p$	Plastic strain
$\epsilon_t$	Total strain
$\rho$	Crack tip radius
$\sigma$	Applied stress

## NOMENCLATURE (Cont'd)

$\sigma_e$	Effective stress
$\sigma_f$	Static tensile strength
$\sigma_o$	Tensile flow stress Also, fatigue strength under reversed shear stress
$\sigma_{rms}$	Root-mean-square stress
$\sigma_{th}$	Threshold stress level, below which SCC will not occur
$\sigma_Y$	Tensile yield strength
$\sigma_1, \sigma_2, \sigma_3$	Principal stresses
$\omega_o$	Expected frequency of narrow band process
COD	Crack opening displacement
cpm	Cycles per minute
HAZ	Heat affected zone
HSLA	High strength-low alloy
mpy	mils per year
NDI	Nondestructive inspection
ppm	Parts per million
PSD	Power spectral density
Q&T	Quenched and tempered
RMS	Root mean square
SCC	Stress corrosion cracking
SCE	Saturated calomel electrode
WG	Weather group

CONVERSION TABLE FOR  
INTERNATIONAL SYSTEM OF UNITS

<u>Multiply</u>	<u>By</u>	<u>To Get SI Unit</u>
in.	0.0254	m. (meter)
lb (force)	4.448	kg·m/s <sup>2</sup> (Newton)
lb (mass)	0.4536	kg (kilogram)
psi	6.895 x 10 <sup>3</sup>	N/m <sup>2</sup> (pascal)
psi./in	1.099 x 10 <sup>3</sup>	N m <sup>-3/2</sup> -

## SHIP STRUCTURE COMMITTEE

The SHIP STRUCTURE COMMITTEE is constituted to prosecute a research program to improve the hull structures of ships by an extension of knowledge pertaining to design, materials and methods of fabrication.

RADM W. M. Benkert, USCG  
Chief, Office of Merchant Marine Safety  
U.S. Coast Guard Headquarters

CAPT F. L. Eareckson, USN  
Head, Ship Systems Engineering  
and Design Department  
Naval Ship Engineering Center  
Naval Sea Systems Command

Mr. M. Pitkin  
Asst. Administrator for  
Commercial Development  
Maritime Administration

Mr. K. Morland  
Vice President  
American Bureau of Shipping

Mr. C. J. Whitestone  
Maintenance and Repair Officer  
Military Sealift Command

## SHIP STRUCTURE SUBCOMMITTEE

The SHIP STRUCTURE SUBCOMMITTEE acts for the Ship Structure Committee on technical matters by providing technical coordination for the determination of goals and objectives of the program, and by evaluating and interpreting the results in terms of ship structural design, construction and operation.

### NAVAL SHIP SYSTEMS COMMAND

Mr. P. M. Palermo - Member  
Mr. J. B. O'Brien - Contract Administrator  
Mr. G. Sorkin - Member

### AMERICAN BUREAU OF SHIPPING

Mr. S. G. Stiansen - Member  
Mr. I. L. Stern - Member

### U.S. COAST GUARD

LCDR E. A. Chazal - Secretary  
CAPT D. J. Linde - Member  
LCDR D. L. Falsom - Member  
CDR W. M. Devlin - Member

### SOCIETY OF NAVAL ARCHITECTS & MARINE ENGINEERS

Mr. A. B. Stavovy - Liaison

### MARITIME ADMINISTRATION

Mr. J. Nachtsheim - Chairman  
Mr. F. Dashnaw - Member  
Mr. F. Seibold - Member  
Mr. R. K. Kiss - Member

### WELDING RESEARCH COUNCIL

Mr. K. H. Koopman - Liaison

### MILITARY SEALIFT COMMAND

Mr. T. W. Chapman - Member  
Mr. A. B. Stavovy - Member  
Mr. D. Stein - Member  
Mr. J. G. Tuttle - Member

### INTERNATIONAL SHIP STRUCTURES CONGRESS

Prof. J. H. Evans - Liaison

### NATIONAL ACADEMY OF SCIENCES SHIP RESEARCH COMMITTEE

Mr. R. W. Rumke - Liaison  
Prof. J. E. Goldberg - Liaison

### U.S. COAST GUARD ACADEMY

CAPT C. R. Thompson - Liaison

### U.S. MERCHANT MARINE ACADEMY

CAPT W. M. Maclean - Liaison

### U.S. NAVAL ACADEMY

Dr. R. Bhattacharyya - Liaison

NOTES

## I. INTRODUCTION

This report constitutes the final report of Project SR-209, "A Study of Subcritical Crack Growth in Ship Steels." The stated purpose of this project has been to:

"... examine the several potential mechanisms exclusive of brittle fracture by which cracks may form from preexisting flaws and by which cracks may grow, and evaluate the importance of these mechanisms and their consequence to the overall structural reliability of ships constructed from high-strength steels."

With the prospect of high-strength, low-alloy steels and their weldments (40-100 ksi tensile yield strengths) being selectively integrated into primary and secondary ship structure, subcritical crack growth looms as a potentially greater threat to ship structural reliability than formerly, when low-strength steels and weldments were used exclusively. This research program made an in-depth study of the problem potential in using HSLA steels and weldments. This was done in two steps. First, a critical assessment was made of the world technical literature related to crack initiation and subcritical crack growth in HSLA steels typical of those proposed for ship structural application, including environmental factors. Second, this information was consolidated into a practical criterion or methodology by which fail-safe structural design may be assured through realistic calculations of the crack initiation and subcritical crack growth potential.

The remainder of this report consists of four technical chapters, plus the references and an Appendix. Chapter II concerns crack initiation and subcritical crack growth in ship steels and weldments, exclusive of environmental factors. This chapter addresses the initiation and growth processes in terms of their microstructural causes and their phenomenological description, residual stress effects, and examines procedures for estimating initiation, growth, and cumulative damage. Chapter III addresses environmental factors important to ship structure, particularly stress corrosion cracking, corrosion fatigue, and preventative techniques. Chapter IV presents a design criterion for estimating crack initiation and subcritical crack growth lives in welded ship structure, and elucidates its use by way of a detailed structural design example. Chapter V summarizes the potential significance of crack initiation and subcritical crack growth in ship steels, and presents a statement of important problem areas in need of further study in order to strengthen the proposed criterion. Following the references given in Chapter VI, the Appendix provides background information related to ship steel and weldment metallurgy, fabrication techniques, ship structural environments, and fracture mechanics.

## II. SUBCRITICAL CRACK GROWTH IN SHIP STEELS AND WELDMENTS

### A. Crack Initiation in Ship Steels

#### 1. Sources of Initiation

Crack initiation is the forerunner to subcritical crack growth and means different things to different people. To a structural engineer, crack initiation usually means the formation of a crack which is small with respect to the critical size, but visible to the unaided eye. Once formed, under suitable conditions of stress and time this crack will propagate subcritically until it either arrests or triggers fast fracture. The materials engineer, on the other hand, views crack initiation as a local transformation of the material, at the crystalline or subcrystalline level, in which micro-surfaces are created. Another difference between these two viewpoints is that the former considers crack initiation to be associated with the first stages of growth from a preexisting geometric or material defect. The materials engineer, however, is usually concerned with initiation as the formation of a defect in an unflawed polycrystalline medium. Thus, the precise meaning of "crack initiation" depends upon one's frame of reference, and, ultimately, upon the means of observation.(1)

Crack initiation considerations are important simply for the reason that ignoring them can lead to underpredictions of fatigue life and overly-conservative design. This is especially true in high-cycle fatigue, where the crack initiation period occupies the greatest proportion of structural life. Figure 1 shows qualitatively the relative contribution of the crack initiation period to total fatigue life for a structural steel. The crack initiation period dominates in the high-cycle regime, provided no crack-like imperfections are present to reduce or eliminate the initiation period in an actual structural component.

The current state-of-the-art regarding crack initiation is almost wholly descriptive. Few quantitative models are available which allow confident prediction of time or cycles-to-initiation as a function of mechanical properties and loading conditions. This is true whether one considers initiation to be flaw formation or initial growth of a preexisting flaw.

It is generally known that subcritical cracks will initiate at, or very near to, the free surface of a structural component. Exceptions to this rule will occur when there is a massive internal defect in the material, such as a fold (over-roll) in plate steel or a slag inclusion in a weld region. Again, depending upon the viewpoint, initiation may be considered to be a process activated on the structural scale or at the material micromechanical level.

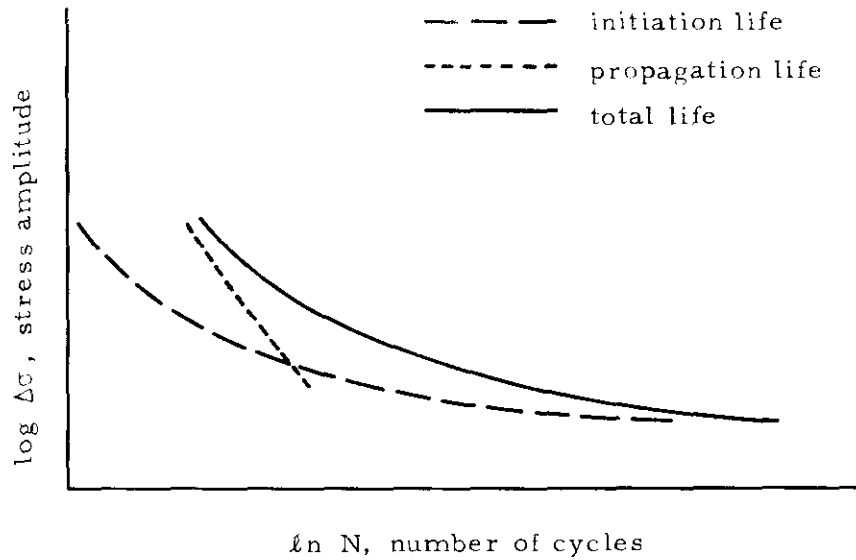


Figure 1. Schematic S-N curves of initiation, propagation, and total fatigue lives (After Barsom, Reference 8)

On the structural level, crack initiation is attributed to the initial growth phase of a preexisting flaw. Such a flaw may have had its origin in structural fabrication, handling, maintenance, corrosion processes, etc. It may take the form of a tool mark, surface scratch, weld undercut, slag inclusion, corrosion pit, or any other similar surface discontinuity. Forman<sup>(2)</sup> has described crack initiation within the context of the fatigue process. In subcritical fatigue crack growth, the relative stress intensity factor range,  $\Delta K/K_C$ , is generally considered to be a key index of crack growth rate. Forman adapted this approach to describe the number of cycles needed to generate a crack of prescribed length from an existing crack. It turns out that  $K_C$ , the fracture toughness, depends upon the initial notch radius, as well as other factors such as specimen thickness. When suitable

- (a) cycles to crack initiation increases with crack tip root radius and decreases with crack length; and
- (b) the approach appears valid for a wide range of crack initiation definitions.

## 2. Influence of Surface and Flaw Geometry

The particular configuration of a given flaw and its relation to the applied stress field has a strong influence on the crack initiation period. Some of the more important aspects are mentioned below. Very little quantitative data are available, however, for comparison.

One of the most important effects is the relative orientation of the flaw with respect to the loading axis. If one considers a notch-like surface defect, the initiation process will develop most rapidly if the plane of the defect is oriented perpendicular to the direction of maximum tensile stress. An existing flaw will not initiate a fatigue crack if the plane in which it lies is parallel to this direction and there are no other stresses acting.

A second important factor is the root radius, or the "sharpness" of the notch. In general, sharper notches accelerate crack initiation. Forman<sup>(2)</sup> has shown that fatigue crack initiation from a preexisting flaw depends upon  $K_C(\Delta K)/\sigma_Y^2\rho$ , and hence is related directly to  $\rho$ , the crack tip radius. Barsom and McNicol<sup>(3)</sup> and Clark<sup>(4)</sup> have examined the applicability of linear elastic fracture mechanics parameters to fatigue crack initiation. The initiation behavior of HY-130 steel as a function of notch tip radius  $\rho$  is illustrated in Figure 2, after Barsom and McNicol. The effect of notch sharpness is very strong in the low-cycle fatigue range, and all but disappears in the high-cycle regime.

There are, of course, other factors which influence the crack initiation period. The size and shape of the flaw affect the initiation period inasmuch as size influences the stress level required to propagate a crack subcritically. Larger cracks require small stresses for initiation, according to the inverse square root relationship  $\sigma \approx L^{-1/2}$ , where  $L$  is a characteristic crack dimension.

The nature of the surface, and the thermo-chemical environment surrounding the structure, can have an important effect on crack initiation. Rough, uneven surfaces contain, in effect, a dense distribution of flaws, all of which potentially can initiate a crack. An aggressive environment, chemical and/or thermal, will accelerate the initiation period. Environmental effects are closely related to stress corrosion cracking and corrosion fatigue, as covered in Chapter III of this report. Unfortunately, very little work has been done to identify crack initiation as a function of environmental variables.

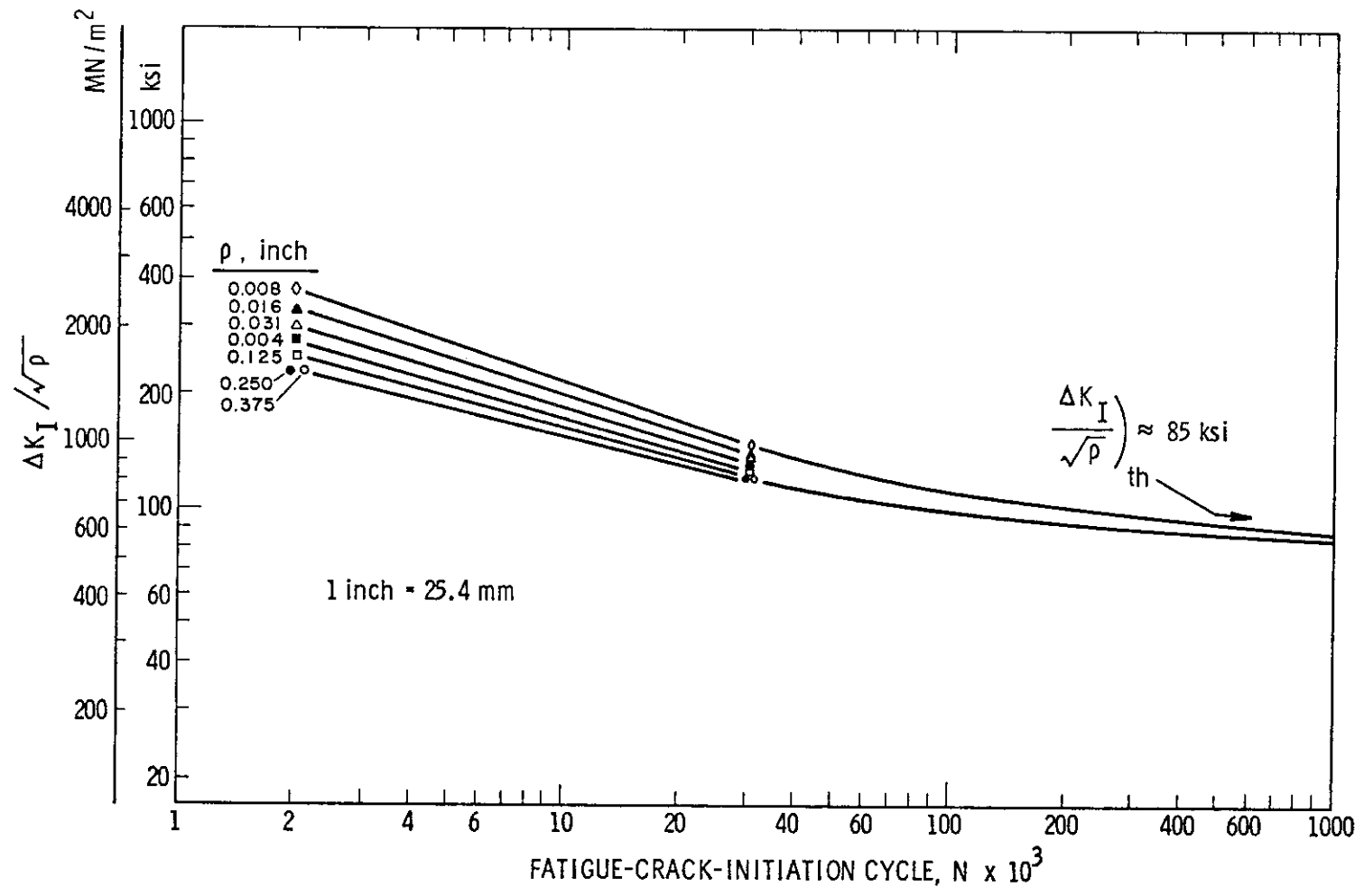


Figure 2. Correlation of fatigue-crack-initiation life with the parameter  $K_I/\sqrt{b}$  for HY-130 steel. (After Barsom and McNicol, Reference 3)

### 3. Model for Crack Initiation

This section describes a quantitative model for crack initiation proposed by Topper, Wetzel and Morrow,<sup>(5)</sup> and subsequently studied by Gowda, et al.<sup>(6)</sup> The procedure is based upon Neuber's notch stress analysis and basically rests on the following equation:

$$K_f \sqrt{\Delta S \Delta \epsilon E} = \sqrt{\Delta \sigma \Delta \epsilon E} \quad (1)$$

where  $K_f$  is the known fatigue concentration factor:  $K_f = 1 + (K_t - 1)/(1 + a/\rho)$  in which  $K_t$  is the usual elastic stress concentration factor,  $\rho$  the root radius of the notch, and  $a$  is a material constant determined from long-life fatigue data for sharply notched specimens in the manner described in Reference (5). Also,  $\Delta S$  and  $\Delta \epsilon$  are the net section stress and strain ranges applied to a sharply notched member, and  $\Delta \sigma$  and  $\Delta \epsilon$  are the local stress and strain ranges at the root of a blunt notch or in a smooth specimen. In Equation (1) the left side represents the average mechanical state in a notched structure, while the right side represents conditions local to the notch tip in an ideal smooth specimen. Thus, the expression implies equal crack initiation periods for notched and unnotched structural elements, provided the net section stresses in the sharply notched specimen are the same as the notch stresses in the smooth specimen. This expression enables determination of fatigue crack initiation lives of notched members using smooth specimen data, or vice-versa. The method is limited to fatigue crack initiation under conditions of zero mean stress.

The procedure involves constructing a "master plot," or graph of effective stress  $K_f \sqrt{\Delta S \Delta \epsilon E}$  versus  $N_i$ , cycles to crack initiation, for the materials of interest. Figure 3 shows one such curve for SAE 1015 mild steel.<sup>(6)</sup> The solid line was constructed from unnotched specimens, for which the value of  $\sqrt{\Delta \sigma \Delta \epsilon E}$  was calculated from steady-state cyclic stress and strain ranges. The data points were taken from experiments with notched plates. The correlation is reasonably good, which tends to validate the theory for this material. This procedure enables initiation predictions for many types of notched specimens from readily available smooth specimen fatigue data. Note that curves of  $\Delta \sigma \Delta \epsilon E$  versus life can be derived from any two of the following curves: stress versus life, total strain versus life, plastic strain versus life, and cyclic stress versus strain.

Aside from the approach just outlined, other investigators have suggested procedures for estimating the number of cycles to initiate a fatigue crack. Manson and Hirschberg<sup>(7)</sup> proposed an empirical method which uses as input the fatigue behavior of unnotched specimens to predict the number of cycles required to initiate an "engineering size" crack. This method is somewhat more complex than that described previously, and there has been little

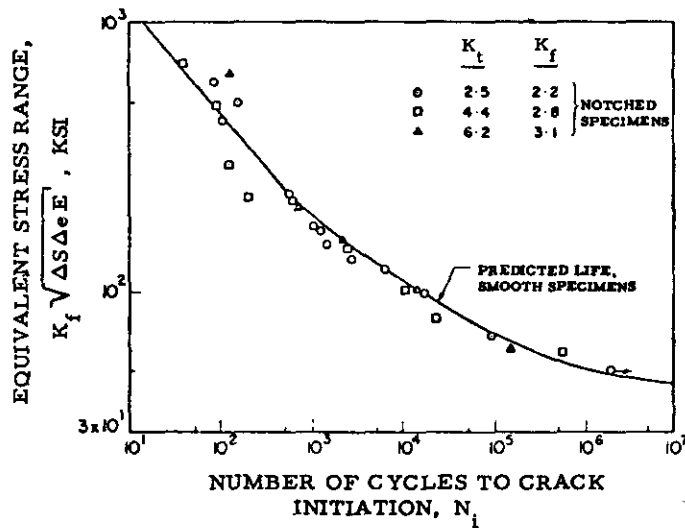


Figure 3. Comparison of Observed Crack Initiation in SAE 1015 Mild Steel Notched Plates With Predicted Values (after Reference 6)

supporting data for evaluating its applicability. Barsom,<sup>(8)</sup> in his review of the subject, suggests that the fatigue crack initiation threshold in martensite steels of various strength levels subject to zero-to-tension fatigue loads may be predicted from the relationship

$$\frac{K}{(\sigma_Y)^\alpha \sqrt{\rho}} = \text{constant} \quad (2)$$

with  $\alpha \leq 1$  and the right hand constant  $\approx 1$ . Here again, however, little corroborating data are available.

#### B. Crack Propagation in Ship Steels

The customary approach to representing the fatigue characteristics of a material is embodied in the S-N (cyclic stress, S, versus number of cycles to failure, N) diagram, an example of which is shown in Figure 4. Such plots for steels (as opposed to many non-ferrous alloys) typically exhibit a cyclic stress level, called the endurance limit, below which specimens never fail. For higher stresses, however, life is finite, usually  $< 10^6$  cycles, and can be divided into two stages, namely, cycles to initiate a detectable crack, and cycles required to propagate such a crack to failure. Large welded structures generally possess a high density of small size flaws, and cracks can readily develop from them. Thus, for welded structures, the greatest portion of the cyclic life is accounted for by crack propagation. In this case local plastic strains develop, caused by crack tip stresses which exceed the yield strength of the material. Under such conditions fatigue

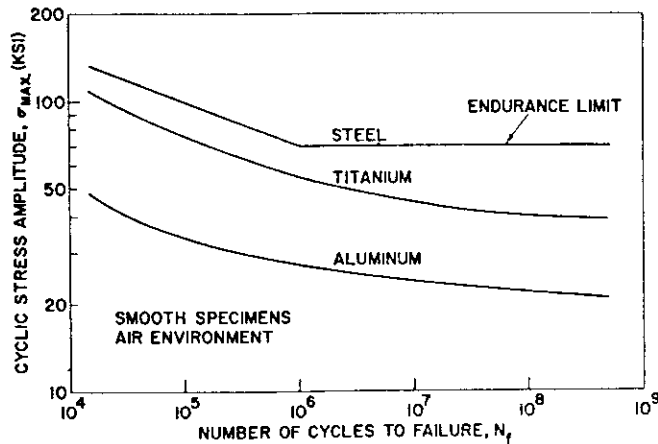


Figure 4. Typical S-N Fatigue Curves for Several Ferrous and Nonferrous High-Strength Alloys. Note the distinct horizontal endurance limit for the steel vs the gradually sloping curves for the nonferrous alloys at long fatigue lives beyond  $10^6$  cycles. (after Reference 13)

is governed essentially by strain, and a description of the fatigue process requires the incorporation of the material parameters which govern cyclic plastic strains. These parameters will be considered within the following subsections, and useful expressions describing fatigue crack growth will be presented and discussed. Factors introduced by welding are developed in Chapter II, Section D.

#### 1. Relation to Strength and Fracture Toughness

It is not presently clear which material properties are most closely related to fatigue crack growth resistance, although some results in the case of steels are available to provide design guidance. In looking at this problem, it is the usual practice to run constant amplitude sinusoidal fatigue tests using standard pre-cracked specimens having controlled initial flaws, and to monitor incremental crack growth microscopically. The data obtained are generally plotted in the form of  $\log (da/dN)$  versus either  $\log \Delta K$  or  $\log K_{\max}$ , where  $a$  is the instantaneous crack length,  $N$  the number of fatigue cycles, and  $\Delta K$  and  $K_{\max}$  represent the stress intensity factor range and the maximum stress intensity factor, respectively (for zero-to-tension cycling,  $\Delta K = K_{\max}$ ). If the resulting data fit a straight line, then one has a relation of the form

$$\frac{da}{dN} = A\Delta K^n \quad (3)$$

where the dependence of crack growth rate on stress intensity is reflected in the slope  $n$  and intercept  $A$  obtained from the plot of  $\log (da/dN)$  versus  $\log \Delta K$ .

Typical crack growth data<sup>(9)</sup> for ferrite-pearlite steels in the strength range of interest to ship construction steels are shown in Figure 5. Despite the wide range in yield stress of the materials and the load ratios involved ( $0 < R < .7$ ), for low values of  $\Delta K$  the data cluster on or above a line described by

$$\frac{da}{dN} = 3.6 \times 10^{-10} (\Delta K)^{3.0} \tag{4}$$

where  $\Delta K$  is expressed in  $\text{ksi} \sqrt{\text{in}}$ . Furthermore, careful study of individual curves shows that a general trend exists according to which  $n$  decreases, and  $A$  increases (cf. Eq. (3)), with increasing yield strength. Evidence of this effect can be seen in Figures 6 and 7, respectively, which present data taken from a different collection of similar low-alloy, hot-rolled plate steels.<sup>(10)</sup> From an engineering design point of view, however, such differences may not be significant, since uncertainty in initial flaw size may well overshadow relatively slight variations in crack growth rate from one material to another.

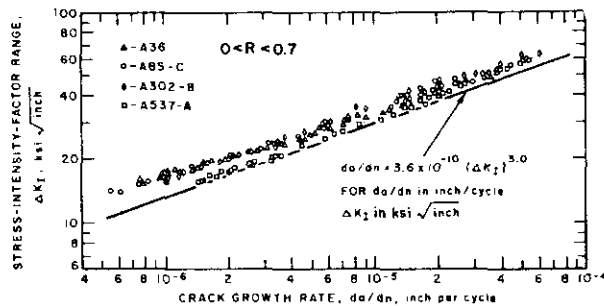


Figure 5. Summary of fatigue-crack-growth data for ferrite-pearlite steels (after Reference 9)

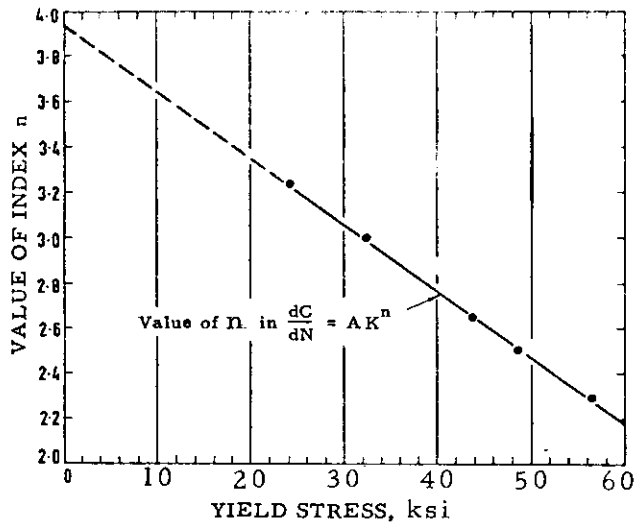


Figure 6. Relationship between the index  $n$  and yield stress (after Reference 10)

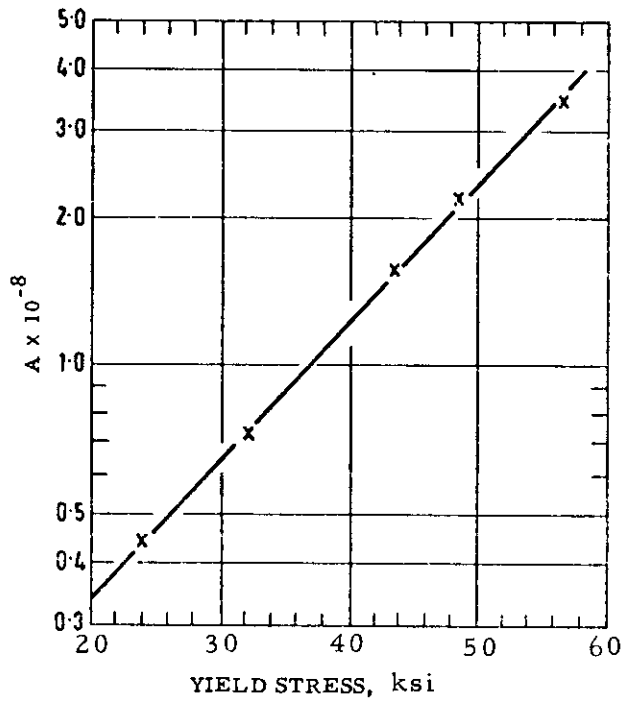


Figure 7. Relationship between  $A$  (in equation  $\frac{da}{dN} = A \Delta K^n$ ) and yield stress (after Reference 10)

If  $da/dN$  versus  $\Delta K$  data are extended to higher values of  $\Delta K$ , an abrupt transition in behavior is observed. Beyond this transition, designated as  $\Delta K_T$ , the rate of fatigue crack growth accelerates markedly, caused apparently by the superposition of a ductile tear mechanism onto the usual cyclic-shear mechanism of subcritical crack growth. The inflection point, which occurs at a relatively constant value of crack opening displacement (COD) of about  $1.6 \times 10^{-3}$  in. in steels,<sup>(9)</sup> divides the low amplitude region of striation formation from the high amplitude region of dimple formation. Such behavior is shown in Figure 8 for a broad sample of quenched and tempered martensitic steels<sup>(11)</sup>; the transition COD generally corresponds to a crack growth rate of about  $1 \times 10^{-4}$  in./cycle. Within the region of accelerated crack growth (dashed lines in Figure 8), the exponent  $n$  governing the magnification of  $\Delta K$  may range as high as 12 for higher strength steels,<sup>(12)</sup> compared to  $2 < n < 3$  below the transition point.

It is useful to consider a realistic structural example in order to appreciate what the foregoing may mean to a designer. The  $\Delta K$  values corresponding to a 0.25-in.-deep semicircular flaw cycled from 0 to 75 percent of net section yield strength for HY-80 and HY-100 are indicated in Figure 8. Although this flaw size and stress level combination should be well within service requirements for these materials, this combination places the designer below, but not very far from, the transition point. It has been found empirically<sup>(11)</sup> that for relatively tough steels (ranging in yield strength from 36 to 184 ksi, and including both martensitic and ferrite-pearlite microstructures), it is possible to estimate empirically the transition  $\Delta K$  level, in  $\text{ksi}\sqrt{\text{in.}}$ , beyond which accelerated crack growth rates would be anticipated ( $\Delta K_T$ ) by using Barsom's relationship  $(\Delta K_T)^2 / E\sigma_Y = 1.6 \times 10^{-3}$ , which results in

$$\Delta K_T = 0.04 \sqrt{E\sigma_Y} \quad (5)$$

There is at present no general relation between fracture toughness and fatigue crack growth, at least for steels within the 40 to 100 ksi strength range. Fracture toughness has sensible influence only on low-cycle life (cf. Figure 9), where the initial flaw size is large or the cyclic stress level is relatively high.<sup>(13)</sup> The effect at long life is negligible. It has been proposed that  $da/dN$  should be inversely proportional to some function of  $K_{IC}$ , but experimental correlation has been inconclusive.\* Other studies on steels

\* Miller<sup>(14)</sup> has obtained some evidence of an inverse relationship between  $n$  and  $K_{IC}$  for a few ultra-high-strength steels with  $\sigma_Y > 200$  ksi, but applicability to ship steels is questionable.

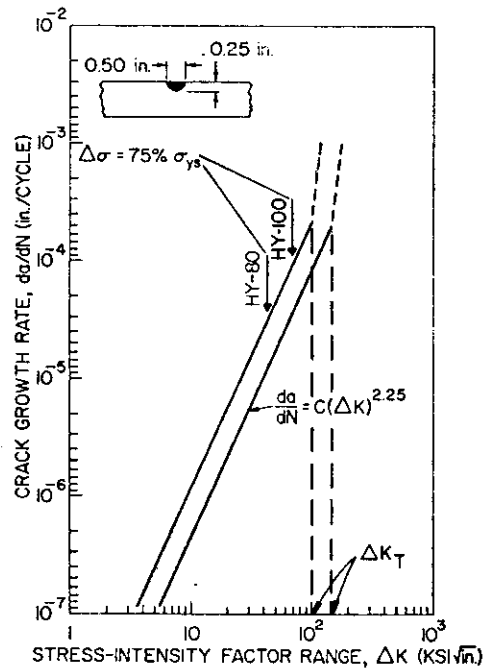


Figure 8. Log-log plot of fatigue crack growth rate ( $da/dN$ ) vs stress-intensity factor range ( $\Delta K$ ) showing the scatterband limits for a broad sample of high-strength steels (after Reference 11)

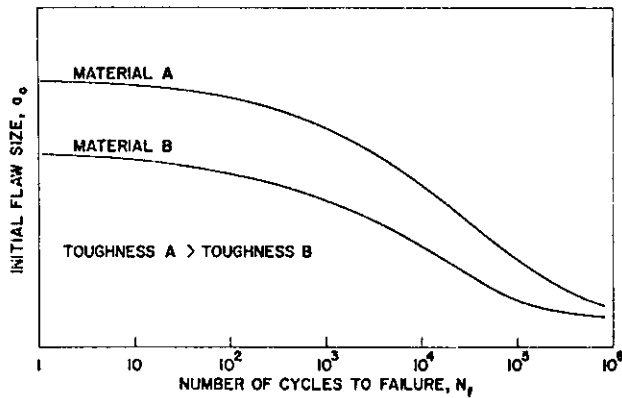


Figure 9. Schematic illustration of the typical effect of fracture toughness on fatigue life in crack propagation. For two otherwise similar materials, fracture toughness, per se, can influence fatigue life in the low-cycle life region ( $N_f < 10^5$  cycles) but will have a negligible effect at long fatigue lives. (after Reference 13)

have shown that the connection between growth rate and fracture toughness is a function of the thermo-chemical environment, with no obvious relationship existing for tests carried out in inert environments.

From the foregoing, it may be concluded that:

- (a) For ship steels having similar microstructure, crack growth rates are essentially independent of material yield strength and fracture toughness.
- (b) The  $\Delta K$  corresponding to accelerated crack growth in ship steels is proportional to  $\sqrt{\sigma_Y}$ .

## 2. Influence of Microstructure

There are a number of microstructural parameters which might be suspected of influencing cyclic crack growth: stacking fault energy, degree of cold work (i. e., initial defect structure), prior austenitic grain size, inclusion content and morphology, and the carbide-ferrite structure. For the case of ship steels, it appears that only the latter two factors are of major significance. The relative insensitivity of crack growth to the other factors has been reviewed by Plumbridge.<sup>(15)</sup> Only a small number of crack growth studies have involved a sufficient variety of steels such that valid, general conclusions may be drawn regarding the role of microstructure. Of these studies, the careful, practical works by Barsom<sup>(9)</sup> and by Heiser and Hertzberg<sup>(16)</sup> offer guidance in the present context.

Barsom studied fatigue crack growth rates in ferrite-pearlite steels ranging in yield strength from 36 to 59 ksi (discussed previously) and in quenched and tempered martensites ranging in strength from 87 to 184 ksi (the lower range included HY-80). All specimens were machined from structural plates ranging from 1 to 2 in. thickness. It was found that the rate of crack growth for ferrite-pearlite steels was described by Equation (4) (earlier), while for the martensitic steels,

$$\frac{da}{dN} = 0.66 \times 10^{-8} (\Delta K)^{2.25} \quad (6)$$

with  $\Delta K$  expressed in ksi  $\sqrt{\text{in.}}$ . From these results, it is evident that prior to the rate-of-growth transition, the crack extension rate at a given value of stress intensity factor is lower in ferrite-pearlite steels than in martensitic steels. Although the exponent in Equation (4) is larger than that in Equation (6), the value of the proportionality constant A is much smaller for the ferrite-pearlite steels than for the martensites. Therefore, Equation (6) may be used as a general, conservative relation for calculating approximate crack growth rates, preceding transition, for both classes of steel.

It can be helpful to understand why these differences in growth rate exist. From the observations of Barsom,<sup>(9)</sup> it seems that two factors combine to lower the net crack growth rate of the normalized-type steels in comparison with the martensites. First, severe secondary cracking (crack branching) is observed in the former steels, but not in the latter. The secondary cracks tend to "share" the crack-tip COD with the main crack, thereby reducing the effective stress-intensity factor for the main crack. Secondly, the ferrite-pearlite matrix microstructure can be looked at as a "particulate composite" material, with the pearlitic carbides playing the role of brittle, strong micro-ligaments, immersed in a relatively ductile ferrite matrix through which the main crack propagates. It has been proposed that as the main crack moves through the ferrite, bypassing certain pearlite colonies, it leaves behind unbroken, load-bearing ligaments of pearlite, which eventually would fracture when loaded to their tensile instability. Because these ligaments carry a portion of the applied stress, the actual stress intensity at the crack tip is further reduced, again tending to lower the measured crack growth rate.

The anisotropy of fatigue crack propagation in hot-rolled alloy steel plate was studied for three mutually perpendicular crack orientations (Figure 10) by Heiser and Hertzberg.<sup>(16)</sup> By heat treating the material appropriately, they produced both ferrite-pearlite and martensitic microstructures with a range of strengths (49 - 144 ksi), having both banded and homogeneous martensite-ferrite and ferrite-pearlite macrostructures. The hot rolling produced a preferential alignment of nonmetallic inclusions parallel to the rolling direction, which was not altered during subsequent heat treatments. Crack growth rates for all of the materials were correlated with  $\Delta K$ . Representative data for banded ferrite-pearlite and banded martensite-ferrite are shown in Figures 11 and 12 (banding versus homogeneous was quite similar). The material constants  $n$ ,  $A$ , and  $\sigma_Y$  (as defined in Equation (3)) are tabulated in Table 1.

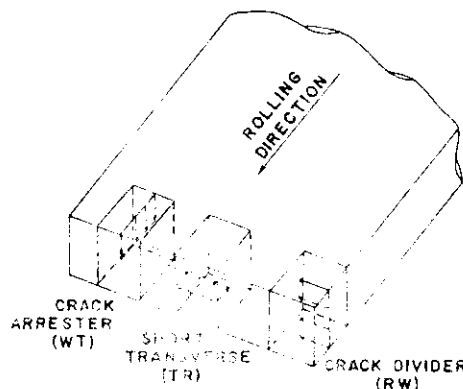


Figure 10. Schematic drawing showing relation of crack to oriented fibered structure (after Reference 16)

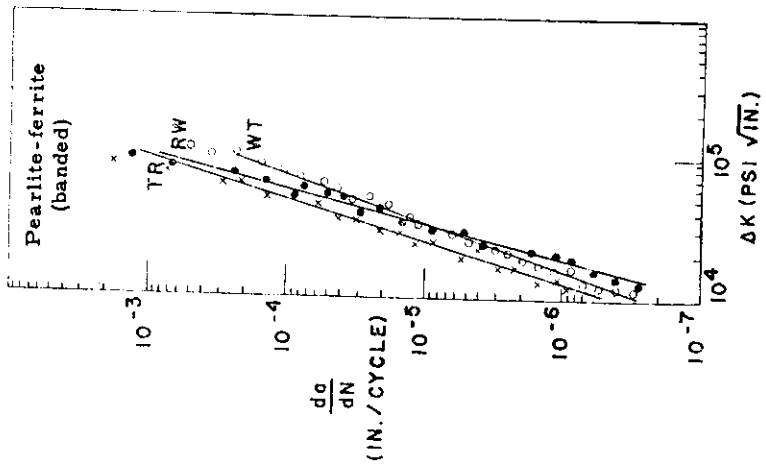


Figure 11. Effect of stress intensity factor range on fatigue crack propagation rate for banded Pearlite-ferrite microstructure (after Reference 16)

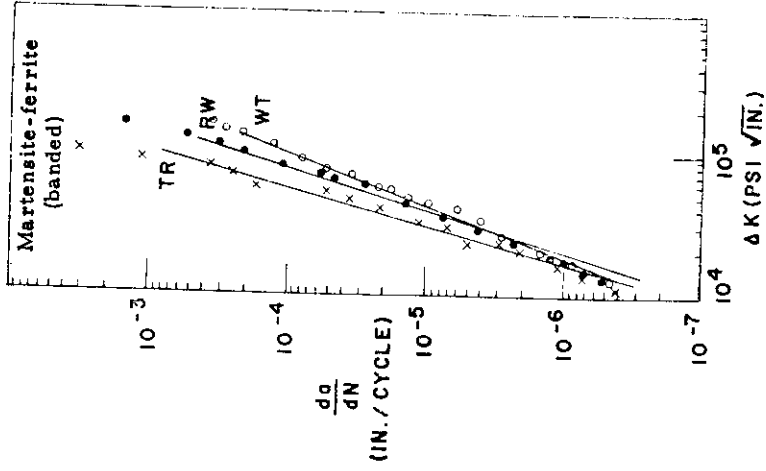


Figure 12. Effect of stress intensity factor range on fatigue crack propagation rate for banded Martensite-ferrite microstructure (after Reference 16)

TABLE 1. MATERIAL PROPERTIES  
(After Reference 16)

	Crack Arrestor (WT)			Crack Divider (RW)			Short Transverse (TR)		
	n	A	$\sigma_Y$ (ksi)	n	A	$\sigma_Y$ (ksi)	n	A	$\sigma_Y$ (ksi)
Pearlite-ferrite (banded)	2.0	$9.0 \times 10^{-19}$	54	3.9	$2.5 \times 10^{-18}$	52	3.5	$2.6 \times 10^{-20}$	49
Martensite-ferrite (banded)	2.8	$2.5 \times 10^{-18}$	70	3.4	$3.3 \times 10^{-20}$	77	3.8	$3.2 \times 10^{-22}$	72

It was observed that the rate of fatigue crack growth was not highly sensitive to microstructural constituents (in agreement with Barsom), but that it was especially sensitive to their orientation with respect to the plane of the crack. For any given microstructure, the effect of microstructural orientation is essentially negligible at low growth rates ( $10^{-7}$  -  $10^{-6}$  in./cycle), whereas large differences in growth rate were observed at higher stress intensity levels. To cite an example, fatigue crack growth rates for the three orientations shown in Figure 10 varied by about 50% at  $\Delta K = 20$  ksi $\sqrt{\text{in.}}$ , but by more than an order of magnitude ( $3.0 \times 10^{-3}$  in./cycle versus  $1.0 \times 10^{-4}$  in./cycle) at  $\Delta K = 95$  ksi $\sqrt{\text{in.}}$ . In this particular case, it is important to note that the transition to the more rapid phase of crack growth already has occurred at  $\Delta K = 95$  ksi $\sqrt{\text{in.}}$  for the TR crack, while for the WT orientation, the transition has not yet occurred. Any general design work for this material based on WT crack propagation data certainly would be unconservative.

The above results were explained by the authors in terms of a fatigue process composed of several different fracture micromechanisms, including fatigue striation formation and inclusion fracture. It was felt that inclusion fracture probably accounts for anisotropic crack growth in "homogeneous" alloys, since, as previously noted, homogenization does not alter inclusion morphology.

### 3. Crack Growth Theories

Many theories of fatigue crack growth have been proposed and utilized in describing various metals and alloys subjected to a wide variety of stress states and environments. In this subsection, some of the work most pertinent to the designer of steel ships will be discussed, thereby excluding many theories which either

- (a) have not been proved valid for ship steels, or
- (b) require "impractical" data as initial input, such as knowledge of the plastic zone size at a crack tip.

Aside from the mechanical properties discussed in the preceding two subsections, other factors which should be incorporated into a general, fundamentally sound crack growth law are: load ratio (R), temperature (T), environment, and the cyclic strain hardening parameters characteristic of the material.

As discussed in Section D of the Appendix, the simple, empirically observed proportionality between  $da/dN$  and  $(\Delta K)^n$  has been modified by Forman, et al., (A-10) in order to account for the effects of load ratio and the instability of the crack growth as the maximum cyclic value of the stress intensity factor approaches the fracture toughness  $K_C$ . The modified equation is given by

$$\frac{da}{dN} = \frac{A (\Delta K)^n}{(1 - R) K_C - \Delta K} \quad (7)$$

and an example of the dramatic effect of R upon the rate of fatigue crack growth in HY-80 is shown in Figure 13. The figure shows crack growth rates for zero-tension and completely reversed loading, all for the same value of  $K_{max}$ . It should be noted that although the above equation has been shown to correlate a broad range of data involving positive R values, the relation is unconservative, for design purposes, when negative ratios, i.e., tension-to-compression cycling, are involved. For this reason, it has been recommended by Crooker(17) that zero-tension crack growth rate data (which often are all that are available to a designer in most instances) be increased by a correction factor of at least 1.5, for applications to low-cycle fatigue situations involving tension-compression cycling.

A number of studies have shown that for a wide variety of high-strength materials, crack growth rate is affected by temperature according to the relation

$$\frac{da}{dN} = A f (\Delta K) \exp \left[ \frac{-U (\Delta K)}{RT} \right] \quad (8)$$

where  $U (\Delta K)$  is an apparent activation energy, and R in this expression is the gas constant, and T is the absolute temperature. However, for ship design it is likely that the temperature dependence, at least in the ductile crack growth range, of crack growth will be a relatively unimportant factor in comparison to certain other parameters.

One of these other factors is the environment, which is known to exert profound control over the growth of fatigue cracks in steel. In fact, both the low-cycle fatigue life and the long-life fatigue limit of carbon steels are significantly lower in water than in air (more hostile environments, such as saltwater, are treated separately in Chapter III). The effect of the environment upon crack growth can be seen in Figure 14. It has recently been shown(18) that such data may be rationalized in terms of a threshold stress

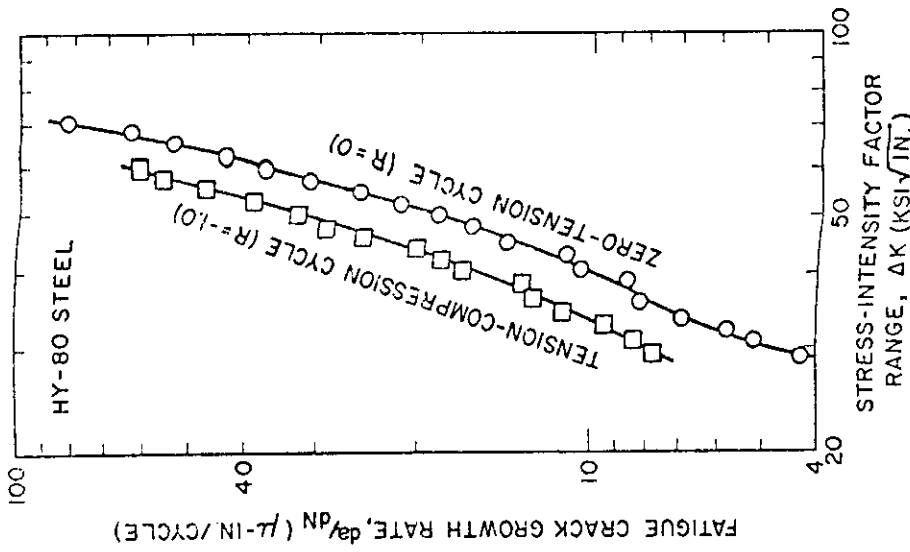


Figure 13. Log-log plot of fatigue crack growth rate  $da/dN$  as a function of the stress-intensity factor range  $\Delta K$ , under conditions of constant  $K_{max}$ . (after Reference 17)

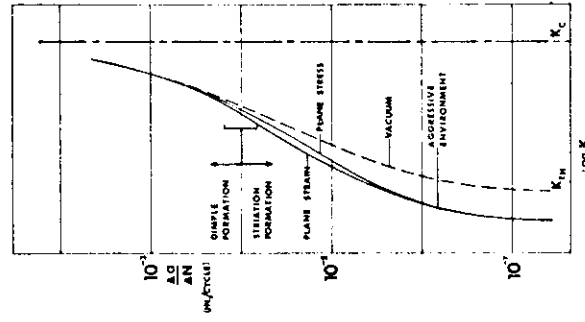


Figure 14. Schematic plot of crack growth rate per cycle ( $\Delta a/\Delta N$ ) with respect to log (stress intensity factor) showing the upper and lower limits of stress intensity factor,  $K_c$  and  $K_{th}$ . (after Reference 18)

intensity factor  $K_{th}$ --characteristic of a given material in a given environment--such that the rate of fatigue crack growth is given by

$$\frac{da}{dN} = \frac{4A}{\pi \sigma_Y E} \left[ \Delta K^2 - K_{th}^2 \right] \quad (9)$$

For  $\Delta K < K_{th}$ , crack growth does not occur. This equation offers a useful, general framework within which to compare and evaluate the relative crack growth resistance of different steels in various environments, although it should be cautioned that the choice of  $n = 2$  as the exponent in Equation (9) may turn out to be not quite so universal as present data seem to indicate. Obviously, this equation is limited in that it does not involve stress ratio, and indeed, to date all correlation of the equation with experimental data has been for  $R = 0$ .

It is an interesting fact that the strain hardening curve for a steel under monotonic, tensile loading

$$\sigma_o = k \epsilon_p^\alpha \quad (10)$$

usually does not coincide with the cyclic strain hardening curve for zero-to-tension, cyclic loading

$$\sigma'_o = k' (\Delta \epsilon_p)^\beta \quad (11)$$

where

$\sigma_o$  = tensile flow stress

$\sigma'_o$  = cyclic flow stress

$\epsilon_p$  = total plastic strain

$\Delta \epsilon_p$  = cumulative cyclic plastic strain

$k, k', \alpha, \beta$  = constants

For steels, typical values of  $\beta$  range from 0.1 to 0.5. Differences in the strain hardening characteristics under monotonic and cyclic loading can be very important, since the material properties which actually control the propagation of a fatigue crack are those characteristic of the material within the small plastic enclave at the crack tip. Under fatigue loading, this region is subjected to repeated plastic strains, although the surrounding material

may experience only elastic strains. Fatigue crack growth is then actually a process of localized low-cycle fatigue, through which small volumes of material undergo plastic strain cycling until local failure occurs, extending the plastic zone further into virgin material.

The consequences of such cycling have been taken into account in a few theories, the most inclusive being that of Tomkins.<sup>(12)</sup> According to this theory, the rate of crack growth for constant stress cycling can be written as

$$\frac{da}{dN} = \frac{\pi^2}{16 \sigma_Y^2} \frac{A}{(2 \Delta K)^{1/\beta}} (\sigma)^{\frac{(2\beta + 1)}{\beta}} \quad (12)$$

This equation has been shown to correlate with excellent fit to low-cycle fatigue data for a wide variety of materials, but it will not account for stress ratio, thermal, or environmental effects. Based on the work of Hickerson and Hertzberg,<sup>(19)</sup> it is likely that better correlation might result from substituting  $\sigma'_0$  (the cyclic flow stress) for  $\sigma_Y$  in the equation. For small strains (high-cycle fatigue), the Tomkins equation reduces to<sup>(12)</sup>

$$\frac{da}{dN} = A (\Delta K)^2 \quad (13)$$

where A is a constant, in general agreement with experiment.

For design purposes, it would be quite useful to have a single equation for crack growth, capable of accommodating all of the factors discussed above, in the presence of multiaxial cyclic loadings. Such an equation would express the connecting design link between the initial detectable flaw  $a_0$  and the ultimate tolerable flaw  $a_{cr}$ , in terms of the calculated lifetime  $N_f$ :

$$N_f = \int_{a_0}^{a_{cr}} \frac{da}{f(\Delta K)} \quad (14)$$

This idealized calculation is represented in Figure 15. It is obvious from the foregoing that there is at present no universal  $f(\Delta K)$  to fit into the above relation, but on the other hand, the useful approximations which have been discussed are available for use under certain prescribed conditions. These approximations to actual fatigue growth rates must be coupled with knowledgeable estimates on the part of the designer concerning principal stress directions, stress gradients within structures, location and size of initial defects, and ultimate failure mode.

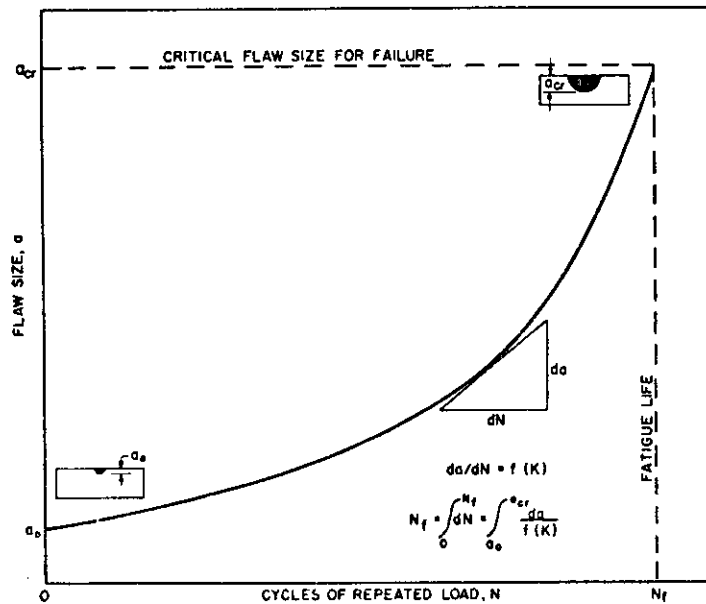


Figure 15. Schematic illustration of failure by fatigue-crack propagation. An initial defect whose size is  $a_0$  grows to a critical size for failure,  $a_{cr}$ , in  $N_f$  cycles. The crack-growth process can be described in terms of the crack tip stress-intensity factor,  $K$ , and  $N_f$  then becomes the integral of this function between the limits  $a_0$  and  $a_{cr}$ . (after Reference 13)

### C. Crack Initiation in Welds and Heat Affected Zones

Fatigue cracks in welds and weld heat-affected zones invariably nucleate either at defects such as voids, preexisting cracks, inclusions, or regions of lack-of-fusion or penetration (seams), or at geometric stress concentrators such as weld toes. It is worth noting that while such defects have little effect on static strength, they can reduce fatigue life to a significant extent. Therefore, as a matter of general policy it should always be the aim, in the fabrication of welded structures, to produce welds free of defects. In practice, this usually is impossible, but on the other hand, absolute freedom from defects is not a necessary requirement in order to assure structural integrity. The various defects encountered during ship hull fabrication are characterized and discussed in the following subsections. For an exhaustive review of both initiation and growth of fatigue cracks in welded structures, the excellent book by Gurney<sup>(20)</sup> is recommended. Unfortunately, as will be shown in the following, most of what is known about fatigue crack initiation in welds is quite qualitative.

## 1. Sources of Initiation

Incomplete penetration generally refers to the condition in butt welds in which the weld filler metal does not reach the root of a joint, so that the depth of the weld metal is less than the plate thickness. Such defects may range from small, localized gaps to large regions of discontinuity, and may occur either as buried internal defects, as when plates are welded from both sides, or as surface defects, if the plates are welded from one side only. Lawrence and Munse<sup>(21)</sup> observed that the initiation period for fatigue cracks nucleated at penetration defects in mild steel butt welds occupied approximately one-half of the total life. This period consisted of the cycles needed to "shake down" the residual stresses in the weld and to transform the lack-of-penetration flaw into an active fatigue crack. A number of investigations have been aimed at relating fatigue strength to defect severity (percent reduction of joined area caused by incomplete penetration). For laboratory-sized specimens, it has been shown that several sets of data can be represented as shown in Figure 16. Burdekin, *et al.*,<sup>(22)</sup> suggested a method of analyzing such results on a fracture mechanics basis, and this approach is discussed in Section II.C.3. Fatigue strength data for surface lack-of-penetration defects are even lower than those of Figure 16, so that every effort should be made to avoid the more readily detectable surface penetration flaw.

Cracks associated with a welded region may occur in either the weld metal or in the parent metal, may form either parallel or transverse to the line of the weld, and may be created by a variety of sources. Concerning cracks which are sufficiently large to be detected by common NDI techniques, the most usual types are solidification cracking, which occurs in the weld metal while it is hot and relatively plastic, and cold (or hard zone) cracking, which takes place in the heat-affected zone (HAZ) material following cooling of the joint. A parameter which looms important (but difficult to quantify) in both these processes is the degree of restraint opposing accommodation of weld-shrinkage, since this provides the effective cracking force. A second factor, important in solidification cracking, is the solidification rate, which determines the local structure and impurity segregation. The solidification rate can be controlled through correct heat input and by preheating, although the latter is primarily used in avoiding cold cracking in the HAZ. Cold cracking is most likely to occur in high-strength steels, due to a hard, brittle microstructure, the embrittling presence of hydrogen, and restraint stresses. It is worth noting that cracking in high-strength, quenched-and-tempered low-alloy steels occurs primarily in the heat-affected zones. This behavior is associated with an unmixed zone and a partially melted zone, which together constitute the fusion line between the apparent heat-affected zone and the base metal.<sup>(23)</sup>

Only limited fatigue research has been devoted to the problem of weld region cracking, i. e., the effect of weld-induced cracks upon fatigue properties. According to Warren,<sup>(24)</sup> at  $2 \times 10^6$  cycles internal cracks,

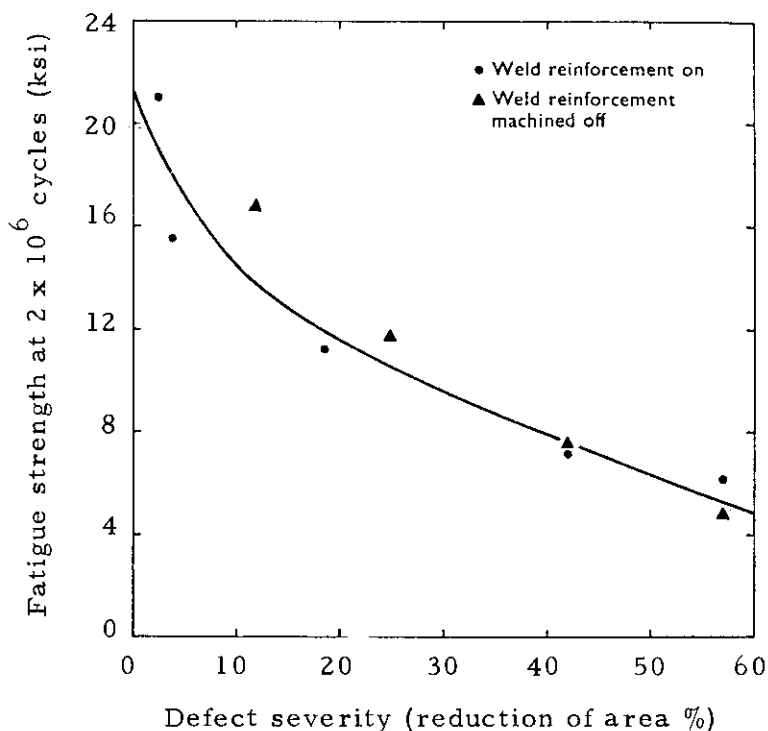


Figure 16. Summary of results relating to the effect of lack of penetration on the fatigue strength of transverse butt welds in mild steel (after Reference 20)

purposely introduced into mild steel by depositing a root run under severely restrained conditions, produced a reduction in fatigue strength of between 55% and 65%. Comparing these findings with Figure 16, one observes that a defect severity as large as 10% produces a reduction in fatigue strength of only about 25%, although lack-of-penetration also is a "planar" defect. This underscores the importance of avoiding true cracks as initial flaws.

Lack-of-fusion is another area of fatigue crack initiation for which few experimental data exist. This type of defect consists of boundaries of unfused metal, generally between the parent and filler metal. In the case of steels, the main cause of the lack-of-fusion is the contaminating presence of foreign matter on the surface to be welded, such as slag or scale, which prevents the metal from reaching the temperature of fusion. This points up the essential importance of proper joint cleaning procedures and of proper deslagging procedures between runs. Incorrect welding current also can cause lack-of-fusion.

The present state of knowledge concerning the influence (relative to other defects and to "geometric" flaws) of lack-of-fusion upon fatigue resistance is quite meager. Only the data of Newman,<sup>(25)</sup> for butt joints in mild steel, are available, and his results are inconclusive, since all observed fatigue failures in these particular specimens initiated from the discontinuity formed by the junction of the weld metal with the backing ring.

"Porosity" refers to the presence of weld metal cavities caused by the entrapment of gas during solidification. These cavities typically are spherical, and may occur in a clustered and/or a scattered distribution throughout the weld. Factors which contribute to porosity include high sulphur content, either in the parent metal or the electrode, excessive moisture in the electrode coating, or, most commonly, wind disturbance of the electrode shield, allowing nitrogen intake.

A considerable amount of work has been performed in an effort to correlate radiographically-deduced defect-severity (% reduction in area caused by porosity) to reduction in fatigue strength. Most of the work has involved butt welds, and typical results of this type are summarized in Figure 17. A few workers have considered fillet welds of varying porosity, and it has been found that in the absence of major geometric stress concentrations, the internal pores formed the major stress raisers, and decreased fatigue strength as above. It has also been observed that for welds of a given (porosity) defect severity, the use of low-hydrogen electrodes can provide an increase in fatigue strength of up to 15% compared, for example, with welds made with rutile electrodes.

Any nonmetallic matter included in a weld joint of steel is commonly referred to as a slag inclusion. This term often is a misnomer, although with the metal arc process the usual source of inclusions seems to be the slag formed by the electrode covering. The most frequent cause of slag inclusions is imperfect cleaning between weld runs. The effect of slag

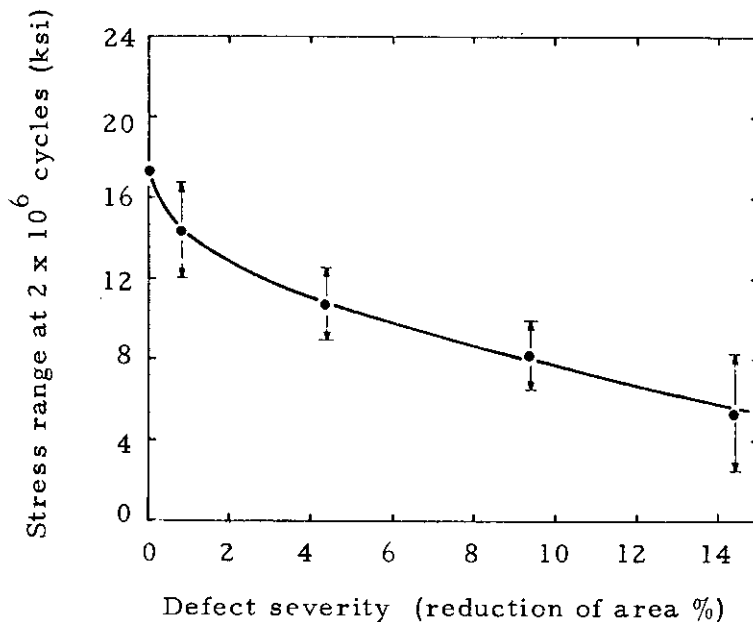


Figure 17. Summary of results obtained for mild steel butt welds containing porosity tested under a tensile mean stress of 19 ksi (after Reference 20)

inclusions has been examined in considerable detail, and they presently are the defect type for which the most comprehensive fatigue data exist.

In this connection, it has been observed that for 1/2-in. -thick specimens containing centerline (midplane) inclusions, there appears to be a reasonable correlation between fatigue strength and defect size, i. e., the radiographically measured length. This relationship, shown in Figure 18, is similar to that for porosity and incomplete penetration, whereby large reductions in fatigue strength are affected by small defects, with the rate of strength reduction decreasing as defect size increases. The number of defects seems to be relatively unimportant, in terms of strength reduction; multiple defects merely increase the statistical chance for crack initiation.

However, defect size is not the only relevant parameter in assessing the effect of inclusions on fatigue strength; in particular, residual stresses and hydrogen can also have significant influence. Tests of thick (1-1/2 in.) specimens have shown that non-stress-relieved specimens with defects near their centers have higher fatigue strengths, because of the compressive stresses around them, than do specimens with near-surface defects.<sup>(20)</sup> On the other hand, thermal stress relief does not reduce the fatigue strength,

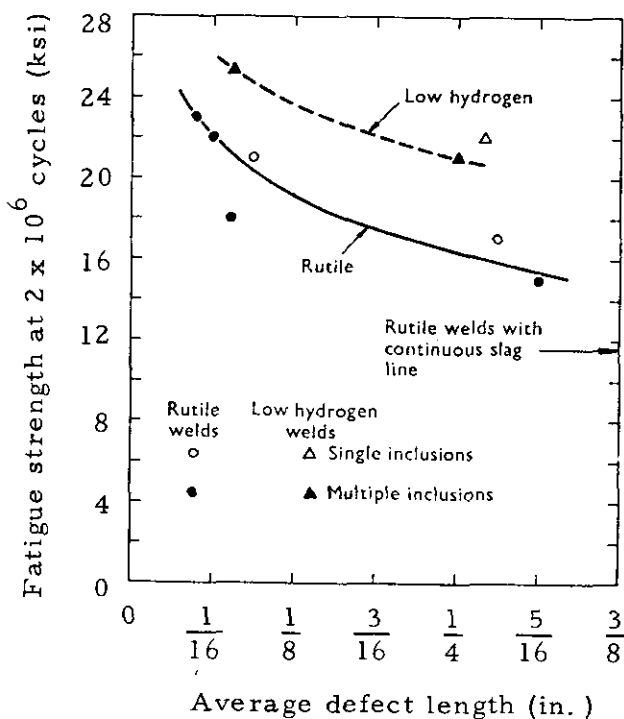


Figure 18. The effect of defect length on the fatigue strength, at  $2 \times 10^6$  cycles under pulsating tension loading, of transverse butt welds containing slag inclusions (after Reference 20)

despite eliminating beneficial compressive stresses, since the thermal process also enables hydrogen entrapped in the defect to diffuse out of the specimen. This effect overrides the loss of beneficial residual stresses, since the effect of molecular hydrogen is so very deleterious to fatigue strength. For thinner specimens, residual stress considerations are less important.

Another way of looking at the preceding discussion is to note that for stress-relieved specimens there is no significant difference between welds made with rutile and with low-hydrogen electrodes. For defect-containing welds in the as-welded condition, however, those made with low-hydrogen electrodes are stronger (see Figure 18). It has been observed that continuous lines of inclusions give a lower fatigue strength than do long discontinuous inclusions, and that preheating of welds containing inclusions has no effect on fatigue strength.

Throughout this discussion, defects have been considered as if they were buried in a continuum and were uniform in shape and orientation. Actually, surface defects, surface geometry, and the specific geometries of both internal and surface defects can further complicate the initiation of cracks in weldments. These factors will be considered next.

## 2. Influence of Surface and Flaw Geometry

In recent years it has become apparent that weld shape, i. e., surface geometry, is the overriding factor in determining the fatigue strength of transverse butt welds, and is a crucial factor for other types of welds as well. While other variables do affect fatigue strength, such as welding process, electrode type, welding position, and post-weld machining, their influence is determined by their effects on the shape of the weld toe. Several researchers have provided dramatic and convincing evidence of the crucial role of weld shape. (On the other hand, it is important to bear in mind that only a very small, but sharp, internal defect is required to override the effect of reinforcement shape.)

Newman and Gurney<sup>(26)</sup> tested several types of butt welds, using both manual and automatic welding procedures. As a quantitative measure of reinforcement shape the angle  $\theta$  between the plate surface and the tangent to the weld at its point of contact with the plate surface was used, since failure usually originated at the point of minimum angle. The measured angles were then plotted against the fatigue strength corresponding to  $2 \times 10^6$  cycles, providing the plot shown in Figure 19. All the experimental points lay within a scatterband defined at its upper end by the strengths of plain plate, with and without millscale.

In order to eliminate complicating effects arising from actual welding, several studies have utilized fatigue specimens with simulated butt welds, i. e., with various weld "profiles" machined in solid specimens of

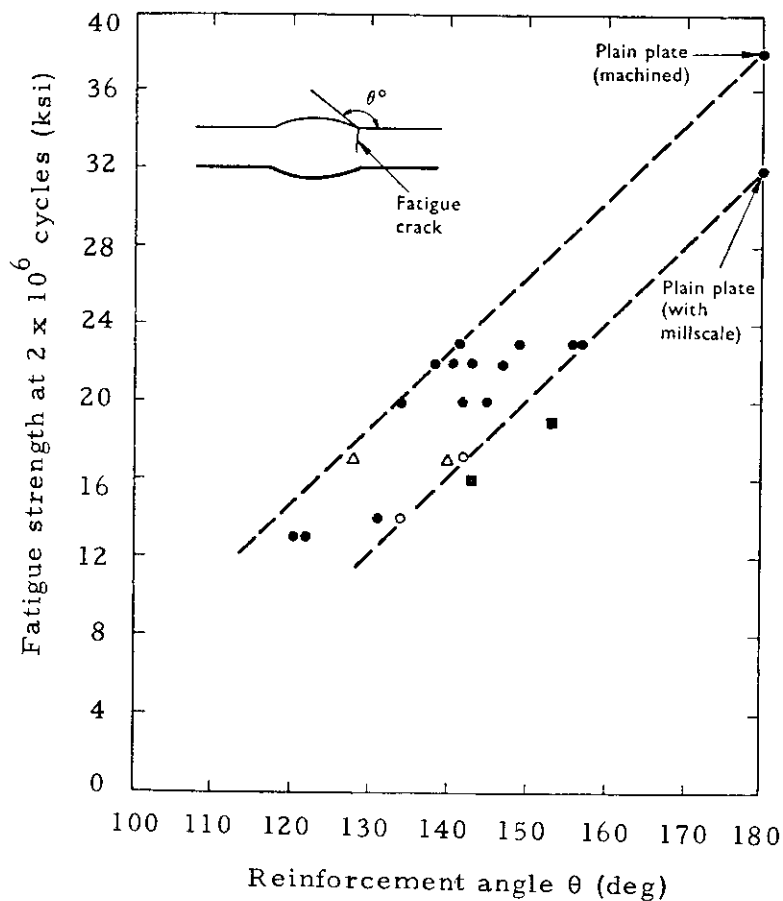


Figure 19. The relationship between reinforcement angle and fatigue strength of transverse butt welds (after Reference 20)

parent metal. The findings agree qualitatively with the previous data derived from actual weldments. For example, results<sup>(27)</sup> obtained using specimens of the shape shown in Figure 20(a) generally agreed with those of Figure 19. However, testing specimens having the configuration shown in Figure 20(b) have indicated that the radius at the weld "toe" also has a considerable influence on fatigue behavior.<sup>(28)</sup> It is thus possible to construct a relationship between the reduction in fatigue strength, reinforcement angle, and toe radius (strength decreases as radius decreases, for  $N_f$  constant), as shown in Figure 21.

Almost any surface irregularity can, in principle, contribute to a reduction in fatigue strength. This is evidenced by the data of Figure 19 for plates tested with and without millscale. Other such superficial but significant surface flaws (as opposed to weld shape) include: machining scratches, variation in weld profile, nicks, and microstructural alterations caused by grinding, welding or stress relief. However, the most severe surface or near-surface defect probably is the slight undercutting along the fusion boundary. This defect is of the order of a few thousandths of an inch in depth and

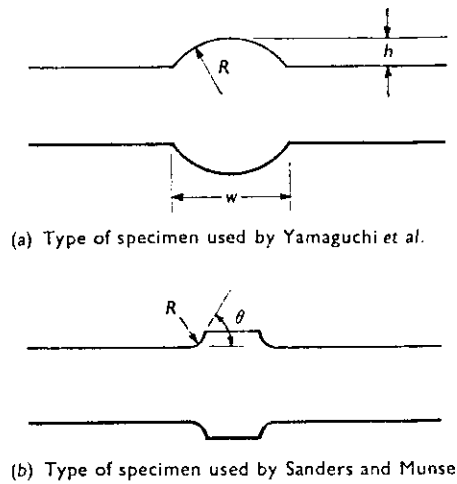


Figure 20. Parent metal specimens used to study the effect of 'weld' reinforcement shape (after Reference 20)

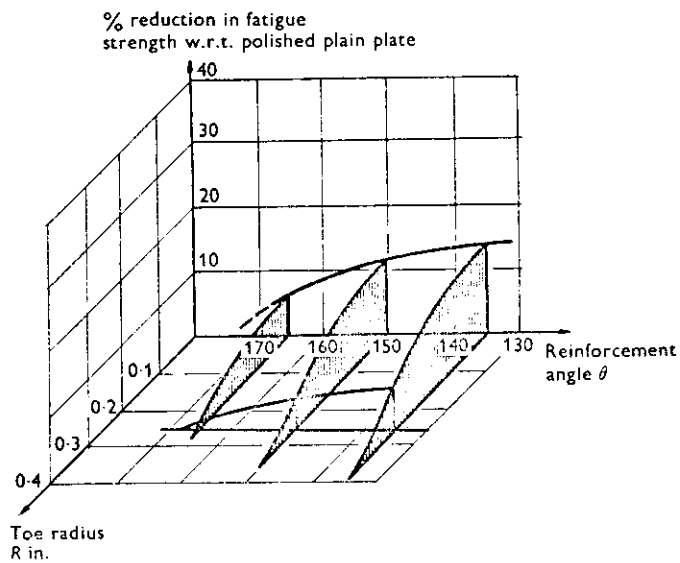


Figure 21. The effect of reinforcement shape found by Sanders, et al., in tests on parent metal specimens subjected to alternating loading (after Reference 20)

is characteristic of nearly all welds. Study has shown<sup>(29)</sup> that this region seems to consist not only of unmelted parent plate, but also of material that had partially melted at some time during the welding operation. This thin region contains an abnormally high concentration of slag inclusions and grain boundary films. The tip radius of these tiny flaws probably is less than 0.0005 inch, so that the local stress concentration is greatly enhanced over that of the weld shape alone. On this basis, there seems good reason to believe that these small, sharp, crack-like defects are the initiating points for cracks emanating from weld toes and heat-affected-zone boundaries, which are easily the most common fatigue crack-starting mechanisms in welded structures. Gurney<sup>(20)</sup> feels that this effect, in fact, accounts for the observation that all steels, when welded, have the same fatigue limit.

A complicating factor introduced by weld reinforcement and weld fillets is the alteration of the applied stress field. Such geometric defects invariably produce local biaxiality even in nominally uniaxial fields. Since the degree of severity of a defect is strongly dependent upon its orientation relative to the local stress field, knowledge of the principal stress state can be very useful in assessing the criticality of a particular known, preexisting flaw. For example, lack-of-penetration defects are extremely detrimental when oriented perpendicular to a uniaxial loading axis, but have little or no effect on fatigue strength when lying parallel to the axis. Similar observations have been made regarding lack-of-fusion. In the case of inclusions, continuous inclusions in butt welds oriented parallel to the applied stress are relatively harmless, indicating that in this case it is the width of the defect, not its length, which is the critical parameter.

### 3. Models for Crack Initiation

In contrast to the situation which prevails for the case of crack propagation, there presently exist no clear-cut, fundamentally sound analytical criteria for predicting crack initiation in weldments. However, a few empirical relationships have been developed to predict cyclic lifetime, which as input parameters include the size and geometry of the initiating flaw, which in turn can be obtained empirically via nondestructive inspection techniques. It should be pointed out that these criteria actually involve crack propagation and that they might better be considered as descriptions of flaw severity, rather than mathematical predictors of cycles to crack "initiation."

The most complete criterion of this type is that formulated by Burdekin, et al.,<sup>(22)</sup> who considered the results of fatigue tests involving incomplete penetration defects in weldments. However, in terms of crack initiation, the most that has derived from this and other similar studies based on fracture mechanics, is guidance as to certain features which any useful initiation criterion should incorporate. In particular, it was concluded that<sup>(30)</sup>

- (a) The ratio of flaw width to plate thickness is dominant in controlling the period spent in crack initiation.
- (b) The position of the initiating flaw relative to the center-line of the weld is an important parameter in determining initiation life.
- (c) In the case of very small flaws, the actual geometry of the flaw is influential in determining the initiation life.

#### D. Crack Propagation in Welds and Heat-Affected Zones

The problem of fatigue crack growth in weldments is considerably more complicated than that of crack propagation in the parent metal. Complications arise from the fact that welding results in residual stresses and metallurgical changes, so that the fatigue crack may initiate in, and propagate through, material having mechanical properties quite different from those of the parent metal. Furthermore, the rate of growth may accelerate or decelerate as the crack passes from weld metal to heat-affected zone to parent alloy. For weldments, the influence of growth rate-controlling factors has not been determined in as systematic and general a fashion as has been the case for the base metals (Sect. II. B), but useful work has been carried out and will be discussed in this Section.

##### 1. Factors Controlling Fatigue Crack Growth in Welds and Heat-Affected Zones

As in the case of base metals, the rate-of-growth of fatigue cracks generally may be described by an equation of the form

$$\frac{da}{dN} = A \Delta K^n \quad (15)$$

It has been shown<sup>(31)</sup> that for weld metal specimens whose tensile strengths range from 50 to 82 ksi, the crack growth rate, as a function of  $\Delta K$ , increases only slightly with yield strength. The data actually cluster within a fairly narrow scatterband, and a transition to a faster, less stable mode occurs between  $10^{-4}$  in./cycle  $< \frac{da}{dN} < 10^{-3}$  in./cycle, in accordance with the discussion of Section II. B. 1. The influence of variations in fracture toughness across the weld zone upon crack growth has not yet been established.

It does appear that microstructural alterations may play a significant, but not yet clearly understood, role in crack propagation. Limited experimental data<sup>(32)</sup> have indicated that for normalized mild steel weldments, the microstructures of the weld metal and the HAZ are more notch sensitive than unaltered base metal. The spheroidized pearlite region of the HAZ is

especially notch sensitive and, further, seems to exhibit the highest rate of fatigue crack growth and the lowest fatigue strength. Grain boundary embrittlement by carbide precipitation appears to account for the higher crack growth rates in weld metal and in the HAZ. These conclusions are at variance with those of other workers,<sup>(33)</sup> studying similar steels, who report that the crack propagation rate within weldments is significantly lower than that observed within the parent metal. It is doubtful if these differences can be explained on the basis of weld metal or welding technique, since Reference (31) employed three different weld metals and two different welding techniques. The insensitivity of fatigue life, and specifically the crack propagation rate, to welding technique and filler metal, has been observed for quenched and tempered low-alloy steels as well.<sup>(30)</sup>

In the case of the latter steels, and HY-80 in particular, it appears that under high-cyclic stresses the fatigue strength of the weld region significantly exceeds that of the softened HAZ, but at stresses near the fatigue limit, this difference is negligible.<sup>(34)</sup> Since cracks nucleate so early in the lives of welded specimens, this difference likely can be ascribed to variations in crack growth rate.

Recent tests<sup>(35)</sup> of mild steel and low-alloy weldments have provided useful insight into crack growth behavior within welds, the HAZ, and the parent metal. Under conditions of constant alternating and maximum stress intensity, for instance, a fatigue crack propagates through the weld metal at a uniform rate only when it is remote from the HAZ. A hard HAZ has been found to reduce the crack propagation rate by a factor of two, although the changes in growth rate were not uniquely related to the condition of the material immediately adjacent to the crack tip. Rather, the shape of the plastic zone at the crack tip was found to control the direction (hence the rate of propagation) of the fatigue crack, and the crack always deviated towards regions of lower flow stress. Generally, cracks did not follow the actual weld/HAZ interface, because of flow stress differences on each side of the interface. It appears that there is no fundamental difference in the crack propagation mechanism between the parent plate and its HAZ for tempered martensitic steels.

Apparently the direction of crack propagation, i. e., whether the crack is growing from the parent metal into the weld, or vice versa, is quite important. This effect is demonstrated in Figure 22, showing the variation in crack propagation rate for a fatigue crack traversing a mild steel HAZ from two different directions. The observed differences in crack growth rate can be rationalized, on a qualitative basis, in terms of the shape and size of the crack tip plastic zone as the crack moves through regions in which the hardness (a reflection of the material strength or toughness) changes. However, there are at present no quantitative theories, either fundamental or empirical, capable of accounting for such effects.

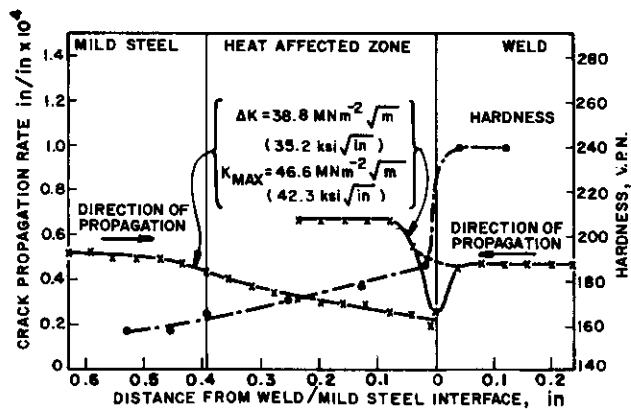


Figure 22. Variation in crack propagation rate and hardness along the fatigue crack path through a mild steel HAZ at 75 deg to the tensile axis (after Reference 35)

## 2. Crack Growth Theories

Most efforts to describe crack growth quantitatively in weld regions have been based on fracture mechanics. However, none of these efforts has as yet been so venturesome as to include as direct parameters the load ratio, temperature, environment, or strain hardening characteristics. Still, useful, fairly simple analytic relations have been developed which are capable of providing conservative, first-order estimates of component life-times as a function of crack growth rate. One of the most complete and physically sound of these approaches<sup>(30)</sup> will be discussed in this section.

It is reasonable to expect that the effect of flaws on the fatigue life of welds should be related to the maximum stress experienced in the material adjacent to the flaw, i. e., to the stress intensity of the defect. On the other hand, the rate of crack growth subsequent to initiation should be little affected by the nature of the initiating flaw, aside from one important point: the characteristic dimensions and spatial orientation of the initial crack will be determined essentially by the dimensions, orientation and location of the originating flaw relative to the effective\* applied stress field. Once a fatigue crack has formed, the number of cycles to failure at any given stress level depends only upon the rate at which the crack propagates through the weld filler material, the HAZ, and the parent metal.

As mentioned earlier, the rate of fatigue crack growth,  $da/dN$ , is given by Equation (15), where  $A$  and  $n$  are material constants. Although these constants do not vary greatly from one high-strength steel to another, or between various filler metals, there can be significant variations in one

\*The external cyclic loading plus any residual stresses present.

or both of these parameters across a given weldment, i. e., as a crack traverses filler, HAZ, and parent metal (see Figure 22). This latter area is insufficiently understood at present and is not taken into account in any current theory.

For tests run at a constant stress range, the number of cycles to failure associated with propagating a crack from an initial length  $a_0$  to a terminal length  $a_{cr}$  is:

$$N_p = \int_{a_0}^{a_{cr}} \frac{1}{A (\Delta K)^n} da \quad (16)$$

where  $\Delta K$  is an analytic expression for the stress-intensity-factor range which describes the character of the growing flaw. If the integration of the resulting expression proves difficult, a finite difference or other numerical technique may be used, e. g.,

$$N_p = \sum_{a_0}^{a_{cr}} \frac{\Delta a}{A (\Delta K)^n} \quad (17)$$

and  $\Delta a$  is a small finite advance of the crack. Although exact solutions for a generalized flaw in a finite body are not available, solutions for simpler idealizations of physical defects do exist.

In Figure 23(a), a simple model of a weld flaw, i. e., a disc-shaped crack in an infinite body, is shown. For this case,

$$\Delta K = \frac{2}{\pi} \sigma \sqrt{\pi a} \quad (18)$$

which, when substituted into Equation (16), yields

$$N_p = \frac{a_{cr}^{(1-n/2)} - a_0^{(1-n/2)}}{(1 - \frac{n}{2}) A (\frac{2\sigma}{\sqrt{\pi}})^n} \quad (19)$$

This equation provides a model for the case of an isolated pore or inclusion, as shown in Figure 24(c).

Similarly, as a second model consider a through-crack in a body which is finite in the direction of crack advance (Figure 23(b)). For this case,

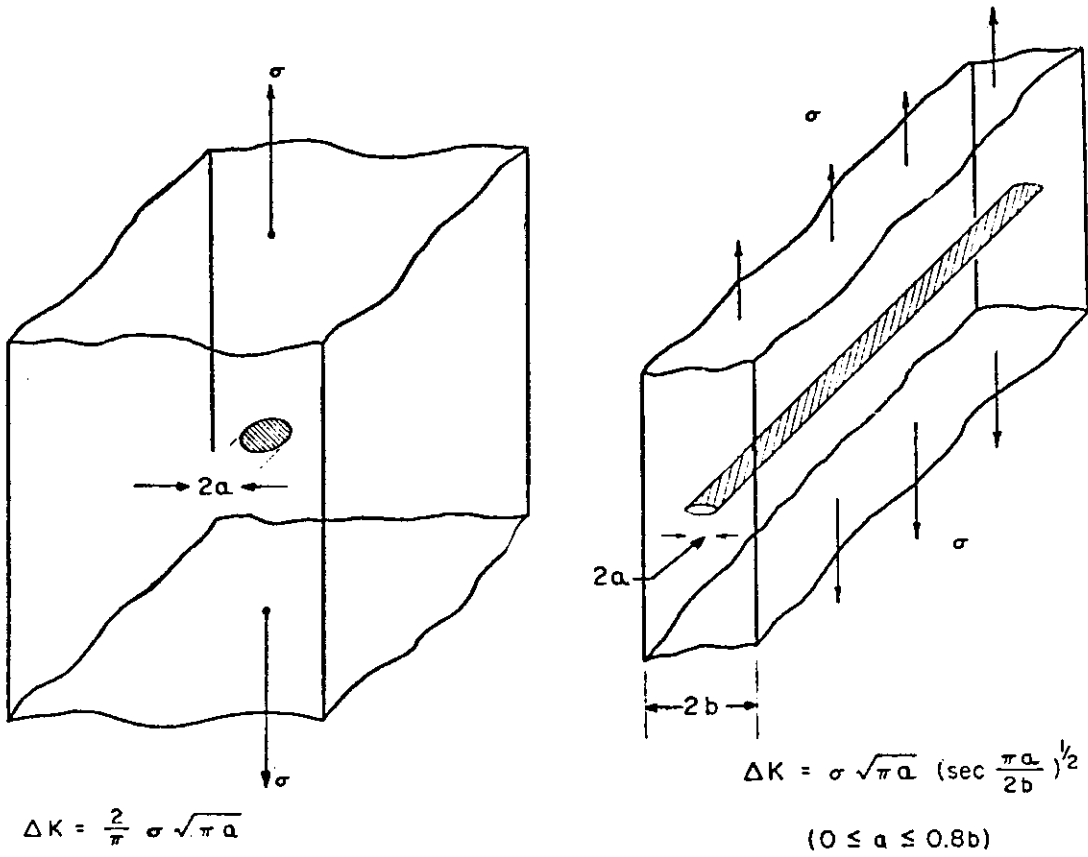


Figure 23. Two models for flawed weldments: left (a) - a disc-shaped crack in an infinite body; right (b) - a through crack in a finite plate. The stress intensity factors are given for each. (after Reference 30)

$$\Delta K = \sigma \sqrt{\pi a} \left( \sec \frac{\pi a}{2b} \right)^{1/2} \quad (20)$$

which can be inserted into Eq. (17) to give

$$N_p = \sum_{a_o}^{a_{cr}} \left[ \frac{\cos \left( \frac{\pi a}{2b} \right)}{a A^{2/n} \sigma^2 \pi} \right]^{n/2} \Delta a \quad (21)$$

This is a reasonably accurate model for the intermittent and continuous linear flaws illustrated in Figure 24(a, b, d).

A characteristic of both of the preceding equations for propagation life is the great sensitivity of the calculated fatigue life  $N_p$  to the choice of initial flaw size  $a_o$ . Since a fatigue crack spends the major portion of its lifetime as a very small crack, the accuracy of the solution will depend in large part upon faithfully modeling the initial size and geometry. This sensitivity is reflected in Figure 25.

Experiments have shown that when good estimates of the initial flaw characteristics are available, Equations (19) and (21) can offer the designer considerable guidance in calculating fatigue life. However, the usefulness of this formalism is compromised by several factors, not the least of which is the fact that so little is known of the factors which determine the period of life spent in initiating an active crack, and the role of flaw size, geometry, and stress level active in determining that life.

Further, techniques for nondestructive flaw evaluation still require further development in order to characterize potential crack-initiating flaws adequately. For example, it is frequently the case that critical fatigue cracks do not start at those flaws which appear to be most severe on the basis of radiographs taken prior to testing. On the contrary, the fatal crack often initiates at a defect not even detected by the radiograph.<sup>(30)</sup>

As mentioned earlier, variations in mechanical properties across a weld still is an area of great uncertainty, capable of seriously distorting idealized predictions based on either weld filler or parent metal laboratory measurements.

Until these factors can be assessed with greater insight than is presently possible,

"The fatigue lives of high-strength steel weldments failing at internal flaws may be estimated by neglecting the crack initiation period and using the concepts of

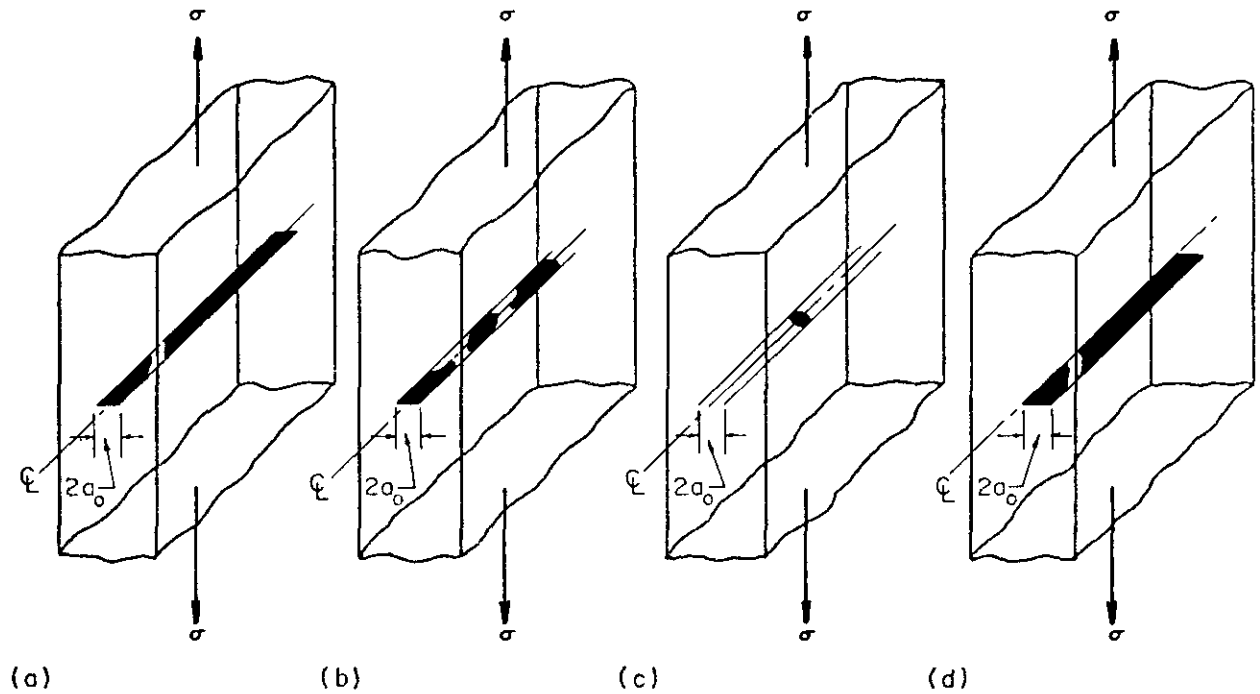


Figure 24. Types of flaws found in weldments: (a) continuous linear defects at the center of the weldment, e. g., lack of fusion, continuous slag; (b) intermittent linear defects at the center of the weldment, e. g., intermittent lack of fusion, intermittent slag, elongated porosity; (c) isolated pores at the center of the weldment, e. g., small voids, pores, very small defects of all kinds; (d) continuous linear defects located off center in the weldment. (after Reference 30)

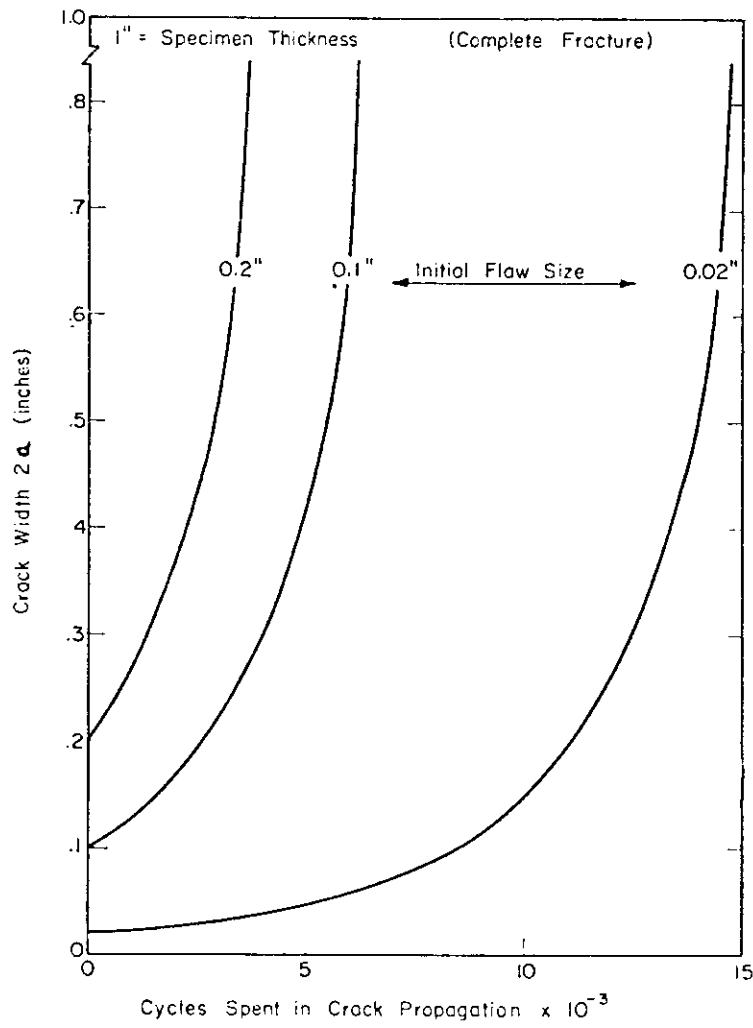


Figure 25. Effect of initial flaw size on the crack propagation life of a flawed 1 in. thick HY-130 weldment. (after Reference 30)

fracture mechanics to (empirically) predict the number of cycles spent in crack propagation and hence the minimum expected total life. Furthermore, from the demonstrated sensitivity of the propagation life to initial width of the flaw, it would seem that the fatigue life of a weldment in service should be assumed to be no better than that resulting from the largest flaw (through-thickness dimension) which may be permitted or remain undetected by the post fabrication nondestructive inspection standards used. "(30)

## E. Fatigue Damage Estimation

The previous sections have discussed in some detail the problems of crack initiation and propagation in ship steels and weldments. This knowledge alone, however, is not a sufficient basis for ship design and structural analysis. In many cases the existence of a dangerous subcritical crack is unknown prior to fast fracture, and therefore data concerned with crack growth rates may be entirely useless. What is needed instead is a set of design principles which will relate the expected life of a structural component to the expected service environment. Such principles are generally known as cumulative damage rules and form the substance of this section.

### 1. Cumulative Damage Analysis

Structural components are subjected to a wide variety of fatigue-producing load spectra. Some structural regions primarily experience simple sinusoidal loads of constant amplitude, whereas others may be subjected to complex nonstationary random loads. Some appreciation for the variety of load environments which can occur may be gained by the following classification of service fatigue problems currently being studied, from Akaike and Swanson:(36)

<u>Dominant Service Loading</u>	<u>Percentage of all Fatigue Problems Currently Under Study</u>
Constant Amplitude Periodic (sine, triangular wave)	7
Programmed Constant Amplitude (blocks of constant amplitude waves)	12
Arbitrary Profile Loadings (repeated one-shot complex loadings)	13
Stationary Random (constant rms to failure)	9
Non-Stationary Random Loadings	13
Quasi-Stationary Random (succession of stationary random blocks)	41
Other	<u>5</u>
	100%

Superposed on this scale are further complicating effects of multiaxial stress fields, variable thermal and chemical environments, etc.

Nearly all models of cumulative fatigue damage are refinements of a basic linear cumulative damage model proposed independently by Palmgren<sup>(37)</sup> and Miner.<sup>(38)</sup> This simple model views irreversible fatigue damage as being introduced with each cycle of load. The rule states that at the  $i$ -th cycle of load with stress  $\sigma_i$ , a damage increment is introduced which is equal to  $1/N_i$ , where  $N_i$  is the number of cycles to failure of a specimen cycled under constant amplitude stress  $\sigma_i$ . Assuming that the amount of damage absorbed by the material in any one cycle is determined only by the load during that cycle, then failure should occur when the summation of the damage increments at each stress amplitude equals unity:

$$\sum_i n_i/N_i = 1 \quad (22)$$

where  $n_i$  is the number of applied cycles at the  $i$ -th load level.

In its usual application  $N_i$  is found from the S-N diagram, in turn constructed from fatigue failure tests with small specimens under sinusoidal loading.  $n_i$ , the number of applied cycles at the  $i$ -th stress level, is derived from an estimate of the expected load spectra under which the structure is expected to operate. The principal difficulties attendant to this procedure are (1) relating the local material response to the overall structural loading environment, and (2) estimating the  $n_i$  from a complex expected load spectrum.

The most common objection with the linear cumulative damage approach is that it does not account for the order of stress application. Load sequencing effects may be important in cases of simple block-type loading, such as  $n_i$  cycles at stress  $\sigma_i$  followed by cycling to failure at stress  $\sigma_j$ . In such cases, it is generally found that the deviation of  $\sum n_i/N_i$  from unity at failure is less predictable, and the linear cumulative law more nearly provides an average estimate of fatigue life. Reported differences among investigators almost surely are due largely to the way in which pseudo-random or true random stress histories are counted as "equivalent" load cycles for use with the damage rule. It is worth mentioning that Saunders<sup>(39)</sup> has recently developed a general analytical probability model from which he showed that the linear cumulative damage rule emerges as the expected value of stochastic fatigue life.

In addition to the nature of the loading environment there are other variables which affect the adequacy of the linear cumulative damage rule. Because of the inherent assumption that the damage increment is independent of the relative position of the load cycle in the spectrum, the rule is strictly valid only for the precrack region. Thus, it tends to be more useful in the "low-cycle" fatigue range, where the major portion of fatigue life is

spent in crack initiation. Moreover, a review of the experimental basis for this rule suggests that it is somewhat in better agreement with test results for structural aluminum alloys than for steels.(40)

In an effort to overcome some of the deficiencies of the linear cumulative damage rule, many investigators during the 1950's and '60's sought to develop new and improved damage rules. Most amounted to empirical modifications of "Miner's Rule." Although some were developed from basic physical principles governing crack initiation and growth, most came as modifications to the original linear cumulative damage rule. O'Neill(41) has provided a critical survey of cumulative damage theories through 1970. He points out that

"None of the rules considered shows a clear superiority to the linear rule. Some are better in particular situations--typically where a few discrete stress levels are applied to a simple specimen run to fracture--but such cases are trivial. However, in random loading of small specimens, which must one day be related to structural behavior, the linear rule is usually unconservative. In part this can be attributed to the common practice of equating cycles and zero crossings and ignoring intermediate fluctuations."

This emphasizes the point that the linear cumulative damage rule is the best one currently available in terms of simplicity and predictive ability, and can be applied to random loading environments provided the random environment is properly interpreted in terms of simple sinusoidal specimen fatigue test data.

## 2. Frequency and Temperature Effects

Fatigue strength is affected by both cyclic frequency and temperature. The frequency effect in HSLA steels is quite small. In the range of about 500-10,000 cpm the frequency effect is in fact negligible.(42) Above this range the fatigue strength shows a continuous, but slow, increase with frequency, due primarily to microstructural effects (such as dislocation generation and movement) which require a finite time scale in which to develop. For typical applications involving primary and secondary ship structure, however, fatigue strength may be considered to be independent of loading frequency.

The effect of temperature on fatigue strength is best understood by considering three separate thermal regimes. In the range up to about 700° F the fatigue and creep properties interact to reduce the fatigue strength sharply. Above 1000° F the fatigue life is very small and is controlled entirely by creep. Within the temperature environments usually experienced by primary and secondary ship structure, creep is not a consideration.

Fatigue strength decreases with increasing temperature and is accompanied by the disappearance of a well-defined endurance limit.

### 3. Multiaxial Stress Fatigue

Although most structural fatigue analysis in practice is based upon the assumption of a one-dimensional stress state, it is unquestionably true that most problem areas involve multiaxial stresses. A good deal of research effort has been given in recent years to understanding this problem,\* and, while substantial gains have been made, there is no single accepted design procedure for fatigue life prediction under multiaxial stresses. It is known, however, that such stress systems can severely reduce fatigue life. Various investigators have attempted to correlate biaxial fatigue failure data by introducing an "effective" stress  $\sigma_e$  (or strain  $\epsilon_e$ ), which is some analytical function of the principal stresses (strains) acting. Among the several expressions proposed for the effective stress are:

$$\sigma_e = \sigma_1 \quad \text{maximum normal stress} \quad (23)$$

$$\sigma_e = \frac{1}{2}(\sigma_1 - \sigma_3) \quad \text{maximum shear stress} \quad (24)$$

$$\sigma_e = \frac{1}{3} [(\sigma_1 - \sigma_2)^2 + (\sigma_2 - \sigma_3)^2 + (\sigma_3 - \sigma_1)^2]^{1/2} \quad (25)$$

octahedral shear stress

In these expressions  $\sigma_1 > \sigma_2 > \sigma_3$  are the principal stresses. As in the case of uniaxial fatigue, the fatigue life may be expressed in terms of the maximum value of  $\sigma_e$  per cycle, or cyclic amplitude per cycle  $\Delta\sigma_e$ , or in terms of the maximum or cyclic amplitude of the effective strain  $\epsilon_e$ . There is no agreement, however, as to which expressions are the most descriptive for a given material and loading spectrum. A good engineering discussion of the use of these various expressions may be found in the book by Marin.<sup>(44)</sup> He recommends that the single most useful design tool is the modified octahedral shear theory. In the case of biaxial stresses ( $\sigma_3 = 0$ ), this theory takes the form

$$\sqrt{(\sigma'_1)^2 + [2 - (\sigma_o/\tau_o)^2] \sigma'_1 \sigma'_2 + (\sigma'_2)^2} + \left(\frac{1-R}{2}\right) \left(\frac{\sigma_o}{\sigma_f}\right) \sqrt{(\sigma'_1)^2 + [2 - (\sigma_f/\sigma_Y)^2] \sigma'_1 \sigma'_2 + (\sigma'_2)^2} = \sigma_o \quad (26)$$

\* Carden<sup>(43)</sup> has published a bibliography on the subject containing approximately 700 references through 1967.

where  $\sigma'_1$ , etc., represent maximum values per cycle, and  $\sigma_0$  and  $\tau_0$  are the tensile and shear fatigue strength, respectively, under completely reversed stress. Also,  $\sigma_f$  and  $\sigma_y$  are the static tensile and yield strengths, and  $R$  is the usual stress ratio:  $\sigma_{\min}/\sigma_{\max}$ . This theory, which assumes that the biaxial stresses are always in-phase, may be used either to predict fatigue strengths  $\sigma_0$  and  $\tau_0$  for given combined stresses, or determine allowable stresses  $\sigma'_1$  and  $\sigma'_2$  for given fatigue properties.

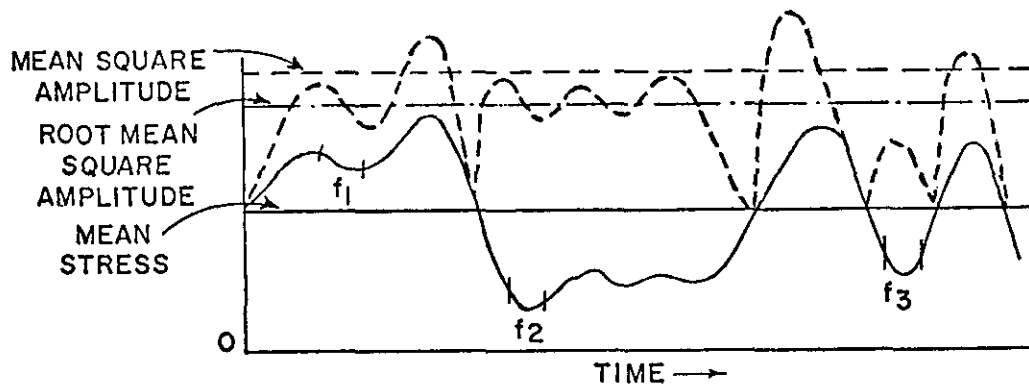
Despite the amount of engineering research devoted to the problem of multiaxial fatigue, little definitive information is available for low-alloy steels of the type employed in ship construction. Blatherwick and Viste<sup>(45)</sup> tested thin tubes of 1020 steel in combined stress fatigue and concluded that the octahedral shear stress correlated their data better than other effective stress measures. Havard and Topper<sup>(46)</sup> conducted similar tests on 1018 steel in oil. They found that fatigue strength conformed to the Basquin relationship  $\Delta\epsilon_e = AN^b$  for elastic strains, to the Coffin-Manson relationship  $\Delta\epsilon_p = CN^d$  for plastic strains, and to the sum  $\Delta\epsilon_t = AN^b + CN^d$  for total strains. Their recommendation for design is to use the maximum shear stress range plus one-twelfth of the sum of the principal stress ranges. Thus,  $\sigma_e = AN^b$ , where

$$\sigma_e = \frac{1}{2} \Delta(\sigma_1 - \sigma_2) + \frac{1}{12} \Delta(\sigma_1 + \sigma_2) \quad (27)$$

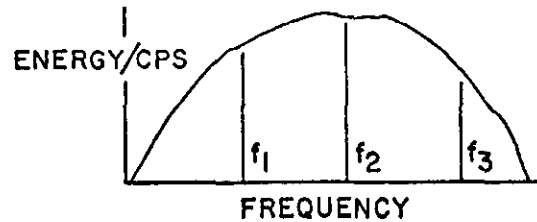
In view of the variety of criteria and recommended practices available, for the time being design for multiaxial fatigue must lean heavily on experimental data generated under conditions closely simulating the expected service environment. Extrapolations of such data to other material conditions and loading spectra can be quite hazardous and should be attempted only when comfortable margins can be designed into the structure.

#### 4. Random Loads

In the analysis of structural fatigue the engineer is faced with the problem of defining the load environment and its relationship to critical structural regions under investigation. First, it is necessary to characterize the service loading as being essentially constant amplitude (such as sinusoidal or blocks of sinusoids) or essentially random, or a combination of random and deterministic loads. If the loading environment has random content, then estimates must be made of statistical quantities which, at least roughly, describe the environment. Some of the basic concepts involved in describing a random signal are illustrated in Figure 26. Figure 26(a) shows a trace of a portion of a random signal as a function of time, and its square, shown dashed. A Fourier analysis of this trace segment would reveal a number of harmonic components; three are illustrated. Figure 26(b) shows the "power spectral density" (PSD) diagram for this trace; PSD is a measure of the energy content



(a)



(b)

Figure 26. Power spectral density plot

of the signal over the frequency spectrum.\* In Figure 26(b),  $f_1 < f_2 < f_3$ , and the principal energy content resides at frequency  $f_2$ .

The second factor to be considered concerns the response of the structure to the load spectrum. The question is whether the structure in question will respond in a single predominant resonance, or will it have a broad-band or multi-modal response. Suppose, for example, that a random signal having the energy content shown in Figure 26(b) is applied to a single degree of freedom structure. If the natural frequency of the structure is much greater than  $f_3$ , it will not respond significantly and fatigue damage accumulation will be small. If, however, the natural frequency is near frequency  $f_2$  the structural response will be strong, possibly leading to a serious fatigue problem.\*\*

\* The actual ordinates for the PSD diagram are sometimes a cause for confusion. The most popular units are  $g^2/\text{cps}$ , where  $g$  is the acceleration being measured. In this case one obtains the mean square value from the integration of the PSD diagram. Another popular ordinate is  $g/\sqrt{\text{cps}}$ . This unit is used so that integration yields the RMS directly.

\*\* The reader interested in obtaining a good basic understanding of the analysis of random fatigue problems is referred to the article by Miles. (47)

Problems in random vibration are commonly classified as "narrow-band" or "wide-band" according to how wide in frequency the PSD diagram is relative to the center frequency. More is known of narrow-band random processes than of wide-band processes. For example, if the process is Gaussian, it is known that the distribution of peak amplitudes is a Rayleigh distribution. (For wide-band processes the distribution is unique to the process.) This fact has made it possible to calculate the expected value of fatigue damage accumulation for narrow-band random processes as a function of time  $t$ . Crandall and Mark (48) have shown that if one assumes an S-N curve of the form  $N\sigma^b = c$ , and uses the linear cumulative damage rule, the expected value of the damage,  $E(D)$ , is:

$$E [D(t)] = \frac{\omega_o t}{c} \left( \sqrt{2} \sigma_{rms} \right)^b \Gamma (1 + b/2) \quad (28)$$

where  $\omega_o$  is the expected frequency of the narrow-band random stress history with zero mean stress (the average number of zero crossings with positive slope per unit time),  $\sigma_{rms}$  is the rms stress level, and  $\Gamma$  is the gamma function, tabulated in standard mathematical tables. It is useful to compare the damage as predicted by the narrow-band random process to that given by the cumulative damage rule for constant-amplitude sinusoidal loading. In the latter case, the time-dependent damage is  $D(t) = \frac{\omega_o t}{c} \sigma_{max}^b$ . On equating this damage with the expected damage from the random process, Eq. (28), one finds an expression of the form  $\sigma_{max} = k \sigma_{rms}$ , where  $k = \sqrt{2} \left[ \Gamma(1 + b/2) \right]^{1/b}$  relating the stresses for the two processes. It is instructive also to compare the calculated value of fatigue damage accumulated under a narrow-band random process with the damage accrued under a sinusoidal stress environment of frequency  $\omega_o$  and maximum stress  $\sigma_{rms}$ . The ratio of the expected damage from the narrow-band random process to that of the constant-amplitude sinusoidal process at the same peak stress level  $\sigma_{rms}$  is  $2^{b/2} \Gamma(1 + b/2)$ . Using a typical value of  $b = 4$  for steels, one finds that the damage accumulation rate for the random process is 8 times that of the "equivalent" deterministic process. This calculation has been borne out by laboratory experience many times. The rates of damage accumulation under the narrow-band random and the sinusoidal loading environments are equal only as the S-N curve approaches a horizontal slope, which is uncharacteristic of any real metal.

The problem of transforming a random loading spectrum into an "effective" sinusoidal environment is a difficult one which has received a great deal of attention recently. It is essential to have a proven procedure for determining the stress levels and numbers of loading cycles in order that sinusoidal specimen data can be used in conjunction with the linear cumulative damage rule. One day undoubtedly more property data will be generated under "standard" random loading conditions, but that day is not yet in sight.

When reducing a random signal for purposes of fatigue analysis it is essential that all "primary" cycles in a given period be considered, but

"secondary" signals can usually be ignored. The meanings of "primary" and "secondary" are established in the following manner<sup>(49)</sup>: First, a mean stress level  $\sigma_{\text{mean}}$  is established for the entire record. Then, the maximum stress occurring between a crossing of  $\sigma_{\text{mean}}$  with a positive slope and a crossing with negative slope is called  $\sigma_{\text{max}}$ . All other local maximum stress values are designated  $\sigma_{\text{ma}}$ . Finally, the minimum stress occurring between a crossing of  $\sigma_{\text{mean}}$  with negative slope and a crossing with positive slope is designated  $\sigma_{\text{mi}}$ . With these definitions, the combination of a  $\sigma_{\text{mi}}$  with the next  $\sigma_{\text{ma}}$  forms a secondary cycle. A simple systematic procedure for cycle counting, which has enjoyed wide use, is the following: If peaks and troughs are normally distributed about a positive mean stress, the damage per cycle caused by all cycles which neither cross nor exceed the mean stress can be neglected.

## 5. Equivalence Between Sinusoidal and Random Fatigue Damage

The structural designer is interested in knowing how to determine the frequency and number of cycles of a sinusoidal loading program that is "equivalent" to a given random loading program. In the present context, the term "equivalent" means the same as "inflicting the same amount of fatigue damage." This sort of a calculated equivalence between sinusoidal and random fatigue loading environments is often necessary in structural fatigue design. For example, it is not uncommon for the fatigue load spectra to be given by a random description, whereas the base-line material behavior (S-N diagram) is available only from the results of sinusoidal fatigue tests.

There is no calculation procedure that can be applied with complete confidence in all cases. In striving for accuracy and generality, a number of research investigators have proposed rather sophisticated procedures in recent years. Rather than follow this trend, however, this subsection will outline the simple method of calculating random-sinusoidal fatigue equivalence discussed in the preceding section. This procedure can be simply applied and should provide realistic answers sufficiently accurate for ship primary and secondary structural design purposes. The problem posed in this procedure is to calculate the constant amplitude sinusoidal fatigue loading which is equivalent (in terms of cumulative damage) to a given random loading environment. This procedure rests on the following assumptions:

- (a) The stress response of primary and secondary ship structure is approximately a narrow-band, stationary Gaussian process.
- (b) The "S-N" curve is log-log linear and described by the equation  $N\sigma^b = c$ .
- (c) The usual assumptions of "Miner's Rule" (Sect. II, E. 1) hold.

The procedure is described by the following six steps.

- STEP 1 Determine the mean or constant component of the random load signal, and use this value as the mean level of the equivalent sinusoidal signal.
- STEP 2 Determine the effective frequency,  $\omega_0$ , of the equivalent sinusoidal signal by using the average number of zero crossings with positive slope per second. (See Sect. II. E. 4 for a further discussion of this procedure.)
- STEP 3 Determine the RMS stress level,  $\sigma_{rms}$ , of the random signal.
- STEP 4 Determine the slope parameter  $b$  of the S-N curve from constant amplitude sinusoidal fatigue test data on the material system of interest. That is, plot  $\log \sigma$  on the vertical axis (where  $\sigma$  is the peak stress per cycle) versus  $\log N$  (cycles to failure); the slope of this line is  $-1/b$ . Note that the slope may be considered to be independent of the value of  $R$ . If the required data are not available, use  $b = 3.5$  for welded structure.
- STEP 5 Calculate the stress equivalence factor  $k$  by the formula  $k = \sqrt{2} [\Gamma(1 + b/2)]^{1/b}$ , where  $\Gamma$  is the gamma function. This equation is plotted for convenience in Figure 27.
- STEP 6 Calculate the peak amplitude of the equivalent sinusoidal signal by the relation  $\sigma_{max} = k \sigma_{rms}$ .

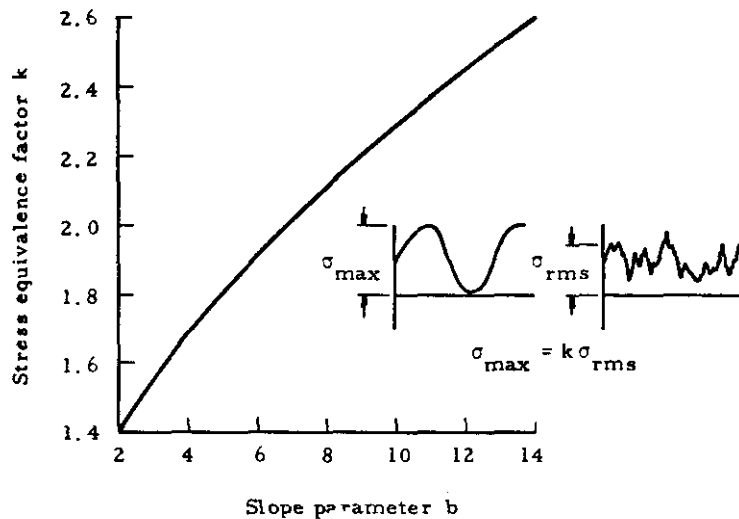


Figure 27. Stress equivalence factor

### III. ENVIRONMENTAL TOPICS RELATED TO SUBCRITICAL CRACK GROWTH

#### A. Stress Corrosion Cracking

##### 1. General Characteristics of SCC

Stress corrosion cracking (SCC) refers to metal failure resulting from the combined action of tensile stresses and a corrosive environment. In the absence of either the stress or the environment SCC will not occur. Certain phenomena are characteristic of SCC in most materials. SCC fractures are brittle in the sense that little macroscopic deformation precedes the fracture; however, the rate of crack growth is usually lower and the microscopic features of fracture surfaces usually are different from those of other forms of brittle fracture in the same alloy. The tensile stresses required for SCC may result from service loads or residual stresses induced by cold working, mismatch during fitup, heat treatment, and welding operations. For each alloy environment combination, time-to-failure increases with decreasing stress and for most combinations there is a stress threshold below which cracking does not occur.

Generally, only a few chemical species cause SCC in a given alloy system and these species usually need not be present in large quantities. An illustration of this is the SCC failures which have occurred recently in certain cold-worked austenitic stainless steel components of boiling water reactors; oxygen in concentrations of 2 to 8 ppm is the responsible species. SCC may be either transgranular or intergranular with respect to the microstructure of the alloy, depending on the metallurgical condition of the alloy and the constituents of the environment.

In many alloy systems, SCC failures of smooth surfaces occur in three distinct phases, as illustrated in Figure 28. The first phase is an incubation period in which a pit is formed and a crack is initiated. The second phase is a state of subcritical crack growth in which the crack propagates under the joint influence of stress and environment. Assuming that the necessary stress is maintained, the third phase is fracture when the crack reaches a critical size.

##### 2. Stress Corrosion Testing

The traditional method of determining SCC resistance of an alloy has been to expose stressed, smooth specimens in the environment. These tests have as their objective either: (1) to determine if the alloy is susceptible to SCC, or (2) to determine if a threshold stress,  $\sigma_{th}$ , below which SCC will not occur, exists. In the first case, specimens usually are exposed under applied stresses near or beyond their yield strengths. Such

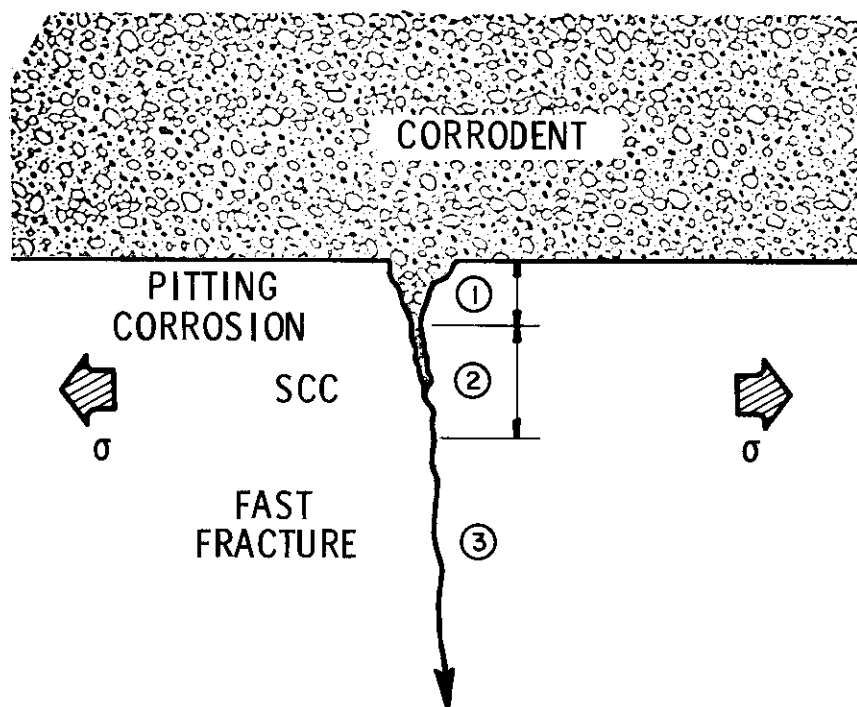


Figure 28. The three phases of structural failure by corrosion. All three phases are not necessary for failure in all cases (after Reference 50)

tests may require months, or even years, depending on the corrosivity of the environment. A relatively recent development in susceptibility testing is the slow-strain-rate test, in which smooth cylindrical tensile specimens are strained in the environment of interest at a constant low-rate in the order of  $1$  to  $4 \times 10^{-6}$ /sec until fracture occurs.<sup>(51)</sup> Relative SCC susceptibility is determined by comparing ductility parameters, e.g., reduction in area or percent elongation, of specimens strained in the environment with those of specimens strained in dry air. This method has the advantage of yielding a definite result within hours or days, regardless of whether the alloy is or is not susceptible to SCC.

In a typical threshold test a series of specimens is stressed at several levels and the time-to-failure of each specimen is determined. Results are plotted to yield curves of the type shown in Figure 29. Such tests have produced much useful information, particularly for low-strength alloys, and are relatively inexpensive to perform. However, basing design upon the results of such tests is nonconservative for many alloy-environment combinations because the time-to-failure represents the sum of the times

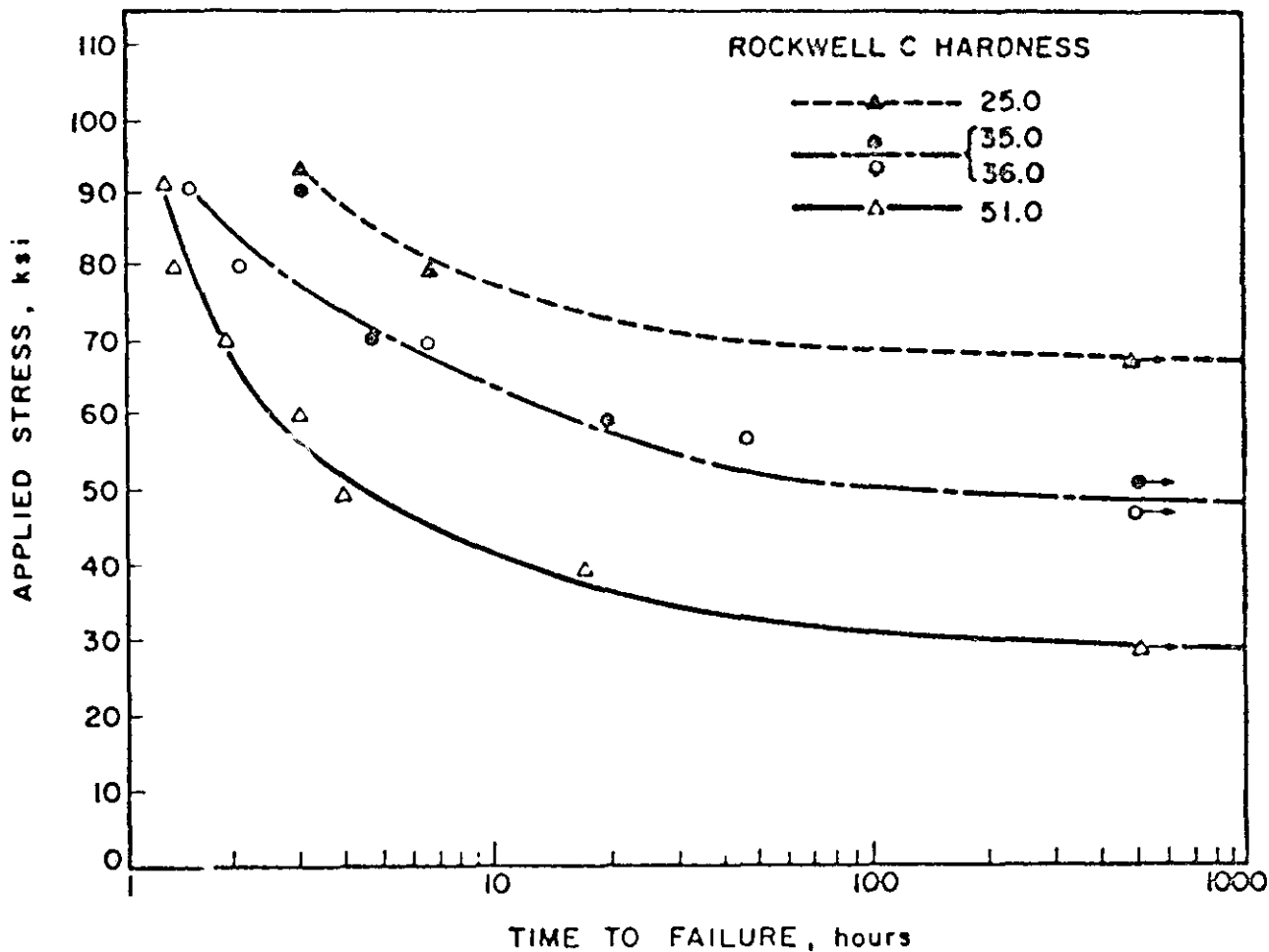


Figure 29. Stress vs. time-to-failure curves illustrating stress-corrosion cracking threshold stresses in an acidified 3.5% NaCl + saturated with H<sub>2</sub>S for an alloy steel heat treated to different hardness levels (after Reference 52)

required for crack initiation, for subcritical crack growth, and for final fast fracture. If an alloy is not susceptible (or is highly resistant) to pitting, smooth specimens may indicate that it is immune to SCC, when, in fact, it may be highly susceptible to stress corrosion crack propagation. High-strength titanium alloys exposed to marine atmospheres behave exactly in this manner.

Testing, using precracked specimens and linear elastic fracture mechanics analysis (see Appendix, Section D), has come into widespread use in recent years. These tests are particularly relevant to high-strength materials with a limited tolerance to defects, where a small stress corrosion crack may initiate catastrophic brittle fracture. A variety of test methods and specimen designs to simulate various loading conditions have been described in the technical literature. (53-55) Since SCC in high-strength materials occurs almost wholly under plane-strain conditions, the fracture mechanics parameter most widely employed in SCC studies is the Mode I plane-strain stress-intensity factor,  $K_{I}$ , hereafter abbreviated  $K$ . Use of precracked specimens eliminates the crack initiation phase of SCC, and  $K$  then is an accurate measure of the mechanical driving force for subcritical crack growth since it expresses conditions at the crack tip. The resistance of metals to SCC has been characterized in terms of the threshold level of  $K$  below which subcritical crack growth is not observed. This characteristic threshold level is designated  $K_{Isc}$  and quantifies SCC resistance for a specific alloy-environment combination with a single number which relates flaw size to nominal stress. Characterization of SCC resistance in terms of critical flaw size is then possible and is most useful since the design of many structures is based on a maximum allowable flaw size, usually determined by the sensitivity or reliability of the nondestructive inspection methods employed. If it is assumed that a long, shallow surface crack is present in a structure, that yield point stresses are present around this crack, and that the value of  $K_{Isc}$  is known for the material in the given environment, the depth of the flaw required to initiate SCC subcritical crack growth may be computed from

$$a = 0.2 \left( \frac{K_{Isc}}{\sigma_Y} \right)^2 \quad (29)$$

where  $a$  is the critical flaw depth and  $\sigma_Y$  is the yield strength. This method of characterizing SCC is convenient for comparing SCC resistance of various alloys, as shown in Figure 30. In this figure  $K_{Isc}$  data for four ultra high-strength steels in salt water are shown as a function of yield strength. Since mechanical properties of a material can vary from point-to-point on one plate and from one plate to another of the same nominal composition, each alloy system is characterized by a zone reflecting a range of properties rather than by a point. The dotted line represents the plane-strain fracture toughness,  $K_{Ic}$ , of the materials. The straight lines represent Equation (29) for two selected values of flaw depth. The significance of these lines is that if a flaw of the depth shown exists and if yield point stresses are present about the flaw, a metal with a  $K_{Isc}$  value below the line will undergo SCC subcritical crack growth.

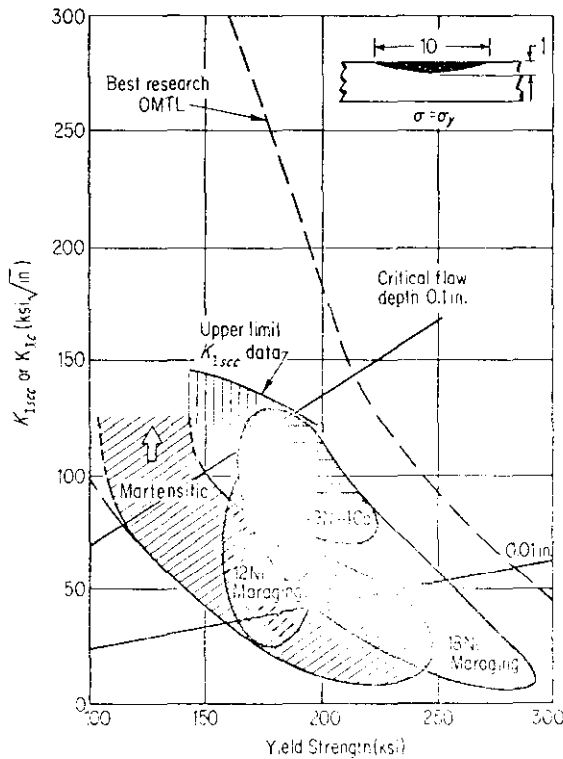


Figure 30. Generalized stress-corrosion cracking resistance of high-strength steels (1 inch plates) in salt water. The OMTL line refers to crack toughness in the absence of a corrosive environment (after Reference 56)

Much research also has been directed toward measurement of time-to-failure with precracked specimens under different loads in the manner used for smooth specimens. The normal experimental procedure is to test specimens over a wide range of  $K$  values in the environment of interest and measure times to failure.  $K_{ISCC}$  is defined to be the value of  $K$  below which SCC is not observed in an arbitrary time, usually 100 to 1000 hours. Figure 31 is a plot of data obtained from such a test series. In the system shown, any combination of stress and crack size which yields an initial  $K$  value equal to or greater than  $K_{IC}$ ,  $68 \text{ ksi}\sqrt{\text{in.}}$ , results in instantaneous fast fracture. Any combination of crack size and stress which yields an initial  $K$  value below  $K_{ISCC}$  is not subject to SCC. Combinations yielding initial  $K$  values between  $K_{IC}$  and  $K_{ISCC}$  result in subcritical crack growth. If the stress remains at a sufficiently high level,  $K$  increases as the crack length increases and fast fracture occurs when  $K = K_{IC}$ .

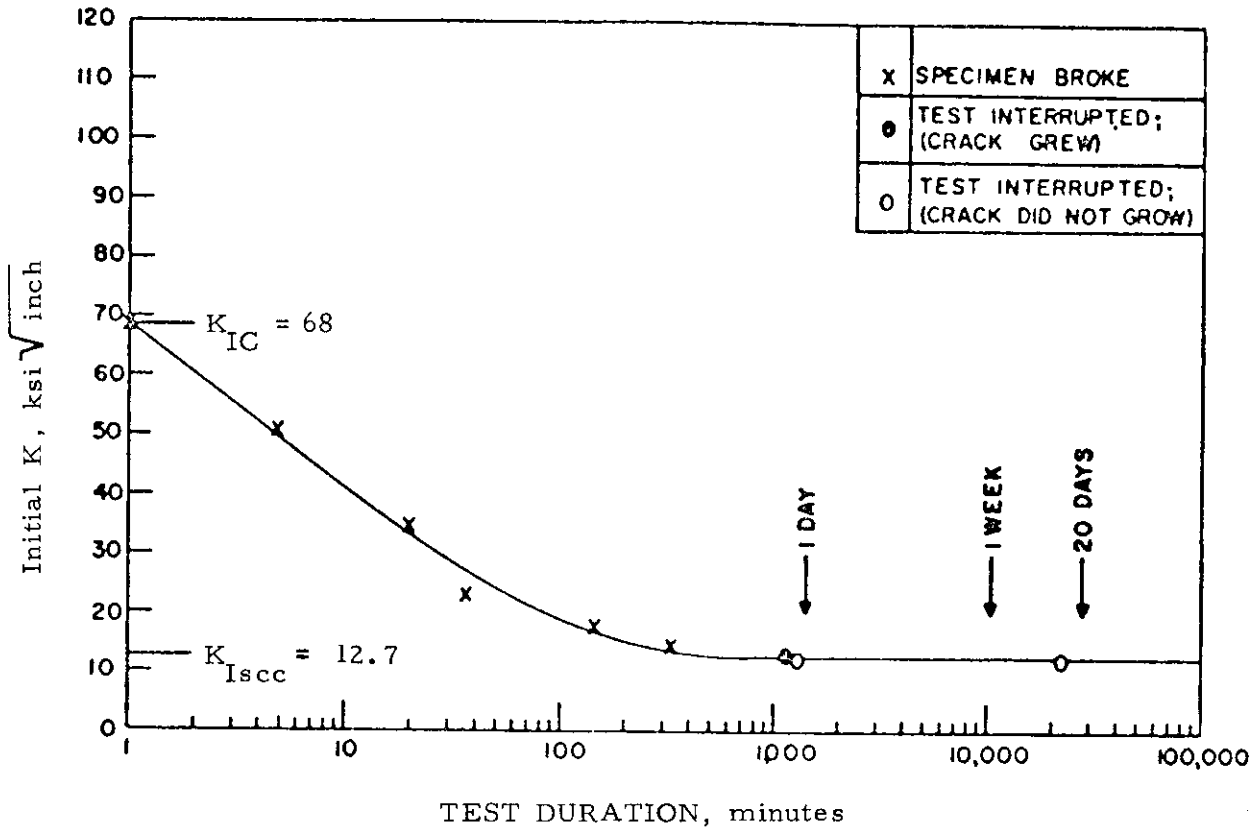


Figure 31. Stress intensity vs. time-to-failure curve illustrating stress-corrosion cracking threshold level,  $K_{Isc}$  (after Reference 52)

### 3. SCC of Ship Steels in Marine Environments

Merchant ship hull structural elements are currently constructed of a wide variety of steels which can be classified into three groups: (1) as rolled or normalized structural carbon steels with yield strengths up to 40 ksi; (2) high-strength low-alloy (HSLA) steels with yield strengths from 40 to 75 ksi; and (3) high-strength low-alloy quenched-and-tempered (HSLA Q & T) steels with yield strengths from 75 to 100 ksi. The structural carbon steels for years have been employed in many applications involving exposure to marine environments, e.g., bridges, drilling platforms, and pipelines, in addition to their use in ship structures. To the knowledge of the authors, SCC has not occurred in any of these applications with structural carbon steels. The literature indicates that these steels are subject to SCC in a relatively few chemical environments, i.e., hot concentrated hydroxides, nitrates, and carbonates, sulfides, cyanides, some hydrocarbons, and coal gas. (57,58) Chlorides, the principal constituent of seawater, have been shown to be incapable of inducing SCC. (59,60) These data, in conjunction with the favorable service experience with structural carbon steels, lead to the conclusion that these steels are immune to SCC in marine environments.

A review of the SCC behavior of HSLA and HSLA Q & T steels by Phelps<sup>(52)</sup> indicates that steels with yield strengths up to about 180 ksi are resistant to SCC in chloride solutions, that steels in the range of 180 to 210 ksi may be susceptible, and that steels with higher yield strengths are highly susceptible. Sandoz<sup>(61)</sup> states that the yield strength limit for SCC immunity of martensitic steels in salt water is about 120 ksi. The results of SCC tests on a number of low-alloy steels in marine atmospheres and seawater reported by Schmitt and Phelps<sup>(62)</sup> are summarized in Tables II and III. Examination of the data in these tables shows that steels ranging in yield strength from 50 to 163 ksi were not susceptible to SCC in marine environments for exposure times ranging up to 2200 days. However, all of these data were obtained from smooth specimens, and it is known that many alloys, particularly higher strength materials, which appear to be resistant to SCC when tested as smooth specimens actually are resistant to crack initiation and may be quite susceptible to crack propagation. Therefore, to categorize completely the SCC resistance of a high-strength materials of the HSLA Q & T type it is necessary to test precracked specimens.

There is relatively little precracked specimen data available for HSLA and HSLA Q & T steels. Novak<sup>(63)</sup> found that artificial seawater had no effect on the SCC resistance of precracked specimens of HY-80 (90 ksi yield strength) and that precracked specimens of HY-130 (T) (135 ksi yield strength) were only slightly susceptible to SCC. Leckie and Loginow<sup>(64)</sup> obtained the same result for HY-80 steels. Smith and Davis<sup>(65)</sup> investigated the effects of 3% NaCl solution on precracked specimens of HY-80 weld metal (124 ksi yield strength) obtained from a 1-inch thick weldment prepared by the shielded-metal-arc process and HY-130 weld metal (145 ksi yield strength)

TABLE II. RESULTS OF SMOOTH SURFACE SCC TESTS ON LOW-ALLOY STEELS IN MARINE ATMOSPHERES 80-FT LOT, KURE BEACH, N. C. (From Ref. 62)

<u>Steel</u>	<u>Yield Strength</u> ksi	<u>Stress Level</u> (Percent of Yield Strength)	<u>Exposure Time (Days)</u>
A 441	52	75	NF* 750
A 242, Type 1	50	75	NF 750
A 572, Grade 50	53	75	NF 750
A 588, Grade A	72	75	NF 750
HY - 80	100	75	NF 1700
HY - 80	100	90	NF 1700
STS	106	75	NF 1700
STS	106	90	NF 1700
A 517, Grade F	115	75	NF 1700
A 517, Grade F	115	Cold worked, welded & stressed	NF 425

\* NF - no failure in time indicated, test terminated

TABLE III. RESULTS OF SMOOTH SURFACE SCC TESTS ON LOW-ALLOY STEELS IN SEAWATER. SPECIMENS EXPOSED 1.5 FT BELOW SURFACE IN QUIESCENT SEAWATER, HARBOR ISLAND, N.C. (From Ref. 62)

<u>Steel</u>	<u>Yield Strength</u> ksi	<u>Stress Level</u> (Percent of Yield Strength)	<u>Exposure Time (Days)</u>
HY - 80	100	75	NF* 2200
STS	163	75	NF 2200
A 517, Grade F	115	75	NF 250
A 517, Grade G	NG**	75	NF 2200

\* No failure in time indicated, test terminated

\*\* Not given; however, would not be expected to be significantly different from Grade F

obtained from a 2-inch thick weldment prepared by the gas-metal-arc process. For the HY-80 weld metal, cracking occurred at a stress intensity level of 12% below the stress intensity level required to cause fracture in air. For the HY-130 weld metal, cracking occurred at stress intensity levels approximately 33% below the air level.

Townsend used precracked specimens to study the SCC resistance of ASTM A 514/517, Type J steel (125 ksi yield strength) in 3.5% NaCl solution<sup>(66)</sup> and found that cracking occurred at a stress-intensity level approximately 10% below the level required for fracture in air. Alternate immersion tests in 3% NaCl solution also were conducted on smooth surface, manually butt-welded specimens. These smooth specimens did not produce SCC after 10,000 hours of exposure. No precracked weld metal specimens were exposed.

Because cathodic protection is known to accelerate SCC of some high-strength materials, its effect on the SCC resistance of some HSLA Q & T steels has been studied. Smith and Davis<sup>(65)</sup> found that HY-80 weld metal (124 ksi yield strength) and HY-130 weld metal (145 ksi yield strength) cracked at stress intensity levels of 19% and 33% below their respective fracture toughnesses in air when cathodically protected to - 1.2 volts vs SCE, a potential approximately 400 MV below the potential normally employed, and, which is known to be capable of causing hydrogen-induced SCC in susceptible materials. Leckie and Loginow<sup>(64)</sup> studied the effects of cathodic protection (- 1.2 volts vs SCE) and plastic deformation on HY-80 (90 ksi yield strength) and HY-130 (T) (135 ksi yield strength) steels. For the HY-80 steel cracking did not occur in strain-free specimens nor in specimens prestrained 1% and 5%. However, the results for HY-130 (T) steel show a significant adverse influence of cathodic protection (Figure 32.); the SCC thresholds of strain-free and 1% prestrained specimens were reduced from about 200% of the yield strength to under 150%, and the SCC threshold for 5% prestrained specimens was only 80% of the yield strength. These results are of considerable practical importance since localized regions of strained metal exist near weldments. They indicate that cathodic protection may be an unacceptable method of corrosion control for HSLA Q & T steels in seawater.

The welding processes and procedures employed in fabrication of high-strength steels also can affect the SCC resistance of the completed structure. In shipyards, most welded joints are prepared by oxygen gas torch cutting, a process which leaves little slag or oxide on the prepared joint. In high-strength steels this process may lead to cracking along the cut edge and will result in a loss of ductility and an increase in strength in the heat-affected zones (HAZ). Welding process and position have been shown to affect the  $K_{I_{SCC}}$  of high-strength steel weld metal.<sup>(67)</sup> HY-130 (T) weld metals deposited by the inert gas shielded metal arc process (GMA) in either flat or vertical-up positions or by the shielded metal arc (SMA) process in the flat position had saltwater  $K_{I_{SCC}}$  values of 125-135 ksi $\sqrt{\text{in.}}$  and nominal SCC thresholds in

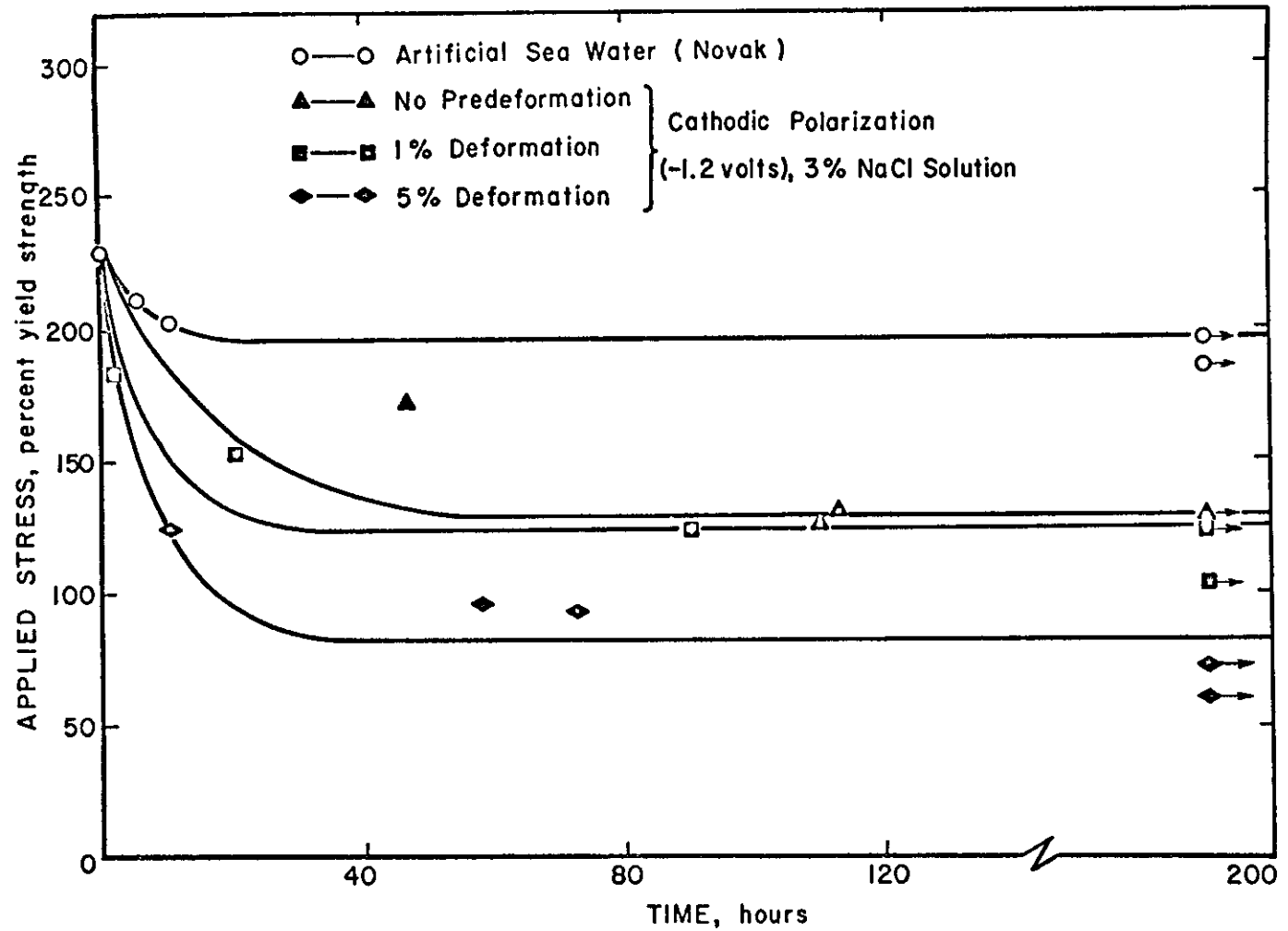


Figure 32. Stress-corrosion behavior of HY-130(T) steel in laboratory studies (After Reference 64)

excess of the yield strength. However,  $K_{I_{SCC}}$  for weld metal deposited by SMA in the vertical-up position was reduced to 90 ksi $\sqrt{\text{in.}}$  and the nominal SCC threshold was reduced to the yield strength.

The data cited above indicate that low-alloy steel-base metals with yield strengths of approximately 100 ksi are immune to SCC in marine environments, but that weld metals and the HAZ adjacent to weldments in which the yield strength is higher may be susceptible, particularly if cathodic protection is applied. A survey<sup>(68)</sup> conducted in 1969 of shipyards and related industries, domestic and foreign, with experience in the use of A514/A517 in merchant ship hulls, indicated that typical yield strength of base metals and submerged arc weldments (as measured by microhardness) ranged from 105 to 115 ksi; however, HAZ yield strengths ranged from below 100 ksi to as high as 175 ksi.

The results of this survey coupled with the limited amount of precracked data on SCC resistance of HSLA Q & T steels suggest that the weld metal and HAZ of these materials may be susceptible to SCC in marine environments. Other factors which increase the probability of SCC in the HAZ of HSLA Q & T steels are: (1) higher residual stresses in HSLA Q & T weldments than in carbon steel weldments because of the higher yield strengths of the HSLA Q & T materials; (2) a lack of sufficient quality control\* of HSLA Q & T base plate used in shipbuilding makes it likely that many of the factors which contribute to weldment cracking (e.g., segregates of nonmetallic inclusions and alloying elements and laminations) may be present and undetected; and (3) HSLA Q & T steels, because of a high yield to ultimate strength ratio, resist blunting of notches and small cracks under occasional high service loads (referred to as "shakedown") so that sharp flaws in regions of yield stress loading may exist during the ship's service life.

## B. Corrosion Fatigue

### 1. General Characteristics of Corrosion Fatigue

Corrosion fatigue is the combined action of a corrosion environment and a cyclic stress leading to premature failure of metals by cracking.<sup>(69)</sup> In general, as in the case of stress corrosion cracking (SCC), neither cyclic stress in an innocuous environment, e.g., dry air, nor environmental attack, alone, will produce results as damaging as their combined action. Unlike SCC, which occurs only in certain specific alloy-environment combinations, most alloys which are subject to corrosion in an environment also are subject to corrosion fatigue in that environment. Corrosion fatigue is an even more complex phenomenon than is SCC in that it is influenced by all of the chemical

---

\*Of the shipyards using A514/517 materials in 1969 only one used radiography and ultrasonic testing for buried flaw detection; the others relied on radiography alone.<sup>(68)</sup>

and mechanical variables which affect SCC, plus the additional variables of the fatigue process, e.g., frequency, ratio of minimum to maximum stress, stress range, and cyclic load wave form.

Corrosion fatigue behavior can be measured in terms of the number of cycles of stress or strain required to produce failure,  $N_f$ , or the rate of crack growth,  $da/dN$ , for a given set of conditions. Figure 33 shows stress versus cycles to failure for a carbon steel in air and in a corrosive environment. The fatigue limit ceases to exist in the corrosive environment and fatigue strength and fatigue life are significantly degraded. Corrosion fatigue cracks are usually transgranular. Failure at smooth surfaces occurs in three stages in the same manner as in SCC: (1) pitting, which initiates a crack, (2) subcritical crack propagation, and (3) brittle fast fracture or ductile rupture. In contrast to ordinary fatigue where there is rarely more than one crack, a number of corrosion fatigue cracks usually are initiated at the bases of pits.

The following sections review the state-of-the-art of corrosion fatigue in steels. In the majority of the cases cited, the steels studied have yield strengths in the range of 150 to 250 ksi. These examples have been used because they illustrate the concepts involved and because yield strengths as high as 175 ksi have been shown to be present in the HAZ of A514/A517 steels<sup>(68)</sup>.

## 2. Analysis of Fatigue Crack Growth

The general fatigue crack growth behavior of a hypothetical steel in terms of stress intensity,  $K$ , in an inert environment is shown in Figure 34a. The principal features of this illustration are: (1) there exists a threshold stress intensity level,  $K_{thi}$ , below which fatigue cracks are not observed to grow in inert environments, (2) fatigue crack growth is terminated when the maximum stress-intensity factor exceeds the material's fracture toughness,  $K_{Ic}$ , and (3) fatigue crack growth rates between (1) and (2) can be described as a power law function of  $K$  or  $\Delta K (K_{max} - K_{min})$  of the form

$$\frac{da}{dN} = A \Delta K^n \quad (30)$$

where  $A$  and  $n$  are material constants. Fatigue crack growth rate is cycle dependent, provided the material is not strain rate sensitive and there are no environmental effects. When these conditions are satisfied, changes in the frequency,  $f$ , of the applied load have no effect on  $da/dN$ , i.e., the rate of crack propagation is frequency independent. The rate of crack

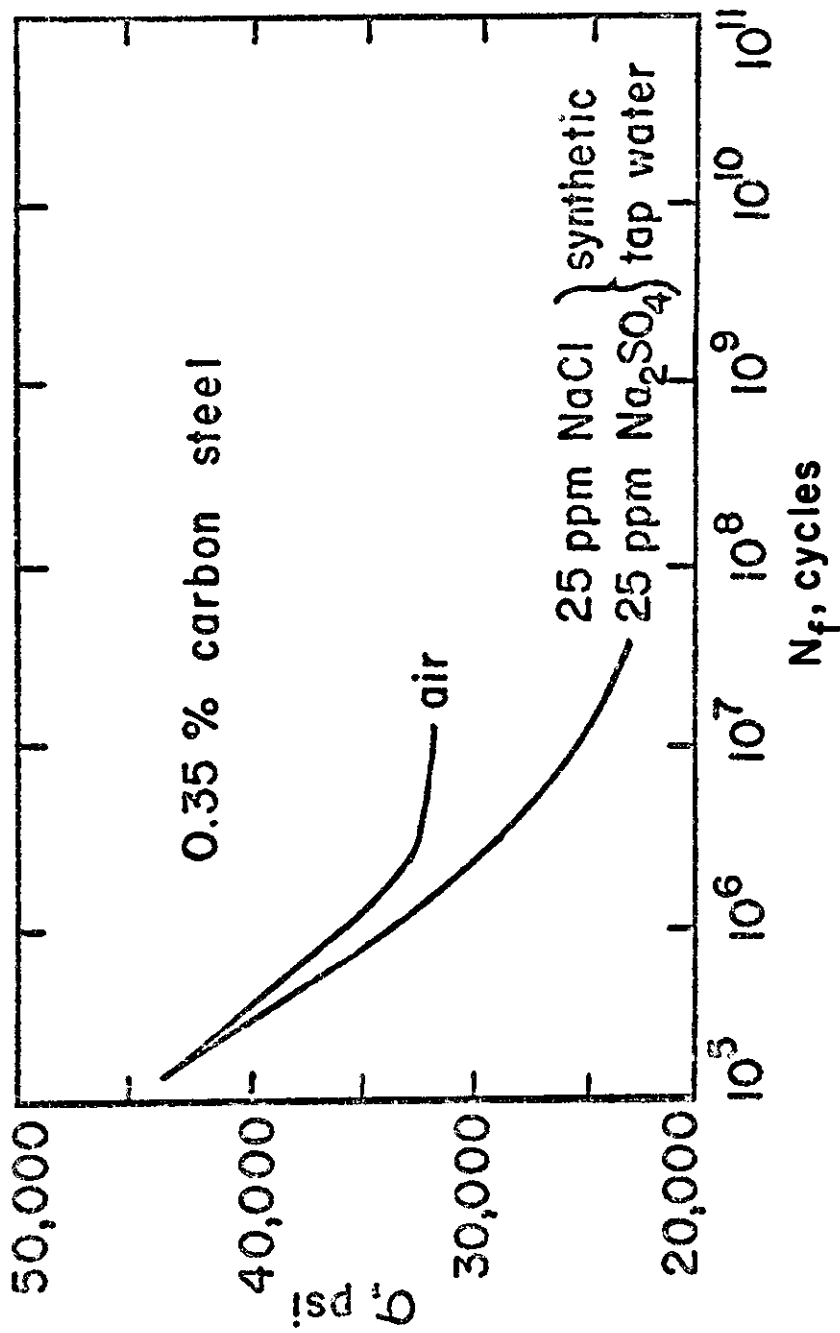


Figure 33. Effect of environment on fatigue properties of a 0.35% carbon steel. (after Reference 70)

growth with respect to time, therefore, may be expressed as

$$\frac{da}{dt} = f(da/dN) \quad (30a)$$

Under such conditions fatigue testing may be accelerated by increasing the frequency.

Corrosion fatigue crack growth may exhibit behavior similar to that for inert environments: there exists a threshold stress-intensity level,  $K_{th_a}$ , for the aggressive environment, which is usually lower than  $K_{th_i}$  for the inert environment. Moreover, crack growth rates are usually greater in the aggressive environment at a given  $K$  or  $\Delta K$  level, as shown in Figure 34a. If the material is susceptible to SCC, the corrosion fatigue crack growth rate curve may exhibit behavior of the type illustrated in Figure 34b. In this case, environmental effects are very strong at  $K$  values above  $K_{IscC}$ , and are negligible at  $K$  values below  $K_{IscC}$ . Crack propagation rates are time dependent for  $K$  values above  $K_{IscC}$  and are cycle dependent for  $K$  values below  $K_{IscC}$ . In reality, most materials exhibit behavior that falls between these two extremes, as illustrated in Figure 34c. The stress corrosion cracking threshold  $K_{IscC}$  provides a convenient separation point between stress-intensity levels which do and do not exhibit substantial environmental enhancement of crack growth rates. In the following discussion, this crack propagation behavior will be referred to as "above  $K_{IscC}$ " and "below  $K_{IscC}$ ."

### 3. Crack Propagation Behavior Above $K_{IscC}$

A study published in 1969 clearly showed the dependence of above  $K_{IscC}$  behavior on the rate of environmental attack<sup>(71)</sup>. Time based crack growth rates were determined for 4340 steel in distilled water as functions of static stress intensity levels and mean fatigue stress-intensity levels for small amplitude ( $\Delta K = 6.3 \text{ ksi } \sqrt{\text{in.}}$ ) tension-tension loading. The results given in Figure 35 show that the two types of crack growth were not significantly different. The corrosion fatigue data, in effect, represent a ripple superimposed on the static SCC growth rate curve. The results of this and other similar studies led to the formulation of the Wei-Landes linear summation hypothesis<sup>(72)</sup> for corrosion fatigue crack propagation rate above  $K_{IscC}$ :

$$\left( \frac{da}{dN} \right)_c = \left( \frac{da}{dN} \right)_e + \left( \frac{da}{dN} \right)_r \quad (31)$$

where  $(da/dN)_c$  is the corrosion fatigue crack propagation rate,  $(da/dN)_e$  is the time dependent environmental (SCC) contribution and  $(da/dN)_r$  is the

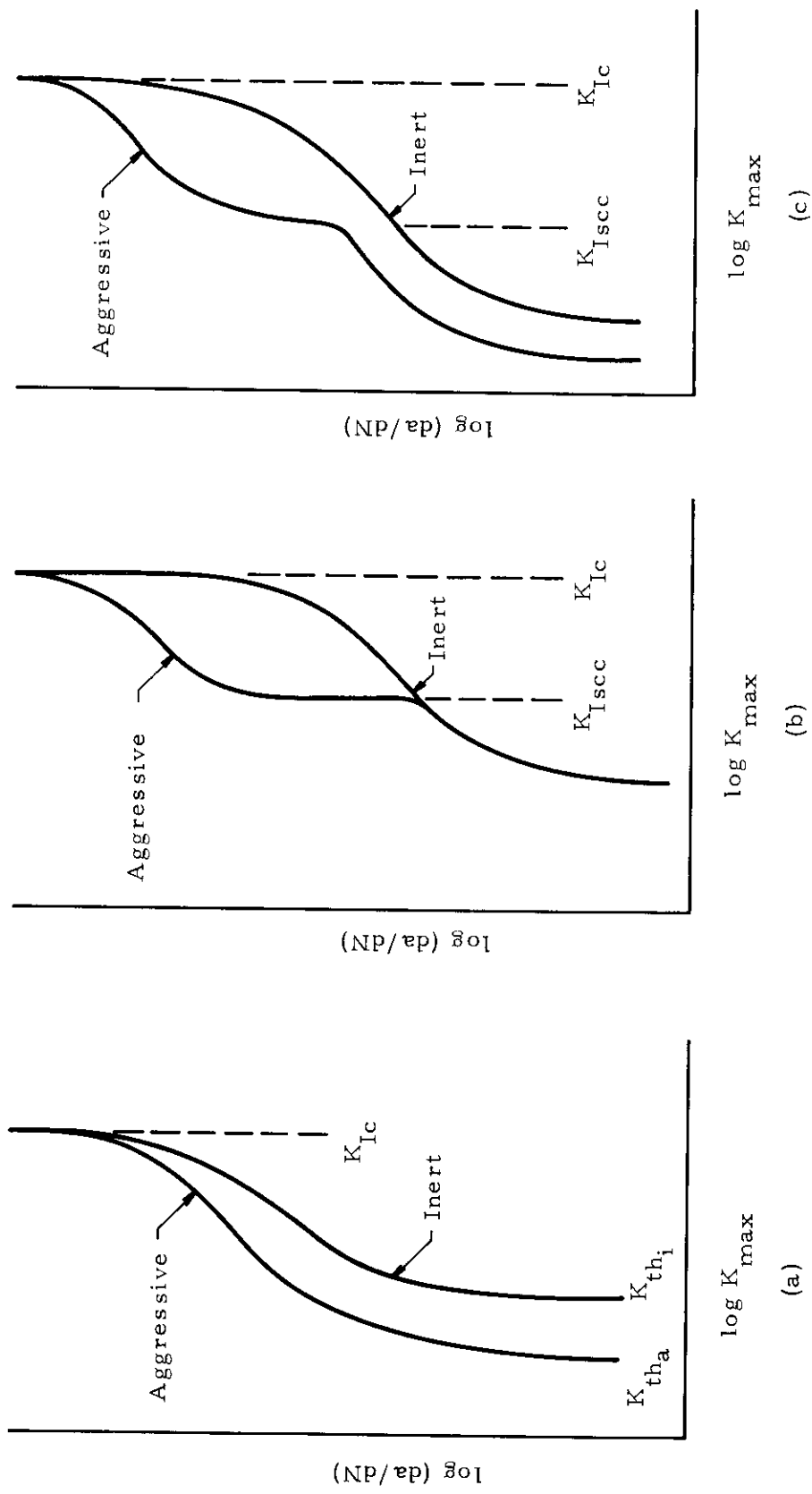


Figure 34. Fatigue crack growth behavior of hypothetical alloy:  
 (a) Below  $K_{Iscc}$  behavior; (b) Above  $K_{Iscc}$  behavior;  
 (c) Combined behavior. (After Reference 70)

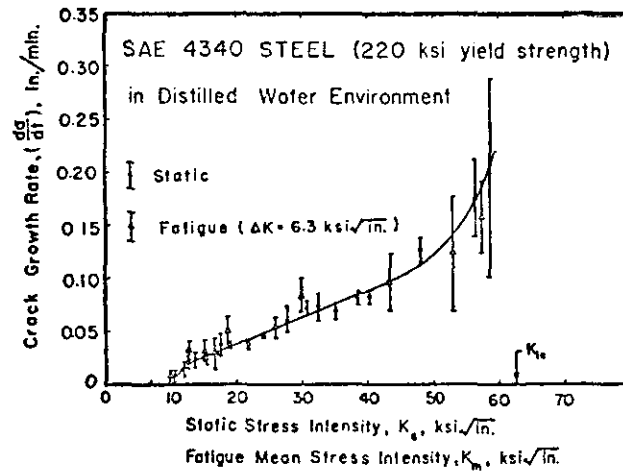


Figure 35. Comparison between static and tension-tension fatigue crack growth rates as a function of the static and mean stress-intensity levels. (after Reference 71)

cycle dependent fatigue contribution. It was further hypothesized that the environmental contribution could be expressed as

$$\left( \frac{da}{dN} \right)_e = \int_{\tau} \frac{da}{dt} (dt) \quad (32)$$

where the integral is taken over one period of loading and the integrand is a time dependent function of stress intensity, i. e.,

$$\frac{da}{dt} = \frac{da}{dt} [K(t)] \quad (33)$$

Using these equations, the rates of corrosion fatigue in a maraging steel in dehumidified hydrogen and of H-11 steel in laboratory air were satisfactorily predicted.

Equation (31) was later expressed in its time-based form

$$\left(\frac{da}{dt}\right)_c = \left(\frac{da}{dt}\right)_e + f_x \left(\frac{da}{dN}\right)_r \quad (34)$$

and adequately predicted the effect of changes in frequency on corrosion fatigue of 4340 steel in saltwater, for fully reversed and sinusoidal loading ( $\Delta K = 39 \text{ ksi } \sqrt{\text{in.}}$ ,  $K_{\text{max}} = 19.5 \text{ ksi } \sqrt{\text{in.}}$ ), as shown in Figure 36.<sup>(73)</sup> The time dependent component  $(da/dt)_e$  is strongly dependent upon wave shape, maximum stress intensity, stress intensity range, and the corrosivity of the environment. Equation (34) and Figure 36 show that whether corrosion fatigue behavior is time dependent or cycle dependent is determined by the relative magnitude of the environmental and fatigue components. A knowledge of the relative contribution of both components is therefore required in designing a component which is to be made of high-strength steel. If the environmental component is at all significant, the structure will be subject to failure by SCC and the alloy should not be used. However, if the fatigue component is one or two orders of magnitude greater than the environmental component, a design based on fatigue loading may be acceptable.

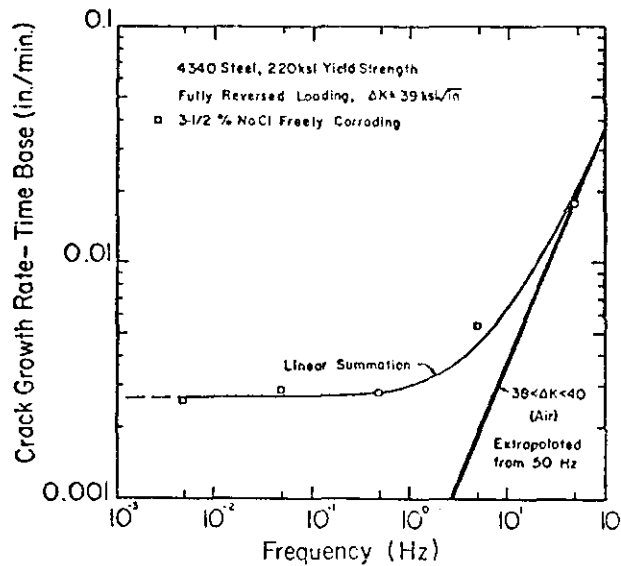


Figure 36. Above  $K_{\text{Isc}}$  corrosion fatigue crack - growth rate behavior of 4340 steel for fully reversed sinusoidal loading as a function of frequency. (after Reference 73)

#### 4. Crack Propagation Behavior Below $K_{Isc}$

Equation (31) indicates that the effect of environment on fatigue crack propagation at stress intensities below  $K_{Isc}$  is negligible. In fact, such behavior is the exception rather than the rule, as it is well known that many relatively innocuous environments can significantly accelerate fatigue damage, e.g., 0.35% carbon steel in tap water, Figure 33. Naval Research Laboratory studies produced the data shown in Figures 37-39, illustrating below  $K_{Isc}$  corrosion fatigue crack propagation behavior in saltwater for several high-strength steels. (74, 75) The steel shown in Figure 37 illustrates the behavior of a steel which is not affected by its environment below  $K_{Isc}$ ; this type of behavior was exhibited by only one of six steels studied. Figures 38 and 39 are typical of the other five steels in which crack growth rates were accelerated by the saltwater environment, with maximum acceleration occurring at the lower stress intensities. Note in Figure 39 that the crack growth rate above  $K_{Isc}$  is not significantly accelerated, indicating that the fatigue crack growth rate is significantly larger than the SCC growth rate.

Frequency has a significant effect on the below  $K_{Isc}$  behavior of high strength steels. Figure 40 compares the effect of frequency on crack growth rates of HY-80 steels at two levels of  $\Delta K$  in saltwater and in a vacuum. (76) This figure indicates that corrosion fatigue attack is accelerated at low frequencies, but that at higher frequencies the corrosion fatigue rate is reduced to the level occurring in a benign environment.

Similar data were obtained in studies conducted at U.S. Steel's Applied Research Laboratory on crack growth rates of four high-strength steels in saltwater. (77, 78) Figure 41 shows that in tension-tension sinusoidal loading at high frequencies (600 cpm), the corrosion fatigue crack growth rate for a 12Ni-5Cr-3Mo steel is not significantly different from the rate in air, but that the environment accelerates crack growth rates as the frequency is decreased (60 and 6 cpm). Unlike the data shown in Figures 37-39, in these studies the rate curves at all frequencies were found to be parallel and to have the same slope as the air data. Similar low-frequency (6 cpm) behavior for three other steels is shown in Figure 42. The data plotted in Figures 41 and 42 indicate that crack growth rates in air and saltwater can be represented by the equation.

$$da/dN = D(t) (\Delta K)^2 \quad (35)$$

where  $D(t)$  is dependent upon the metal-environment combination and upon frequency. For all of the steels evaluated,  $D(t)$  was constant and independent of frequency in air. The susceptibility of each steel to the environment may be evaluated by comparing the values of  $D(t)$  in the environment and in air.

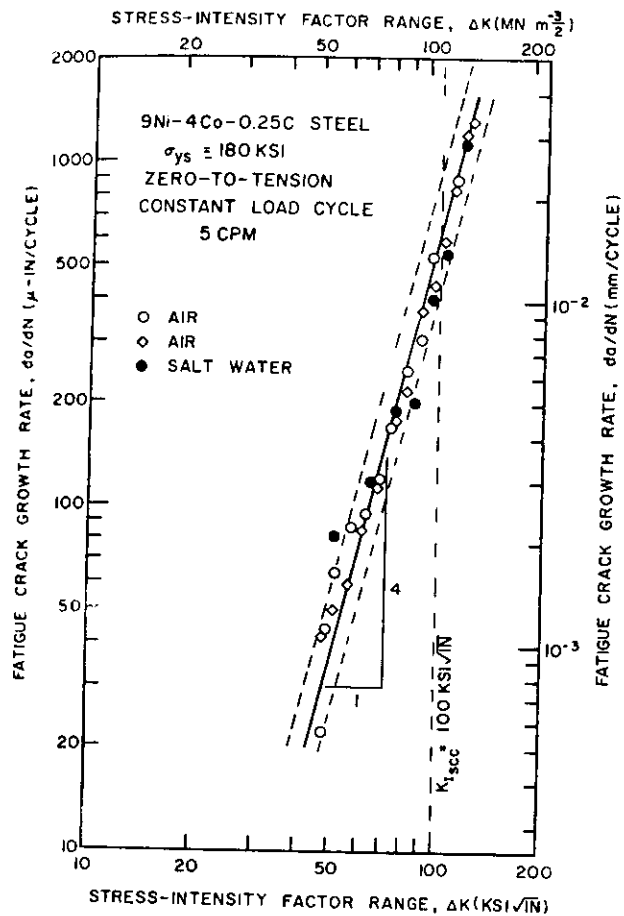


Figure 37. Air and salt water fatigue crack growth rate behavior of 9 Ni-4 Co-0.25 C steel. (after Reference 74)

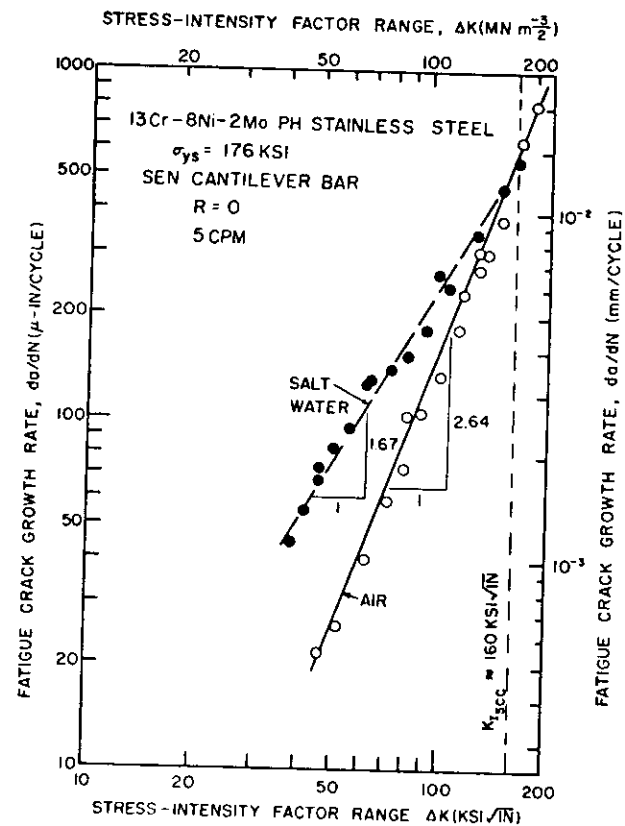


Figure 38. Air and salt water fatigue crack growth rate behavior of 13 Cr-8 Ni-2 Mo PH stainless steel. (after Reference 75)

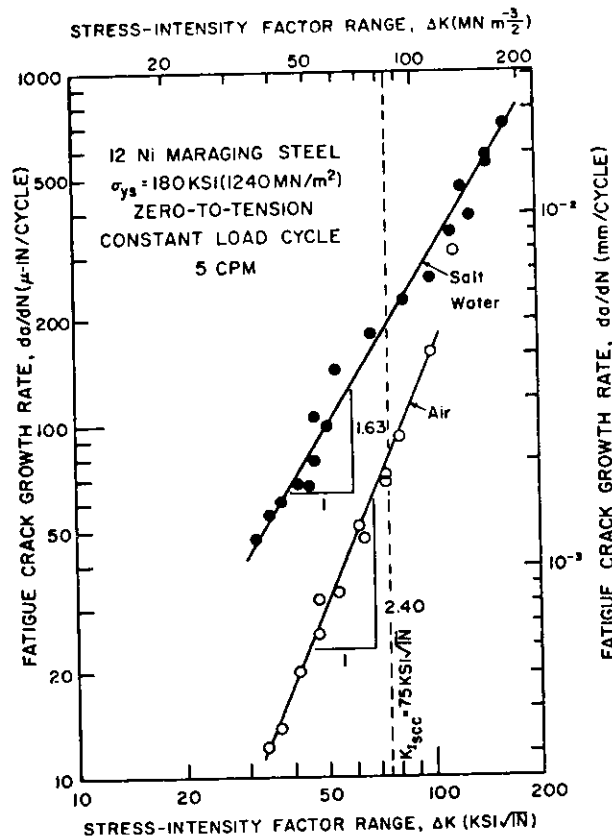


Figure 39. Air and salt water fatigue crack growth rate behavior of 12 Ni (180) maraging steel. (after Reference 74)

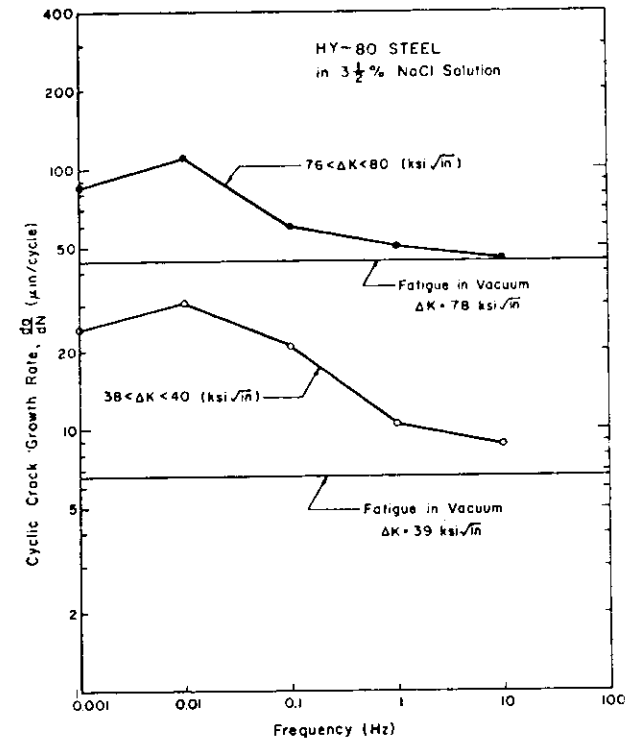


Figure 40. Below  $K_{Isc}$  corrosion fatigue crack growth rate behavior as a function of frequency. (after Reference 76)

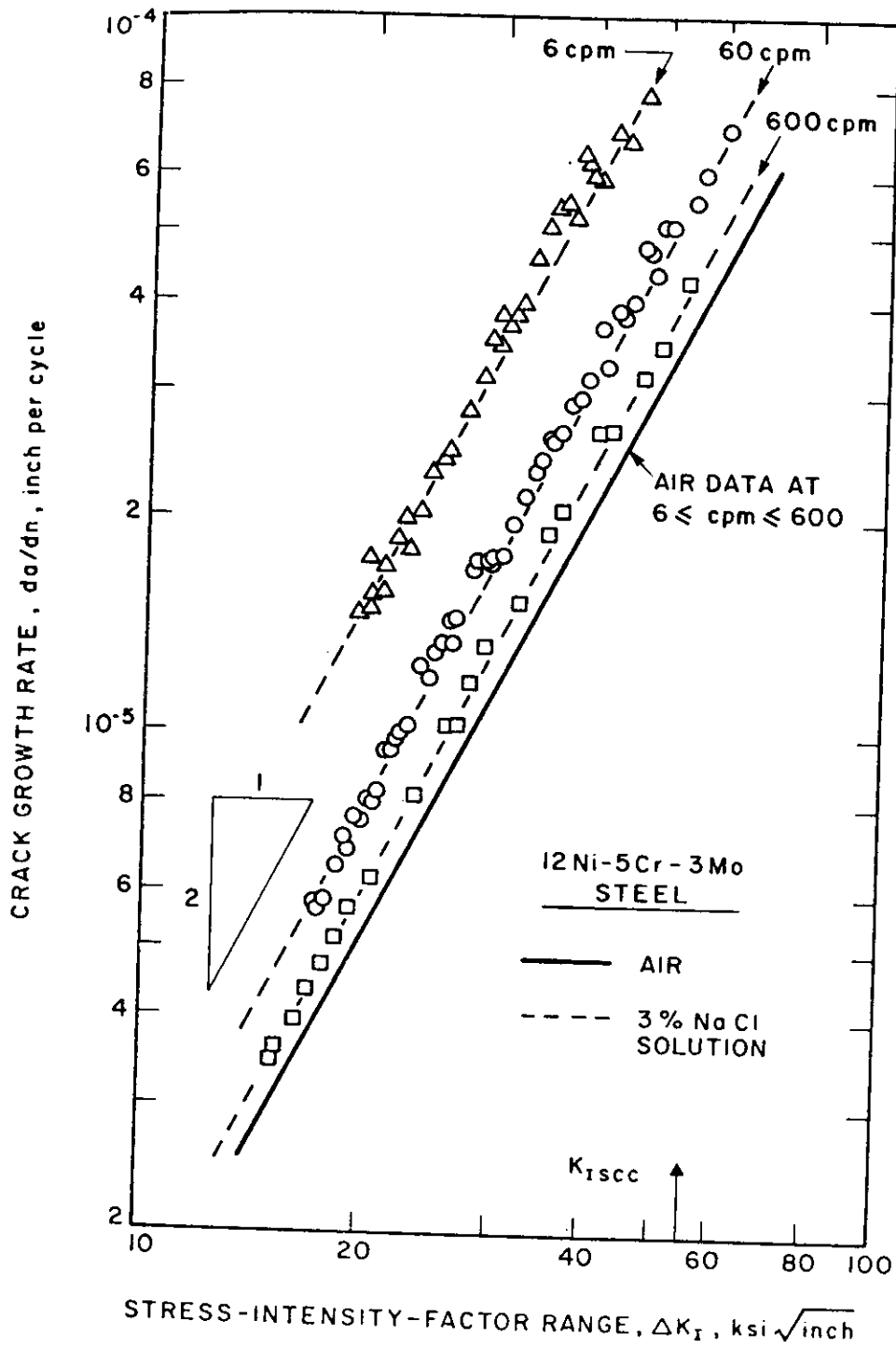


Figure 41. Corrosion-Fatigue Crack-Growth Data  
As a Function of Test Frequency  
(After Reference 78)

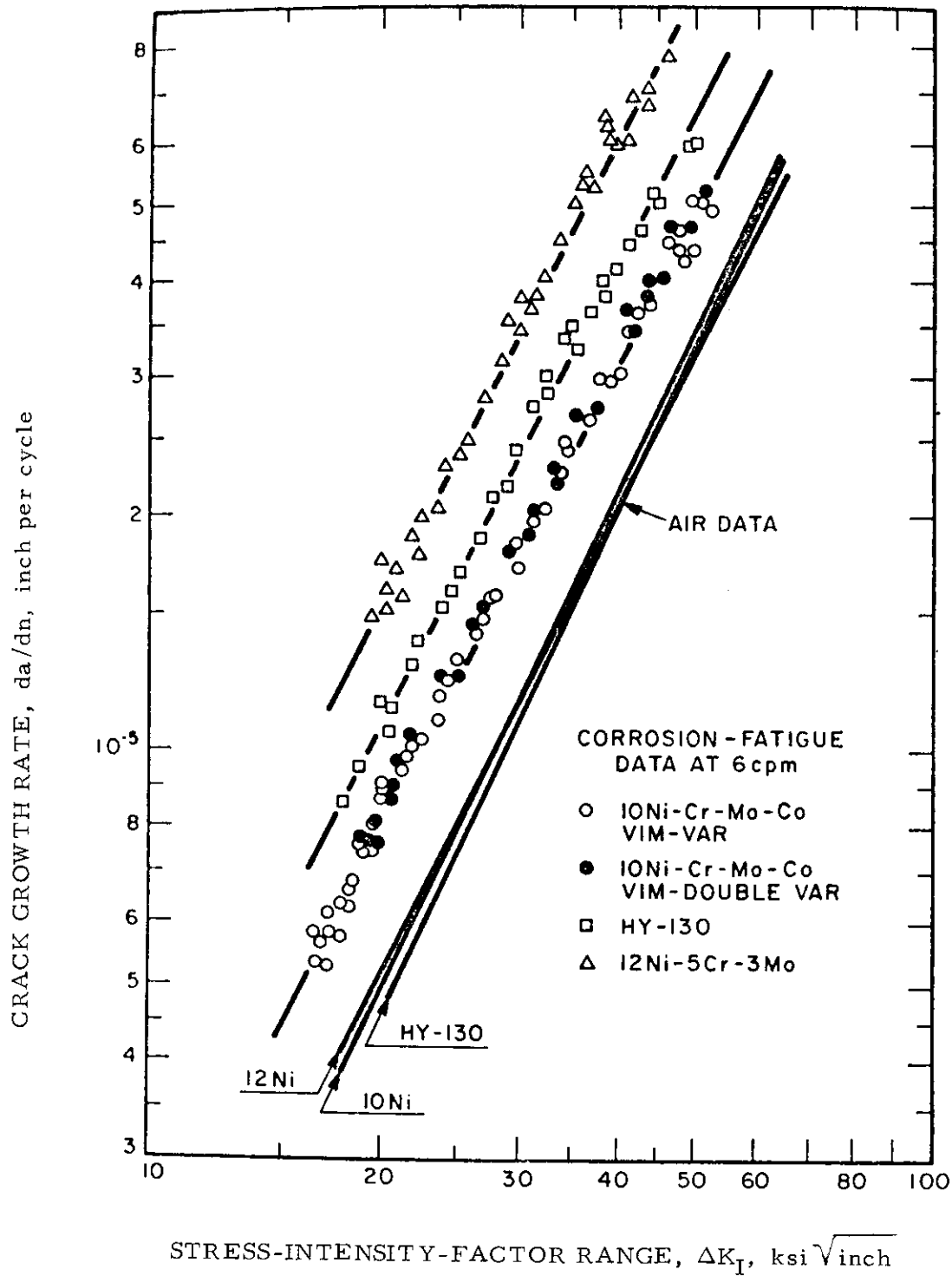


Figure 42. Fatigue-Crack-Growth Rates in Air and in 3% Solution of Sodium Chloride Below  $K_{Isc}$  for Various High-Yield-Strength Steels (After Reference 78)

Figure 43 depicts  $D(t)$  as a function of frequency for four steels and indicates that at any given frequency the saltwater environment had the least effect on the 10Ni-Cr-Mo-Co steel.

An important conclusion of the U. S. Steel study is that below  $K_{Isc}$  crack propagation behavior of high-strength steel is markedly affected by the cyclic loading wave form. Figure 44 shows that crack growth rates for 12Ni-5Cr-3Mo steel specimens exposed in air are the same under square, triangular, and sinusoidal loading wave forms. However, at 6 cpm in saltwater, under sinusoidal and triangular wave loading, crack growth rate acceleration is significantly greater than under square wave loading, Figure 45. The combined effect of loading wave form and frequency on  $D(t)$  is shown in Figure 46. At low frequencies a significant environmental contribution occurs under sinusoidal and triangular wave loading, but at high frequencies very little environmental effect is seen. Under square wave loading, the effect of the environment is negligible, regardless of the frequency. Additional studies<sup>(78)</sup> showed that environmental effects occurred only during the time the material is undergoing plastic deformation, i. e., during the increasing-tensile loading portion of the cycle, and depend primarily upon the time spent in such loading. At a given frequency, wave forms producing the same total time of increasing tensile loading have equivalent effects on crack growth rates, Figure 47. Under negative sawtooth and square waves, the time of tensile loading is short and both wave forms have negligible effects on crack growth rates, while under positive sawtooth, triangular, and sinusoidal wave forms the time of tensile loading is much longer and all three produce significant crack growth acceleration. The time at maximum or minimum tensile stress (the hold time) was investigated with skewed square wave forms and was found to have no effect. Additional studies on other steels are needed to confirm or deny the universality of these observations.

##### 5. Factors Affecting Corrosion Fatigue Crack Growth Rates

In the previous sections the primary parameters governing corrosion fatigue crack growth of very high-strength steels were shown to be sensitive to SCC, stress-intensity range ( $\Delta K$ ), frequency of applied loading, and, in the case of below  $K_{Isc}$  behavior, the cyclic loading wave form. The effects of a number of other factors on a variety of steels have been studied and some of these are described below. It should be noted, however, that in the past most corrosion fatigue studies were performed with smooth specimens and that only time-to-failure was reported. These procedures are not recommended because time-to-failure data combines initiation and propagation data, but such work does provide some indication of the effects of solution composition, electrochemical potential, and metallurgical variables, and other such factors on corrosion fatigue rates.

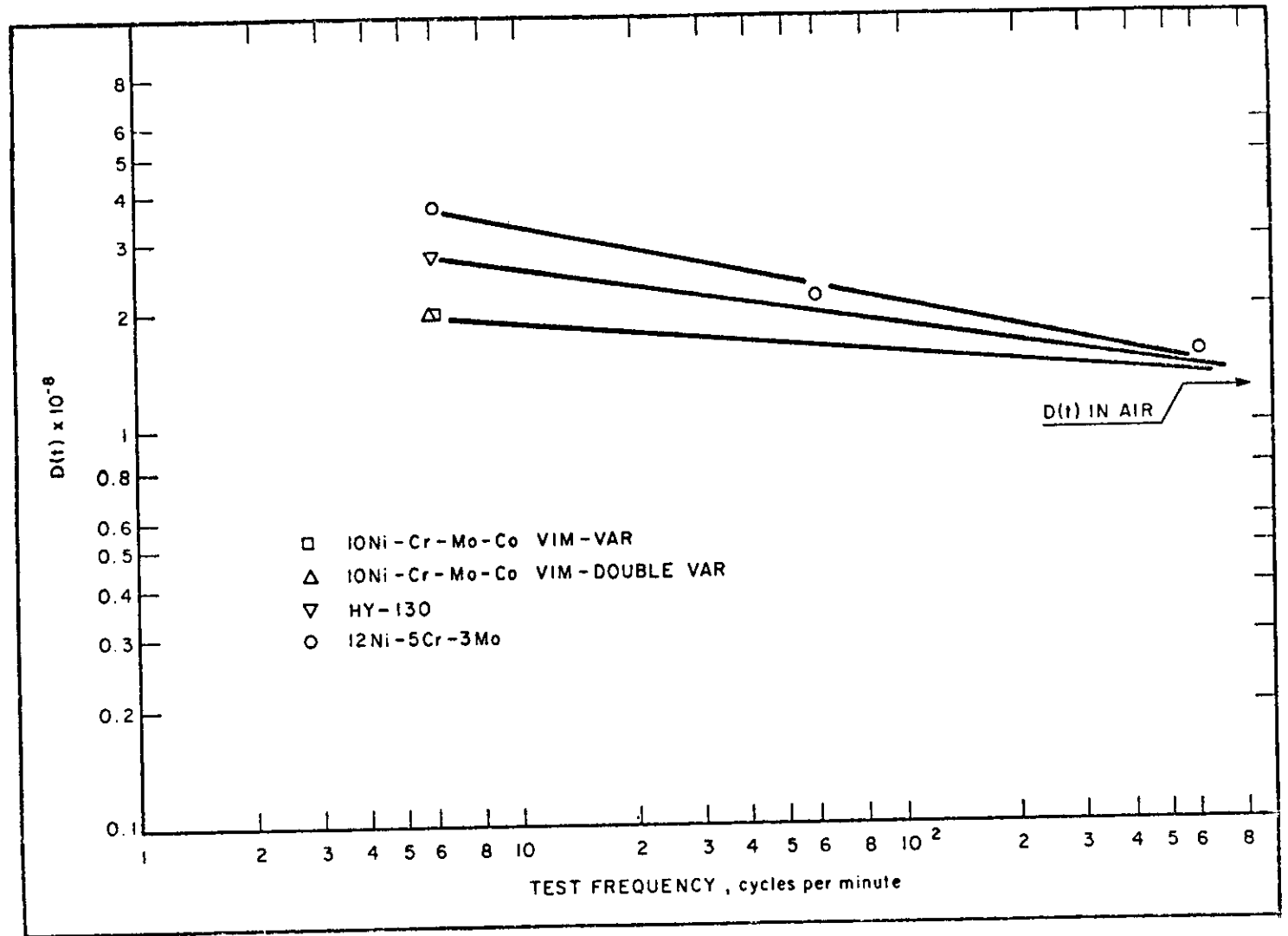


Figure 43. Relationship Between  $D(t)$  and Cyclic-Stress Frequency in Various Steels Subjected to Sinusoidal Loading in 3% Solution of Sodium Chloride (After Reference 78)

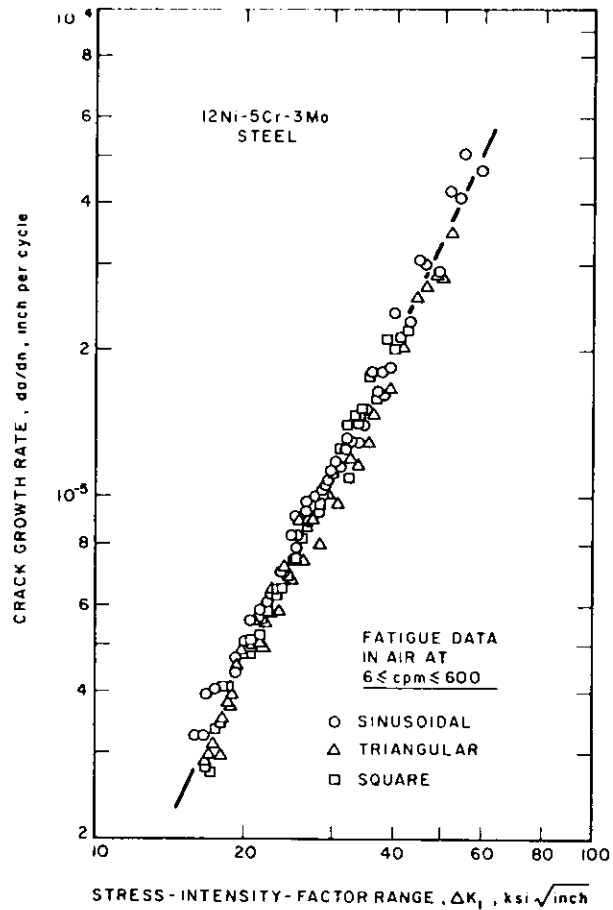


Figure 44. Fatigue crack growth rates in air under sinusoidal, triangular, and square loading wave forms. (After Reference 77)

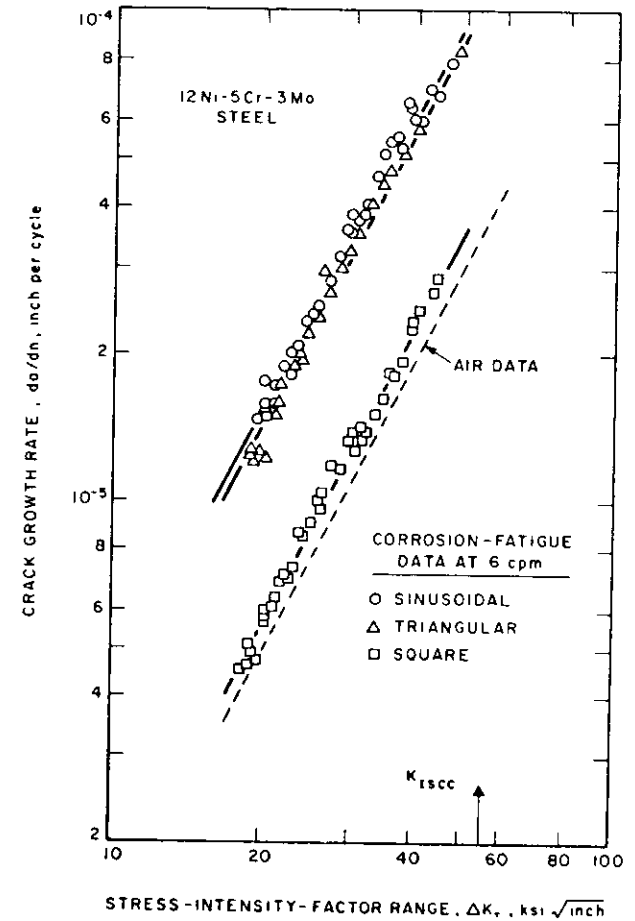


Figure 45. Corrosion fatigue crack growth rates below  $K_{Isc}$  under sinusoidal, triangular, and square loading wave forms. (After Reference 77)

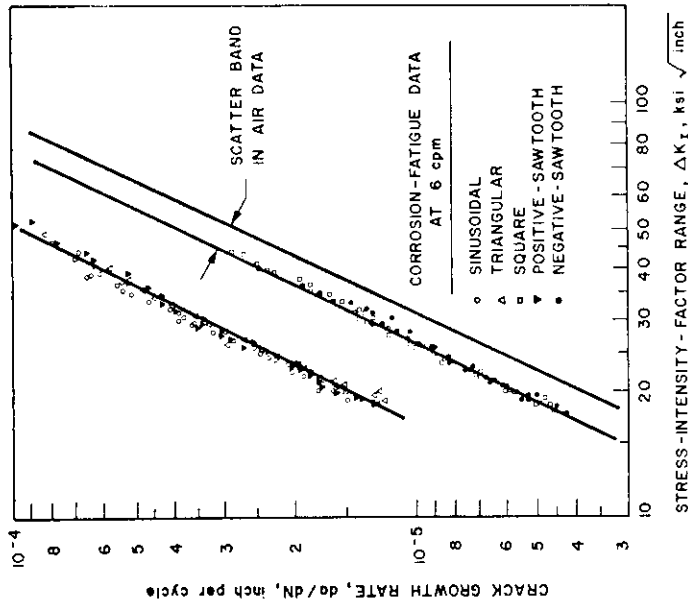


Figure 47. Corrosion fatigue crack growth rates in 12Ni-5Cr-3Mo steel in 3% solution of sodium chloride under various cyclic loading wave forms with different stress-time profiles. (After Reference 77)

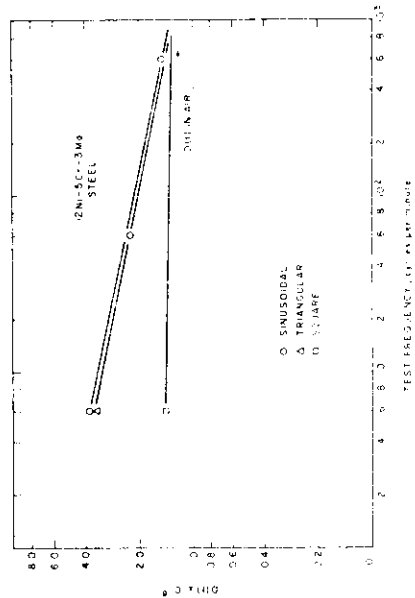


Figure 46. Relationship between  $D(t)$  and cyclic stress frequency in 12Ni-5Cr-3Mo steel in 3% solution of sodium chloride under sinusoidal, triangular, and square loading wave forms. (After Reference 77)

a. Temperature. A study of mild steel at 8 ksi in artificial seawater at constant solution temperatures indicated that an increase in temperature from approximately 60 to 115° F reduced the fatigue life by approximately 50% in the  $10^7$  cycle range. (79) In a 2.5% NaCl solution at temperatures approaching the boiling point of water, it was found that fatigue life of a drilling steel was improved. (80) The causes of these differences are not apparent. Increasing temperature would be expected to increase corrosion rates and would therefore be expected to reduce corrosion fatigue life where environmental effects are controlling. However, if crack growth is caused by hydrogen embrittlement, temperatures near 212° F are known to drive hydrogen out of steel and might be expected, therefore, to increase corrosion fatigue life. As these examples indicate, the role of temperature in corrosion fatigue is far from clear.

b. Alloy Composition and Structure. Essentially no data are available on the effects of alloy composition and microstructure on corrosion fatigue crack growth rates. However, the linear superposition rule for above  $K_{Isc}$  behavior suggests that compositions and heat treatments which render an alloy susceptible to SCC would cause the corrosion fatigue crack growth rate to increase. For below  $K_{Isc}$  behavior at frequencies, levels of  $K$ , and under loading wave forms where environmental factors are most significant, one would expect any change in composition or heat treatment which renders the alloy less susceptible to corrosion also to reduce its susceptibility to corrosion fatigue.

c. Method of Applying Stress. In fatigue tests stress is applied either axially or in bending. Some investigators have reported results which show that applying the stress in bending decreases the corrosion fatigue life compared to results obtained by axial loading, while others have produced opposite results. (81, 82)

d. Environment. The time-to-failure of mild steel in saltwater has been shown to decrease as pH becomes more acidic; above a pH of 12, the corrosion rate of mild steel in saltwater is equivalent to the rate in air. (83) The reduction in corrosion damage at the alkaline pH levels is believed to reflect an inhibitive effect on crack initiation, rather than crack growth, since it is well established that the pH at the tip of an existing crack or at the bottom of a pit is 3 to 4 for steels, regardless of the pH of the bulk solution. (69, 84) The amount of dissolved oxygen in saltwater has been shown to have a major effect on corrosion fatigue life of mild steel; specimens exposed in deoxygenated 3% NaCl solution were found to have the same fatigue limit as in air. Since corrosion rates of steel in water are controlled by diffusion of oxygen to the metal surfaces, these results suggested that corrosion fatigue rates were controlled by the corrosion rate, and, therefore, a critical corrosion rate should exist below which the environment exerts no influence on fatigue properties of steel. (85) Critical corrosion rates for mild steel and 4140 in deaerated 3% NaCl have been determined and reported to be

approximately 0.9 mpy, regardless of the strength level of the steel or the maximum applied stress level. (83, 86) These results, in turn, suggested that cathodic protection or other techniques which would reduce the general corrosion rate of a steel also would be effective in eliminating the influence of environment on fatigue.

e. Electrochemical Potential. A number of investigators who have studied the effects of cathodic protection on mild and high strength steels in neutral and acid pH saltwater environments have reported that polarizing the metal to a level of -0.75 to -0.85 v vs SCE (approximately 0.20 v below the freely corroding potential) or lower effectively eliminates the influence of environment on fatigue to the point that the fatigue limit in saltwater is essentially the same as in air. (83, 86, 87) These data clearly suggest that cathodic polarization is beneficial.

However, other studies have produced somewhat different results for moderate-to-high strength steels. (88) and another study concluded that effects of cathodic protection are dependent upon specimen geometry. (89) Figures 48 and 49 show cycles to failure and crack growth rates for HY-80 steel at low frequencies as a function of electrochemical potential. The data shown in Figure 48 are reported to be essentially initiation data, since cracks were observed to grow to failure quite rapidly once initiated. On this basis the curves indicate that polarizing the steel approximately 200 mv below the freely corroding potential delays crack initiation. Figure 49 indicates that, at the low frequencies shown, cathodic polarization accelerates propagation. Similar results were obtained for 4340 steel at a frequency of 90 cpm. (88) The implication of these results is that cathodic polarization to a level of approximately 200 mv below the freely corroding potential inhibits crack initiation by retarding the formation of pits, but once pits are formed, cathodic polarization accelerates crack growth, the degree of acceleration being inversely proportional to the frequency of loading. Such behavior is consistent with a hydrogen embrittlement mechanism for high-strength steels. The apparently contradictory results as were reported for more negative potentials (86, 88, 90, 91) are stated by Brown (88) to be due to two factors: (1) tests showing beneficial effects at potentials lower than 200 mv below the free corroding potential almost always are conducted with full reversal of stress; and (2) the cycle rate is high, i. e., in the order of 1000 cpm or greater. Under such conditions it is conjectured that the loading rate is too rapid for hydrogen to exert its effect and that going into compression in some manner redistributes hydrogen and reduces its potential to inflict damage.

f. Stress Ratio. The term stress ratio, R, refers to the ratio of the minimum stress (or stress intensity) to maximum stress (or stress intensity). Therefore, in zero-to-tension loading R is zero, in tension-to-tension loading R is positive, and in tension-to-compression loading, R is negative. The rate of fatigue crack growth is affected by R in both inert and

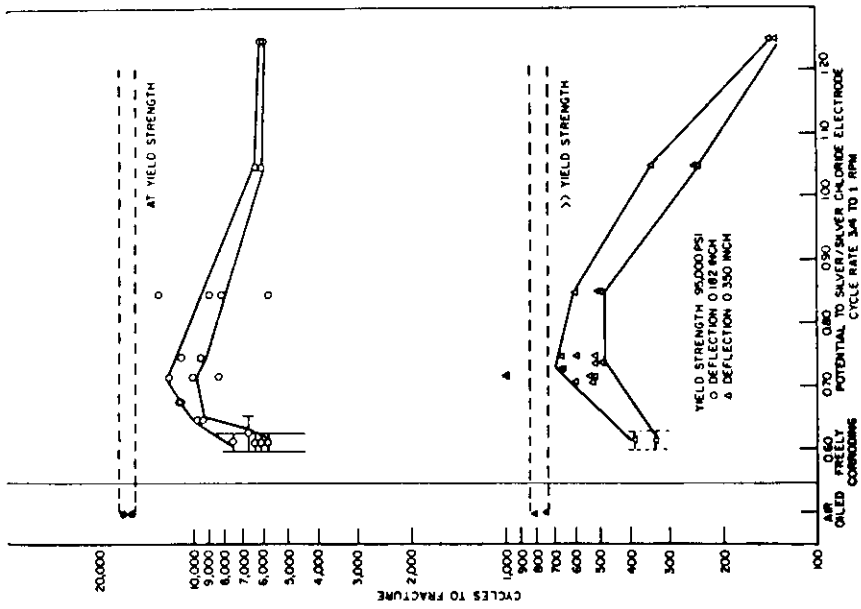


Figure 48. Effect of potential on corrosion fatigue life of smooth-surface HY-80 specimens in salt water at two stress levels. (After Reference 89)

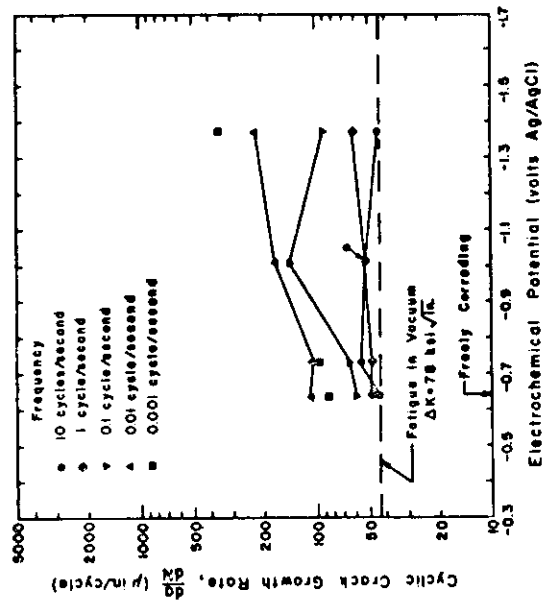


Figure 49. Corrosion fatigue crack growth rates for pre-cracked HY-80 specimens in salt water as a function of electrochemical potential for high amplitude fatigue loading ( $\Delta K \approx 78 \text{ ksi} \sqrt{\text{in}}$ ).

corrosive environments. For a given value of  $\Delta K$ , the crack growth rate is proportional to R and may vary by as much an order of magnitude as R varies from 0 to 0.50<sup>(92)</sup>, as illustrated in Figure 50. However, for design purposes crack growth rates for R = zero.<sup>(13)</sup>

g. Surface Discontinuities and Stress Concentrations. Figure 51 demonstrates the effects of surface discontinuities and stress concentrations on the fatigue strength of A517F Q&T steel. Scratches perpendicular to the principal stress axis are shown to reduce the fatigue strength from an as-received plate value of 45 ksi to approximately 35 ksi. Leaving the weld reinforcement intact produces the maximum stress concentration at the toe of the weld and reduces the fatigue strength to approximately 15 ksi. However, grinding down the weld reduces the stress concentrations and increases fatigue life. Figure 51 indicates that grinding the weld down from 1/16-in. height to 1/64-in. height nearly doubled the fatigue strength, and removing the weld reinforcement completely, followed by polishing, essentially restored the fatigue life to the as-received plate value. These data clearly indicate that (1) designers must minimize stress concentrations by careful attention to design of details and (2) design should be based on data from material fabricated by the process to be used, rather than on as-received plate data, or that the as-received plate data must be modified to account for effects of discontinuities and stress concentrations.

#### C. Control of Stress Corrosion Cracking and Corrosion Fatigue

The techniques available for control of stress corrosion cracking (SCC) and corrosion fatigue in ship structure can be classified into two groups:

- (a) design measures, and
- (b) protective measures.

Design measures include such important steps as minimizing discontinuities and stress concentrations through careful attention to details of design and holding stresses below critical values. They also include a thorough knowledge on the part of the designer of the structure and the structural material if crack propagation technology is to be applied successfully. The designer must anticipate where to look for flaws in the structure, what type of flaws to look for, and a reliable means for flaw detection. Quality control and inspection procedures must be considered in the light of the properties of the materials. Weldment joint design and welding procedures must be carefully specified to minimize flaws, stress concentration, and residual stresses that could degrade performance of components below threshold values. The necessary knowledge for satisfactory use of structural carbon steels in ship hull construction is well established. The task remains to establish like factors for higher strength HSLA Q&T steels to provide equal serviceability and permit economic shipyard construction and marine service.

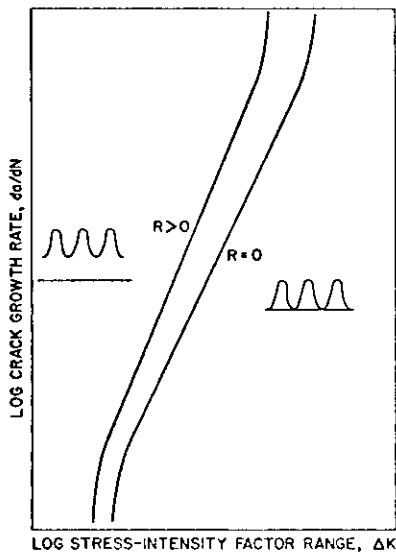


Figure 50. Schematic illustration of the typical effect of stress-ratio on fatigue-crack propagation. Positive R values (tension-to-tension cycling) tend to displace the entire curve above the curve for  $R = 0$ . (After Reference 13)

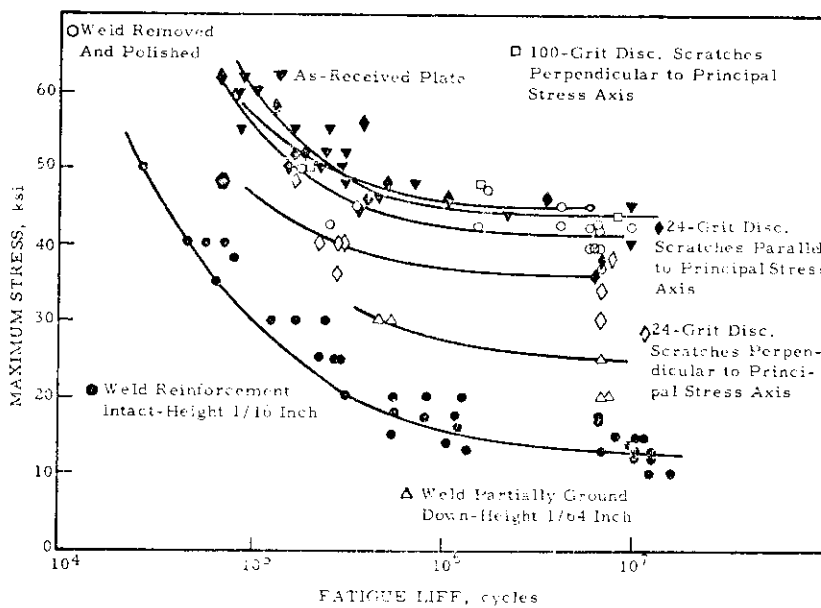


Figure 51. Effect of Removal of Weld Reinforcement on Axial-Load Fatigue Strength of Transversely Butt-Welded 1/4-in.-Thick Construction Alloy Steel Plates ( $R = -1$ ) (After Reference 93)

The common protective methods available for minimizing environmentally induced cracking phenomena in seawater are:

- (a) reducing stress concentrations,
- (b) reducing residual tensile stresses,
- (c) use of cathodic protection,
- (d) use of coatings,
- (e) combinations of these.

Stress concentrations have a major effect on fatigue and stress corrosion cracking resistance of materials exposed to corrosive environments. The effects of weld discontinuities and associated stress concentrations are shown in Figure 51 and are discussed in Section B.5.g. Every effort should be made to minimize stress concentrations by careful attention to design of weld joints, notches, penetrations, changes in section thickness, and similar details of design. Further, actual construction should be carefully supervised and inspected to assure that design specifications are followed.

Residual stresses may be removed by thermal stress relieving, but this obviously is impractical for large structures. Residual surface tensile stresses may be reduced or eliminated by the use of shot peening to introduce compressive surface stresses which effectively raise the applied stress level required to initiate cracking. However, to be effective the compressive stresses must be continuous and extend far enough below the surface so as not to be removed by general corrosion. Shot peening, too, is clearly impractical for the extensive welds on primary ship structure.

Cathodic protection is an effective method of minimizing general corrosion and may be helpful in minimizing SCC and corrosion fatigue to the extent that if a critical corrosion potential for cracking exists, the potential of the structure can be lowered below that potential. However, as noted in the previous sub-section, cathodic protection may cause hydrogen-induced SCC in HSLA Q&T steels. It therefore should not be used for these materials without careful testing to ensure design integrity.

Coatings are the most widely used means of protecting steel against corrosion in seawater. The various types of organic coatings that have performed well in seawater include vinyls, epoxies, urethanes, and coal-tar epoxies. These coatings function as barriers preventing the corrodent from reaching the steel surface. To be most effective they must be sufficiently ductile to withstand rupture, particularly under dynamic strain conditions present in corrosion fatigue. Metallic protective coatings of sprayed or vapor deposited aluminum have been found effective in preventing atmospheric SCC of Q & T steels with yield strengths in the 200 ksi range; zinc-rich paints were similarly effective.<sup>(94)</sup> A wide variety of coatings has

been evaluated in a seaside exposure with bent-beam SCC tests. The coatings tested and the results are shown in Tables 4 and 5. Of these, only aluminum deposited after austenizing was effective for both steels. Robinson and Uzdarwin<sup>(95)</sup> conducted bent-beam tests on H-11 and 18% Ni maraging steels in a 3% NaCl solution using polyurethane, inorganic zinc, and inhibited epoxy coatings. These coatings also were evaluated in air saturated with water at 140°F. Representative results are shown in Table 6. The inhibited epoxy was the most effective in both environments. These data indicate that although certain coatings appear promising as preventive measures against SCC of high strength steels, the reliability and effectiveness of a given coating must be evaluated for each situation. No data are available on the effects of coatings on the corrosion fatigue resistance of Q & T steels.

TABLE 4. COATINGS TESTED  
(After Reference 94)

Coating	Description	Measured Average Thickness (in.)
Ni-Cd electroplate	Specification AMS 2416; electroplated Ni 0.002 to 0.0004 in., followed by electroplated Cd 0.0001 to 0.0002 in., followed by diffusion at 630°F for 1 hr.	0.0005
Electroless Ni	Coated to 0.002-in. thickness, followed by postbaking heat-treatment.	0.0017
Electroplated Ni	"Gray Nickel" plate	0.0025*
Chromium	Commercial electroplating	0.0013
Aluminum	Al-metallizing, followed by dip coating with hydrolyzed ethyl silicate.	0.0057
Al-pigmented silicone	Baked 2 hr. at 425°F	0.0013
Silicone	Baked 2 hr. at 425°F	0.0005
Zinc chromate iron oxide alkyd paint	Primed and painted, air-dried.	0.0019
Zinc chromate primer	Air-dried	0.0009
Zinc-dust dibutyl titanate	An experimental zinc-dust dibutyl titanate primer, air-dried	0.0021
Rust-preventive wax	Coating was applied to stressed specimens immediately before exposure	0.0012
Rust-preventive grease	Coating was applied to stressed specimens immediately before exposure	Not measured
Strontium chromate aluminum paint	Air-dried	0.0008
Aircraft-type zinc chromate primer	Specification: MIL-P-6889A Type I, air-dried.	0.0002

\* Coating peeled off during stressing on some specimens. These specimens were excluded from the test.

TABLE 5. EFFECT OF PROTECTIVE COATINGS ON STRESS  
CORROSION OF AIRCRAFT ALLOYS\*  
(After Reference 94)

Coating	Time to Failure (days)	
	12 MoV	Die Steel
Not Coated	0.7	1.5 to 3
<i>Coatings that prevented stress corrosion</i>		
Aluminum applied after austenitizing	NF	NF
<i>Coatings that delayed stress corrosion</i>		
Ni-Cd electroplate	NF	263**
Zinc-dust dibutyl titanate	NF	395**
Aluminum applied before austenitizing	4 to 66	46**
Al-pigmented silicone applied after austenitizing	7**	147**
Aircraft-type zinc chromate primer	2 to 17	-
Electroplated Ni	405**	0.7
<i>Coatings with no appreciable effect on stress corrosion</i>		
Electroless Ni	0.7	0.7 to 1
Electroplated Cr	0.7	0.01 to 4
Al-pigmented silicone applied before austenitizing	0.7	2 to 3
Silicone	0.7	0.7 to 5
Zinc chromate iron oxide alkyd paint	0.7 to 3	0.7 to 13
Zinc chromate primer	0.7 to 1	-
Rust-preventive wax	0.7 to 13	0.7 to 4
Rust-preventive grease	0.7 to 3	0.7 to 5
Strontium chromate aluminum paint	0.7 to 1	-

NF = No failure in 420 days.

- Results of exposure at Kure Beach, N.C.
- \*\* Some specimens have not failed after 420 days.

TABLE 6. BENT-BEAM STRESS-CORROSION TESTS FOR  
COATINGS EVALUATION  
(After Reference 95)

Base Metal	Coating	3% NaCl Solution		140°F Water-Sat. Air	
		Failure Ratio*	Median Failure Time (hours)	Failure Ratio*	Median Failure Time (hours)
A-11 steel	None	4/4	1.5	2/2	64
A-11 steel	Polyurethane X-500	3/3	1380	6/6	3500
A-11 steel	Inorganic zinc - 11	2/2	687	2/2	821
A-11 steel	Inhibited epoxy 454-1-1	0/2	NF 3100	3/3	2720
18%-nickel maraging steel	None	3/3	119	3/3	535
18%-nickel maraging steel	Polyurethane X-500	1/3	4488	3/3	1560
18%-nickel maraging steel	Inorganic zinc - 11	3/3	288	3/3	140
18%-nickel maraging steel	Inhibited epoxy 454-1-1	0/3	NF 4990	2/3	1870

\* Ratio of samples failed to samples exposed.

#### IV. CRACK INITIATION AND SUBCRITICAL CRACK GROWTH CRITERION

##### A. General Principles Governing Ship Design with HSLA Steels

The first requirement in establishing a crack growth criterion is to determine the general design objectives which the structural designer must set before himself. Up to the present time, ships have been designed and built without specific reference to fatigue crack growth. Performance success has been achieved due to the conservatism with which loads spectra were established and design allowables defined. In addition, the low-strength, low-alloy mild steels used have had relatively high toughness, which is often an index of resistance to crack growth. With the prospect of HSLA steels being used on a selective basis in primary ship structure, the possibility of crack growth is now of much more concern. Thus, the designer is immediately confronted with the following choices: he may either

- (a) design to prevent fatigue cracks from developing,
- or
- (b) design to ensure overall integrity of the structure even if fatigue cracks propagate substantially in some areas.

The first of these two design philosophies is referred to as a safe-life criterion. From this viewpoint, the structure is designed such that crack propagation is only remotely possible. At the end of the design life the structure is either scrapped or reworked extensively, as there is no reliance on periodic NDI and repair in the design framework. According to the safe-life design principle, if fatigue cracks do develop and grow, whether due to changes in service conditions or design error, they may well prove to be fatal.

The alternative to the safe-life principle is the fail-safe principle. According to this philosophy, the design is based on the premise that cracks will develop and grow, and hence there must be sufficient structural redundancy (load paths) and crack arrest devices to ensure that the structure can be used safely until the crack can be discovered and repaired. Thus, this design scheme assumes an inspection schedule will be performed periodically during service life. The fail-safe philosophy is usually less conservative than the safe-life philosophy, and results in a lighter, more efficient structure.

Heretofore, ship design has been based on a combination of the safe-life and the fail-safe design principles. Traditional ship design methodology has not specifically included structural fatigue analysis. Operating stresses

in primary and secondary structure have been kept low relative to endurance limits, and structural redundancies have been designed in to ensure structural integrity in the event of fast fracture in one region. On the other hand, past designs have assumed that periodic NDI inspections would be performed so that any cracks that do develop would be repaired or replaced at some stage in their growth. Thus, unlike aircraft structures, which are often designed according to strict fail-safe principles, ship structural design currently represents an intermediate position between the two complementary philosophies. This approach, coupled with conservative design factors and a long history that records only rare instances of fatigue crack propagation in primary structure, has proved to be a successful design philosophy for ship structures. However, as design stresses are increased in both mild and in HSLA ship steels used in primary structure, it will be necessary that design philosophies move closer to the fail-safe position, by including crack growth criteria in structural design.

The criterion that is set forth in this chapter is to be considered a tentative design tool by which the designer/architect can evaluate tradeoffs between stress levels and fatigue damage resistance of ship structural weldments. It is tentative because the data on which the criterion is based are in some respects inadequate to develop a complete, reliable design process. The criterion concerns crack initiation and subcritical crack growth specifically, and does not address fast fracture.\* It assumes that the designer can identify the potentially critical stress areas in the structure and has some knowledge of the loading environment which these regions experience.

#### B. Purpose of the Criterion

The purposes of the criterion described in this chapter may be stated briefly as follows.

- (a) To identify the relative merits of mild and HSLA steels with regard to crack initiation and subcritical crack growth in ship structure,
- (b) to permit the ship designer to place realistic estimates on the permissible fatigue-producing stresses in primary structure so that adequate service life can be assured,
- (c) to enable the ship designer to make recommendations, on the basis of expected subcritical crack growth rates, of the required resolution and frequency of nondestructive inspection procedures,

---

\*The reader interested in an introduction to fracture design is referred to the Appendix; in general it is to be emphasized that the plane-strain fracture toughness  $K_{Ic}$  can lead to excessive structural weight since the apparent fracture toughness,  $K_c$ , is usually somewhat higher than  $K_{Ic}$ .

- (d) to have a basis for estimating the level of conservatism now present in primary ship structural design,
- (e) to identify areas in need of further investigation so that the confidence level and applicability of the criterion may be increased.

C. Rationale for Criterion

1. Technical Basis

The Criterion set forth in Section IV.D should be considered to be a tentative procedure which may be applied by a ship designer or naval architect to make realistic design decisions concerning the application of mild and HSLA ship steels, when subcritical crack growth may be of concern. This Section presents the rationale behind the suggested criterion, i. e., the technical basis and the assumptions which were used in developing the criterion. To begin with, it is useful to establish the interpretation of the word "criterion" as used in this report. One authoritative source\* defines the word "criterion" as "A standard, rule, or test on which a judgment or decision can be based." This interpretation is to be given in the criterion to follow. The principles which guided the development of this particular criterion were:

- (a) Simplicity of use, consistent with sound, accepted principles.
- (b) Incorporation of the best state-of-the-art data generally available.
- (c) Establishment of a framework that will permit updating the criterion as improved data and procedures become available.
- (d) Viewpoint that the criterion must be easily usable by designers having at best a marginal knowledge of fatigue and fracture processes.

These principles are clearly subjective and open to varying interpretations. Nevertheless, they provide useful guidance to the overall understanding of the criterion.

The criterion is based on the premise that small discontinuities (as distinguished from cracks) are inherently present in ship structure, and hence may be assumed to exist in critical stress regions. In time, due to exposure to the loading environment, these discontinuities may develop (initiate) into true fatigue cracks, which can then propagate subcritically

---

\*Taken from the American Heritage Dictionary, Houghton-Mifflin Co., 1969.

for a period of time. Given sufficient exposure to the loading environment, one or more such cracks may eventually attain a critical length associated with structural failure through fast fracture, excessive deflection, leakage, or some other form of structural malperformance. The total number of load cycles to failure,  $N_f$ , associated with a crack propagating to a critical length is, therefore,  $N_f = N_i + N_p$ , where  $N_i$  is the number of cycles required to initiate a fatigue crack, and  $N_p$  is the number of cycles active in propagating the crack to its critical length.

The number of cycles,  $N_i$ , required to initiate the crack is defined in different ways by different people. It may, on the one hand, be taken from micromechanical considerations as the number of cycles required to trigger cyclic growth from a pre-existing flaw site under the expected loading environment. On the other hand, it is sometimes more useful to consider  $N_i$  as the number of cycles required to grow a crack to the minimum length which can be detected reliably by the structural NDI means to be employed. This criterion uses the latter interpretation, for reasons to be explained shortly.

Sustained load stress corrosion cracking (SCC) does not need to be accounted for in applying this criterion. At the present time SCC effects are generally thought to be negligible for the class of materials and environments relevant to ship structures. Moreover, the criterion as presented applies only to welded joint structural regions, since experience has shown that fatigue cracks will initiate and propagate in these areas at lower stresses long before developing in the base material. Because of the residual stresses created in weld regions by confinement forces and by the welding process itself, the weld region may experience a load ratio  $R$  quite different from the load ratio applied to the structure. According to Gurney and Maddox<sup>(96)</sup> the current knowledge of residual stresses in as-welded structures suggests that  $R$  is irrelevant to fatigue life because of the inevitability of high tensile residual stresses. Thus, members subjected to applied compressive stresses would need to be designed as if they were subjected to tensile stresses. While this assumption requires some further experimental clarification, for purposes of this criterion subcritical crack growth in welded structures is taken to depend purely on the stress range. Cycles which nominally are partially or even wholly compressive are assumed to be just as damaging as cycles which are fully tensile.

There presently exists in the technical literature a substantial body of test data concerned with the fatigue life,  $N_f$ , of various welded structural joints.<sup>(20, 96, 97)</sup> These data can be presented in the form of plots of stress range  $\Delta\sigma$  vs  $N_f$  as shown in Figure 52. The test data consistently show that, for mild and HSLA steels of interest to this work, the  $\Delta\sigma - N_f$  curve depends strongly on the particular type of welded joint configuration, and also upon the strength level of the base material at stress levels associated with a failure life

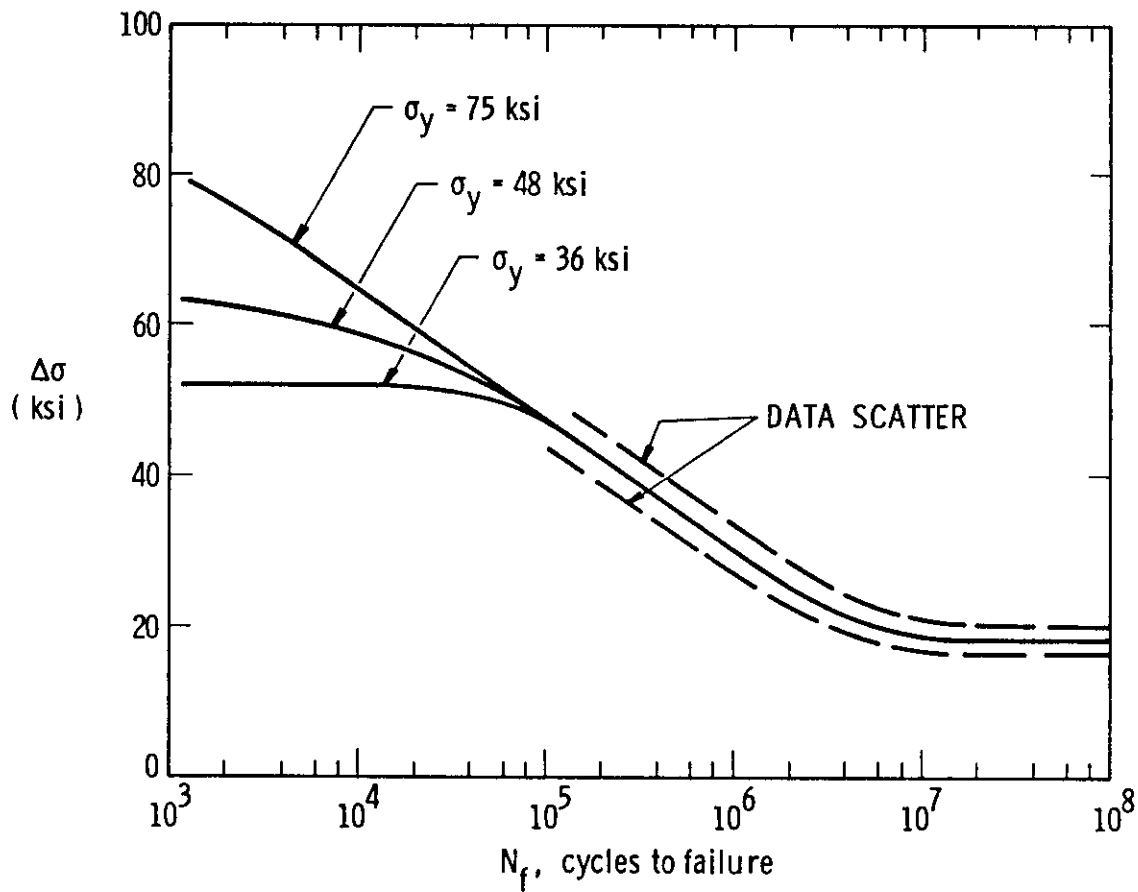


Figure 52. Typical  $\Delta\sigma$ - $N_f$  curves for structural weldment (after Reference 20)

$N_f$  less than about  $5 \times 10^5$  cycles. However, for  $N_f > 5 \times 10^5$  cycles, the  $\Delta\sigma - N_f$  curve and the endurance strength (stress level for unlimited fatigue life) are independent of the base material strength level for a given weld - ment type.

The implication of this finding is that if the structure is exposed predominately to low-cyclic stress levels, i.e., those associated with failure  $N_f > 5 \times 10^5$  cycles, the fatigue life is the same for mild and HSLA ship steels. Since the ship design life is considerably in excess  $5 \times 10^5$  cycles, \* differences between the fatigue life of mild and HSLA ship steels will arise only due to the infrequent stress overloads where the  $\Delta\sigma - N_f$  curve is yield-strength-dependent. This "strength effect" of fatigue life, which is dependent on the mean or rms stress level in the structure and the spectral response of the ship to the various sea states encountered, can be expected to be very small for conventionally designed ships wherein the operating stresses are low. That is, while high-yield-strength steels do provide an extra margin of protection against infrequent high overload cycles, the occurrence frequency of these cycles is so small that the fatigue strength of the ship to spectral loading is expected to be insensitive to yield strength.

While  $\Delta\sigma - N_f$  data of the type discussed above are important in design and, in fact, form the cornerstone of the proposed criterion, they give no information as to the relative proportions of life associated with initiation,  $N_i$ , and propagation,  $N_p$ . At the present time, there is no reliable and accepted procedure for independently determining the crack initiation period  $N_i$  for welded structural joints. On the other hand, sound engineering data are generally available for the propagation rates associated with sub-critical crack growth in welded martensitic and pearlitic parent steels.<sup>(9, 98-102)</sup> These data can be represented by curves similar to that shown in Figure 53 where the crack propagation rate,  $da/dN$ , is plotted as a function of the stress intensity factor range,  $\Delta K$ . Over a certain range of  $\Delta K$  this relationship is log-log linear, bounded from below by  $\Delta K_{th}$ , the threshold value, and from above by  $\Delta K_T$ . Below  $\Delta K_{th}$ , the crack growth rate  $da/dN$  is so small as to be considered negligible for all practical purposes. Above  $\Delta K_T$ ,  $da/dN$  is so large that serious structural fatigue damage may occur within a relatively small number of cycles.  $\Delta K_{th}$  is generally considered to be independent of the strength level (although it appears dependent upon the load ratio R).<sup>(8)</sup> Between the limits of  $\Delta K_{th}$  and  $\Delta K_T$ ,  $da/dN \approx (\Delta K)^n$ . The slope of this portion of the curve is not sensibly affected by the material's strength level. For martensitic steels in the strength range 80 - 300 ksi,  $da/dN \approx (\Delta K)^{2.25}$ , while for pearlitic steels of lower strengths (40 - 60 ksi) the exponent is usually

\*The design fatigue life for primary structure in a ship having a hog/sag frequency of 6 cpm and a design life of 20 years at 200 operational days/year is  $6 \times 60 \times 24 \times 200 \times 20 = 3.456 \times 10^7$  cycles.

taken as 3.0. (9, 101, 102) Crack growth rates are almost always somewhat higher in the parent material than in the weld or HAZ, and to be design-conservative, crack growth rates should be those associated with the base metal. (8)

Since there is a known proportionality between  $da/dN$  and  $\Delta K$  in the region  $\Delta K_{th} \leq \Delta K \leq \Delta K_T$ , this expression may be integrated to give  $N_p$ , the number of cycles required to propagate the crack from an initial length  $a_o$  to a critical length  $a_{cr}$ . For simplicity, this criterion assumes that the initial crack configuration is a surface crack, with a length equal to twice the depth, and that this crack aspect ratio does not change during crack growth. With these assumptions, the following calculation procedure directly determines  $N_p$ : The crack growth expression  $da/dN = 0.66 \times 10^{-8} \times (\Delta K)^{2.25}$  is adopted for purposes of this criterion from the work of Barsom, (101) for application to design for both martensitic and pearlitic steels in the strength range 40 - 300 ksi. In this expression,  $\Delta K$  is expressed as  $\text{ksi}\sqrt{\text{in.}}$ , and the instantaneous crack depth  $a$  is in inches. Combining this with the expression  $\Delta K = 1.24\sqrt{a}\Delta\sigma$  for the surface crack with a length equal to twice the depth, (103) there results

$$\int_{a_o}^{a_{cr}} da = 0.66 \times 10^{-8} (1.24\sqrt{a}\Delta\sigma)^{2.25} \int_0^{N_p} dN \quad (36)$$

from which

$$N_p = \frac{7.47 \times 10^8}{(\Delta\sigma)^{2.25}} \left( \frac{1}{a_o^{1/8}} - \frac{1}{a_{cr}^{1/8}} \right) \quad (37)$$

where  $\Delta\sigma$  is expressed in ksi, and  $a_o$  and  $a_{cr}$  are in inches. Thus, under the assumptions mentioned earlier,  $N_p$  depends only upon the applied stress range, and the initial and final crack depths, but is otherwise independent of material strength.

The manner in which the initial and critical crack lengths,  $a_o$  and  $a_{cr}$ , are defined influences the calculated value of  $N_p$ . One method of determining these quantities is to calculate them from fracture mechanics principles. According to this approach, since  $\Delta K = 1.24\sqrt{a}\Delta\sigma$ , then  $a_o = 0.65 (\Delta K_{th}/\Delta\sigma)^2$  and  $a_{cr} = 0.65 (\Delta K_T/\Delta\sigma)^2$ . Furthermore, while  $\Delta K_{th}$  (and hence  $a_o$ ) is independent of the yield strength,  $\Delta K_T$  (and hence  $a_{cr}$ ) does depend upon  $\sigma_Y$ . In particular, there is convincing evidence showing

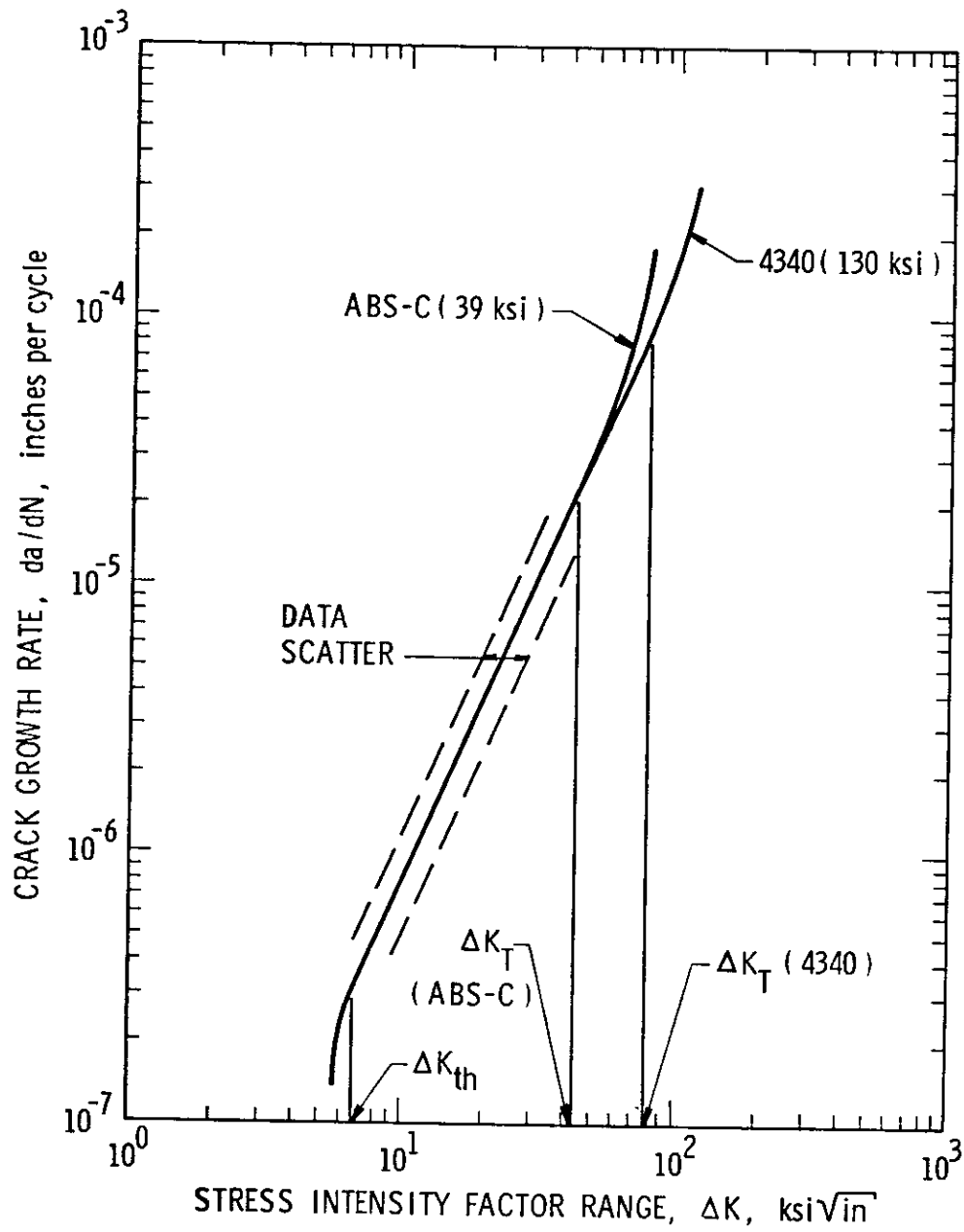


Figure 53. Typical crack growth data for welded steel plate (after References 9 and 102)

that  $\Delta K_T \approx \sqrt{\sigma_Y}$ . (9, 11, 102) The net result, then, from this approach is that the calculated value of  $N_p$  increases slightly with yield strength because of the increase in  $a_{cr}$  with  $\sigma_Y$ .

While this approach for defining  $a_o$  and  $a_{cr}$  is physically appealing, it is to some extent unsatisfying in application. One inconsistency lies in that the calculated value of  $a_{cr}$  may greatly exceed critical crack sizes found in laboratory specimens. Moreover, the implication of such an approach is that for a fixed  $N_f$ , since  $N_p$  increases with  $\sigma_Y$  (slightly, through  $\Delta K_T$ ), then it follows that  $N_i$  decreases with  $\sigma_Y$ . This implication is not supported by common laboratory observations.

This criterion takes a different and more pragmatic approach for defining the crack lengths  $a_o$  and  $a_{cr}$ . The initial crack length  $a_o$  is fixed as the smallest crack reliably detectable by the usual NDI methods employed in the inspection of ship structures. Thus, the crack initiation period  $N_i$  is that number of cycles needed to produce a perceptible crack. This crack length is of the order of the plate thickness, and depends upon the type of NDI employed and type of crack found. (104, 105) For purposes of this criterion,  $a_o$  is taken to be one-half the thickness of the thinnest plate in the welded joint under consideration. (104, 105) In other words, the surface crack length, which is twice  $a_o$ , is the thickness of the plate.

For the critical length,  $a_{cr}$  is taken to be 5 in. long, i.e., a surface crack of length 10 inches. This approach avoids the difficulties inherent in applying fracture mechanics to obtain realistic values of  $a_{cr}$ , and merely defines a crack 10 in. in length as being critical in some operational sense. It should be noted, however, that for a surface crack to achieve a length of 10 in. in conventional steel plate, its geometry would necessarily change, a factor not accounted for in the criterion. To account for the change in crack shape from a surface to a through-crack would have the effect of decreasing somewhat the computed value of  $N_p$ , but the effect would not be a strong one. It should also be understood that once the crack approaches its critical length  $a_{cr}$ , its growth rate is very high, so that its length will change considerably in a comparatively small number of cycles.

Using the value  $a_{cr} = 5$  in. as discussed above, the calculated value of  $N_p$  becomes, from Equation (37),

$$N_p = \frac{7.47 \times 10^8}{2.25 (\Delta\sigma)} (a_o)^{-1/8} (0.81777) \quad (38)$$

This expression was used in developing the data for the crack initiation period  $N_i (=N_f - N_p)$  presented in the criterion.

Using the approach for the calculation of  $N_p$  outlined above, it is concluded that  $N_p$  does not depend directly on the yield strength properties of the base material.  $N_p$  does, however, depend indirectly on  $\sigma_Y$  in that HSLA steels, as contrasted with mild steels, will be employed in ship structure in plates of reduced thickness, and thus  $a_o$  as defined by the criterion will be smaller for HSLA than for mild steel construction. The result is that  $N_p$  will be somewhat greater for the HSLA application, when compared on the basis of equal  $\Delta\sigma$ . This comparison is only partially correct, however. HSLA steels are employed to raise the working stresses through reduced plate thicknesses, and the commensurate increase in stress amplitude will tend to counteract the effect just mentioned of increasing  $N_p$  through smaller values of  $a_o$ . The net effect is that  $N_p$  is considered not to be significantly influenced by the strength level of the base steel used.

The rationale for the proposed criterion, as thus far outlined, implies that  $N_f$  is independent of  $\sigma_Y$  in the medium-to-high-cycle design regime, and depends only on the welded joint configuration under consideration. Moreover,  $N_p$  is, for all practical purposes, independent of  $\sigma_Y$ . Therefore, it follows that  $N_i (=N_f - N_p)$  is essentially independent of yield strength, so that the whole process of crack initiation and propagation to a critical length is at most only weakly dependent upon yield strength. Thus, insofar as crack initiation and subcritical crack propagation in ship steels are concerned, there is no important benefit or penalty associated with yield strength. Indeed, HSLA steels emerge as having no less fatigue resistance than mild steels, and the benefits that accrue from using HSLA steels to withstand the static design loads with reduced structural sections may be enjoyed without sacrifice. HSLA steels may also be expected to possess enhanced fatigue resistance due to greater ability to withstand the overload cycles which, while few in number, do inflict increased fatigue damage on the structure. More is said about the implications of the criterion in the subsection to follow.

The criterion proposes two complementary approaches for estimating fatigue life and permissible cyclic stress levels. The first, and most conservative of the two, makes use of a constant-amplitude sinusoidal loading environment to replace the true narrow-band random environment experienced by the primary structure. The assumption of a narrow-band process itself implies that high-frequency loading components associated with dynamic slamming are disregarded. These loading components, however, are generally considered to be unimportant to the fatigue damage process. (106)

Using the constant-amplitude sinusoidal loading environment approach, the criterion provides a conservative estimate of the maximum fatigue loads that can be sustained for an indefinite or for a finite life. These data are derived from the  $\Delta\sigma - N_f$  curves shown as Figures 54-59. It is important that this simplification, which is commonly employed in other structural design criteria, be understood and appreciated by users of the criterion. Figures 54-59 present fatigue life design data for typical welded joint configurations, and form the basis for life estimates for the criterion. The data are based upon results from Gurney<sup>(20)</sup> and Frost and Denton<sup>(97)</sup> obtained in pulsating tension experiments. These curves reflect the assumption (Frost and Denton<sup>(97)</sup>) that the fatigue strength approaches the ultimate tensile strength as the life  $N_f$  is decreased to zero. It is also assumed, after Gurney<sup>(20)</sup>, that the fatigue endurance limit is reached at  $10^7$  cycles, and it is further assumed to be equal to 75% of the fatigue strength at  $2 \times 10^6$  cycles. (As mentioned earlier, the stress range to be used in the criterion is the algebraic difference between the maximum and minimum cyclic stress values, i.e.,  $\Delta\sigma$  includes any compression component of the loading cycle that may be present.) These figures furthermore permit estimates of the scatter effect in the high-cycle portion of the fatigue life to be made. They also reveal that  $N_f$  is independent of yield strength for cyclic lives above  $10^5$  cycles, for all weldments considered.

Primary ship structure is exposed to a large number of narrow-band process random load cycles, typically  $10^7 - 10^8$  cycles, and thus ship structural fatigue design is inherently in the high-cycle regime. In this regime, as mentioned previously, for welded structures base metal strength effects vanish and the  $\Delta\sigma - N_f$  curves are independent of  $\sigma_y$  out beyond about  $10^5$  cycles. However, the spectral distribution of the loads about the mean value can affect the fatigue resistance. The (relatively few) load cycles of high intensity that can be expected statistically to occur do influence crack initiation and growth behavior, and it is here that yield strength effects can emerge. High-strength steels can accommodate those few load cycles of high intensity much better than mild steels. In general, it can be expected that due to the increased low-cycle fatigue resistance of HSLA ship steels, these materials will perform somewhat better under actual spectral loading conditions than conventional mild steels insofar as crack initiation is concerned.

Several recent research studies<sup>(107-109)</sup> conducted under the auspices of the Ship Structure Committee have addressed the problem of describing structural loading spectra for cargo ships deployed in service. Certainly each ship has its own peculiar structural response to given sea conditions, and the operational mission pattern also will vary from ship-to-ship. Therefore, it is unrealistic to expect there to be a single load spectral distribution which will closely characterize the total envelope of variable loads experienced by all cargo ships. Nevertheless, it is useful to examine the subcritical crack growth and failure implications of a representative load spectrum.

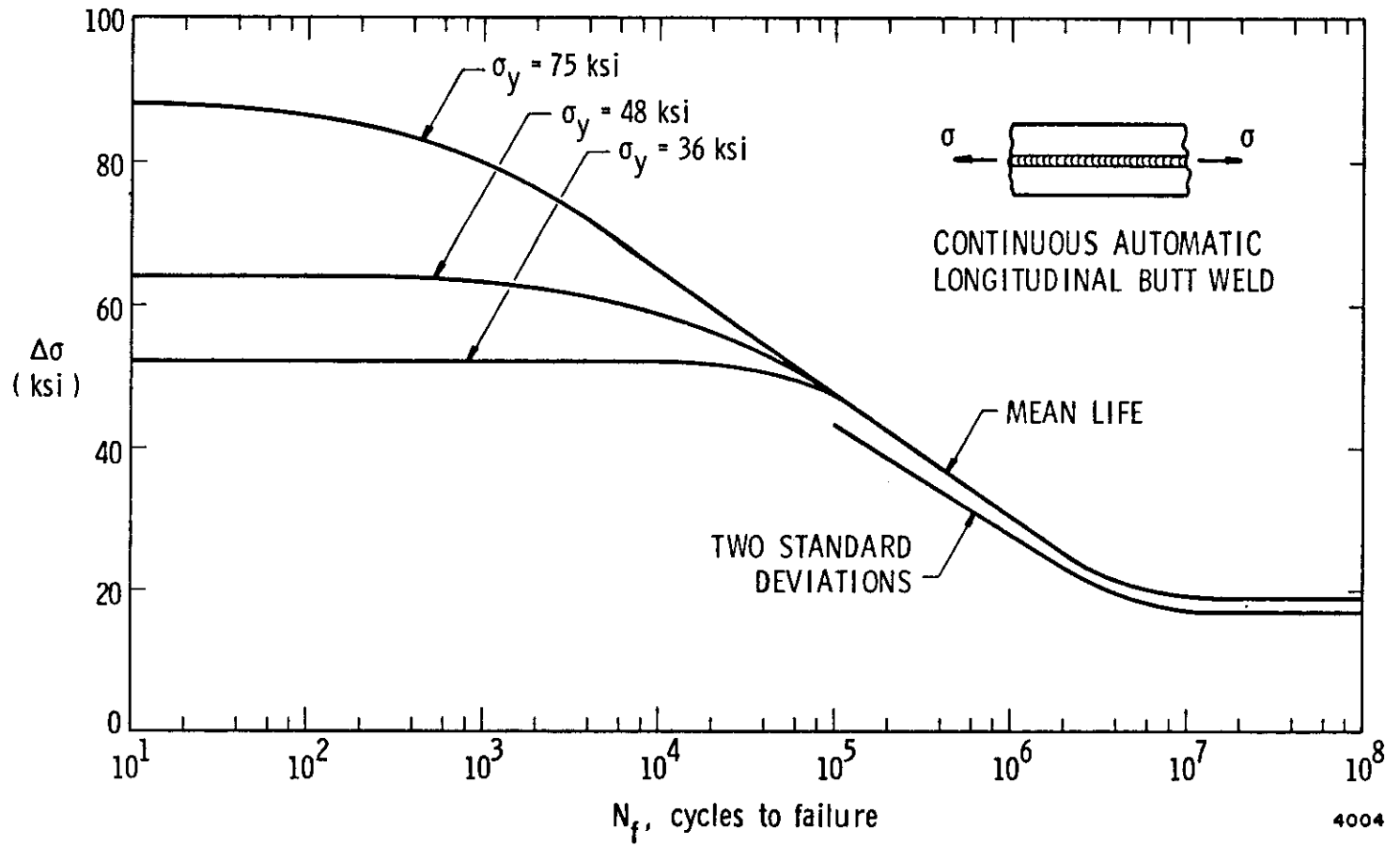


Figure 54.  $\Delta\sigma$ - $N_f$  curves for Type 1 weldments

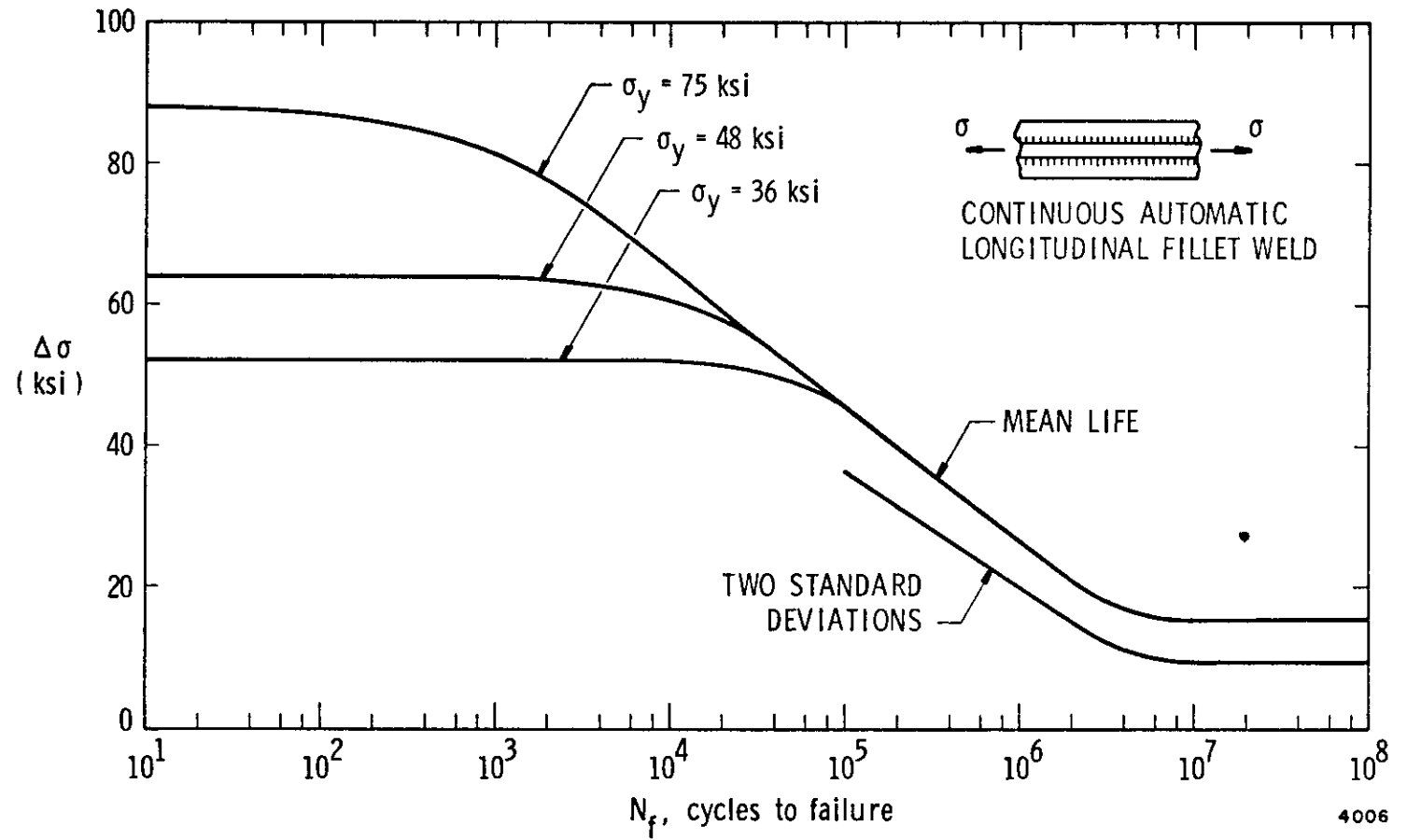


Figure 55.  $\Delta\sigma$ - $N_f$  curves for Type 2 weldments

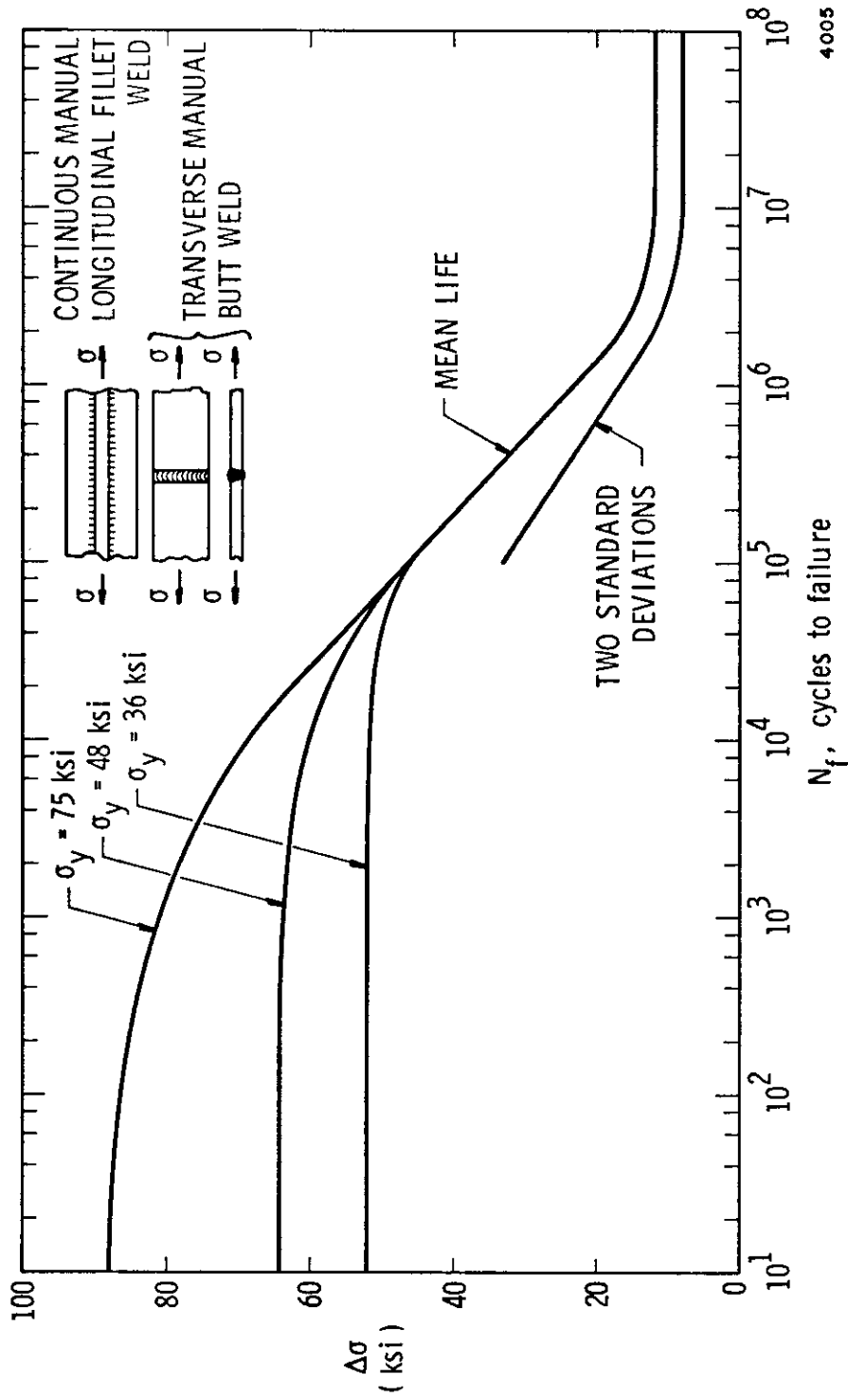


Figure 56.  $\Delta\sigma$ - $N_f$  curves for Type 3 weldments

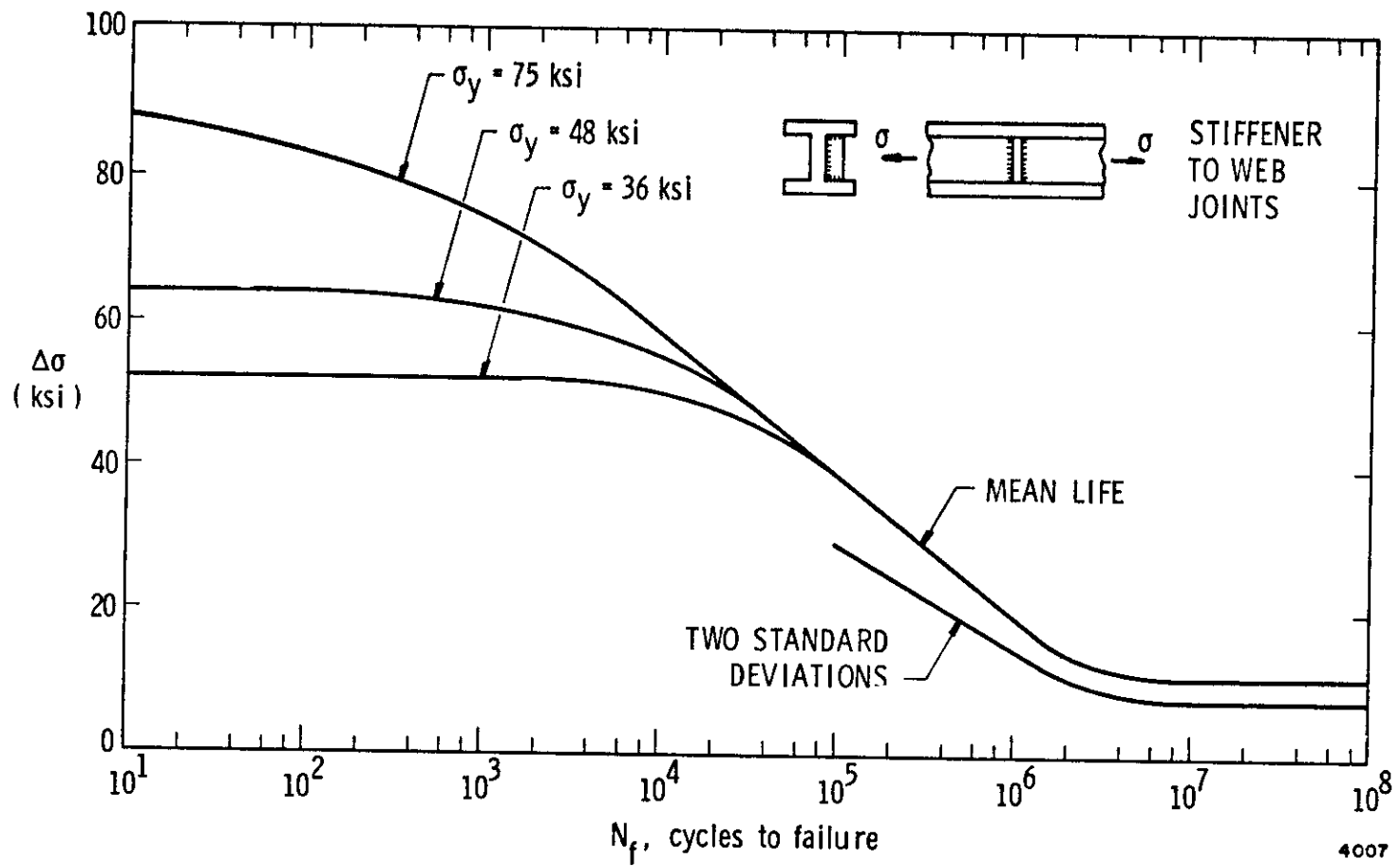


Figure 57.  $\Delta\sigma$ - $N_f$  curves for Type 4 weldments

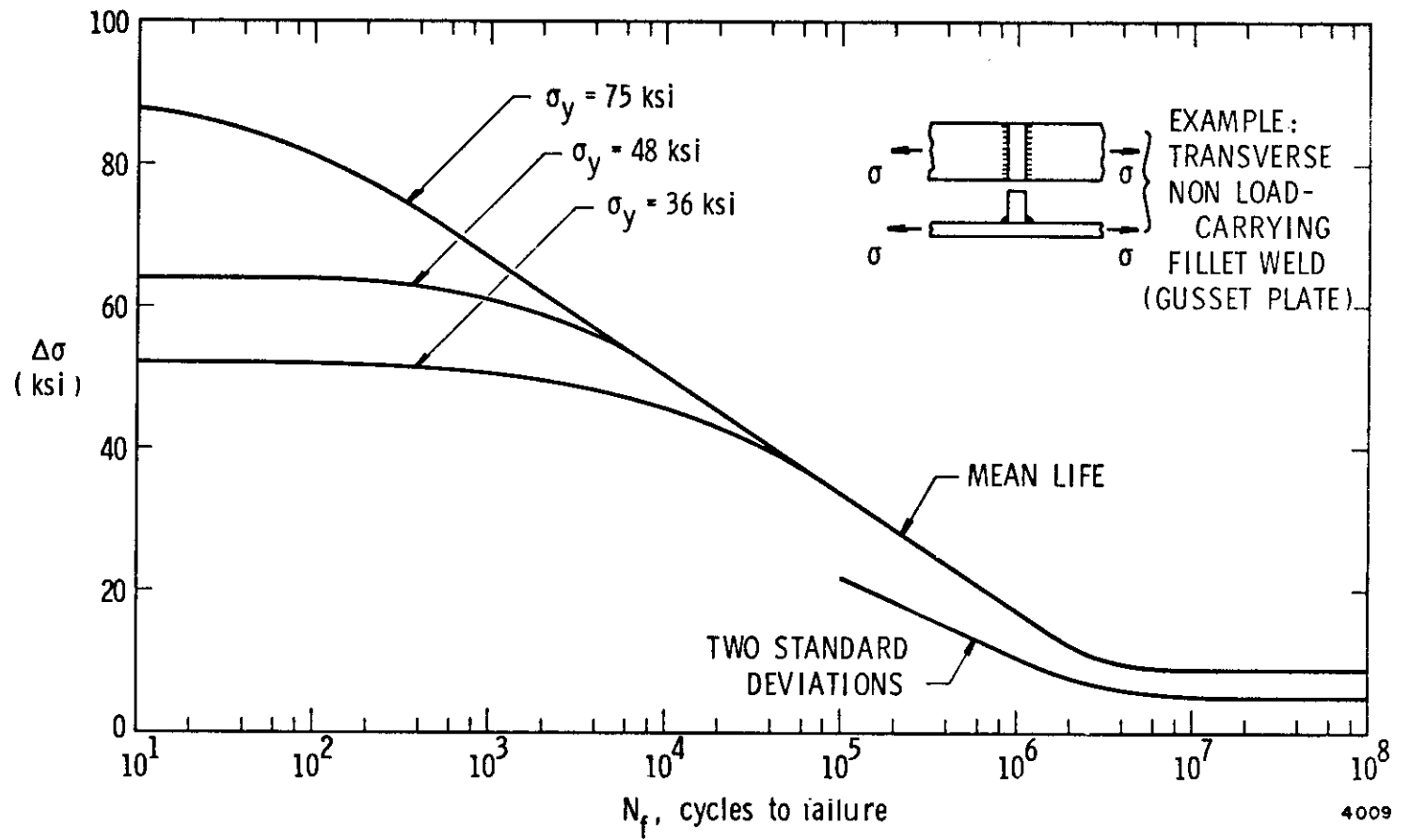
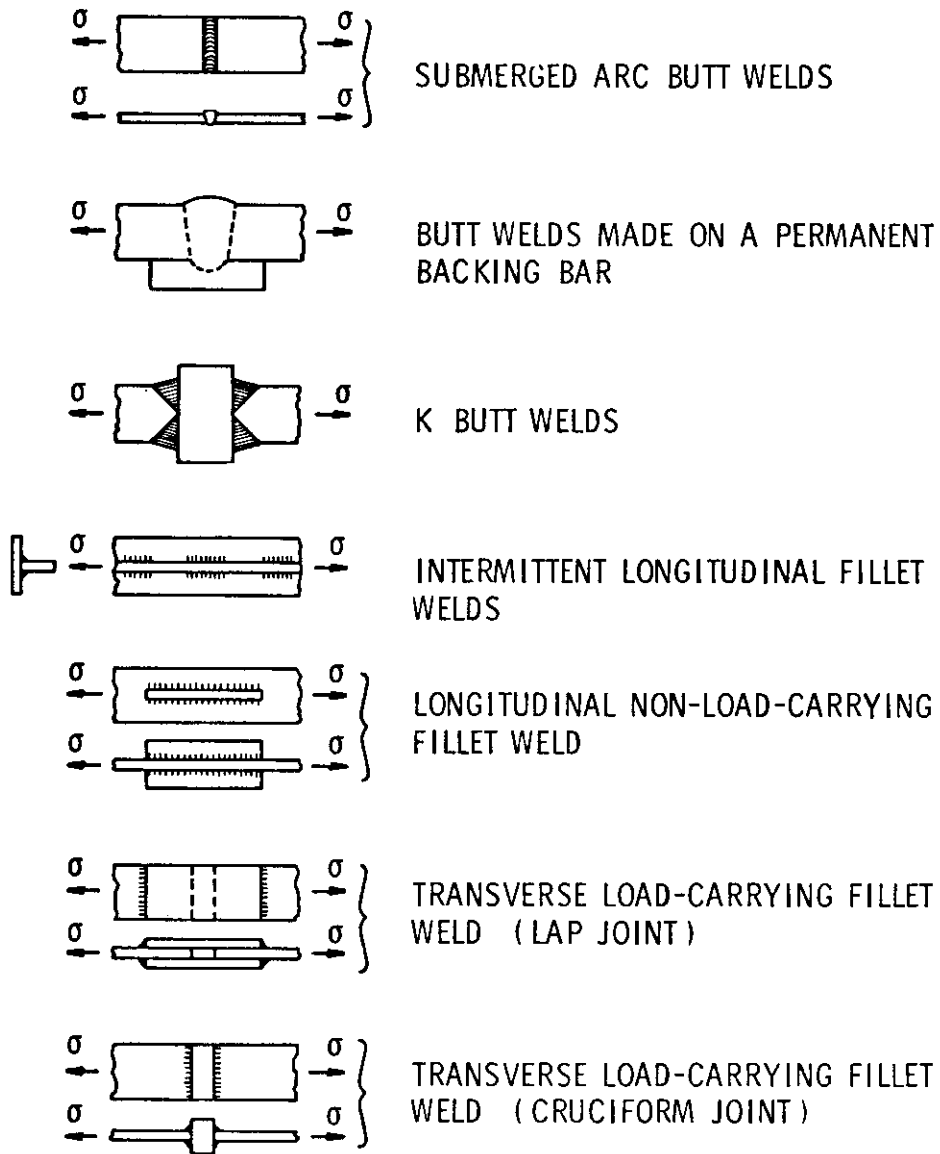


Figure 58a.  $\Delta\sigma$ - $N_f$  curves for Type 5 weldments

## TYPE 5 GEOMETRIES



4010

Figure 58b. Common geometries for Type 5 weldments

1001

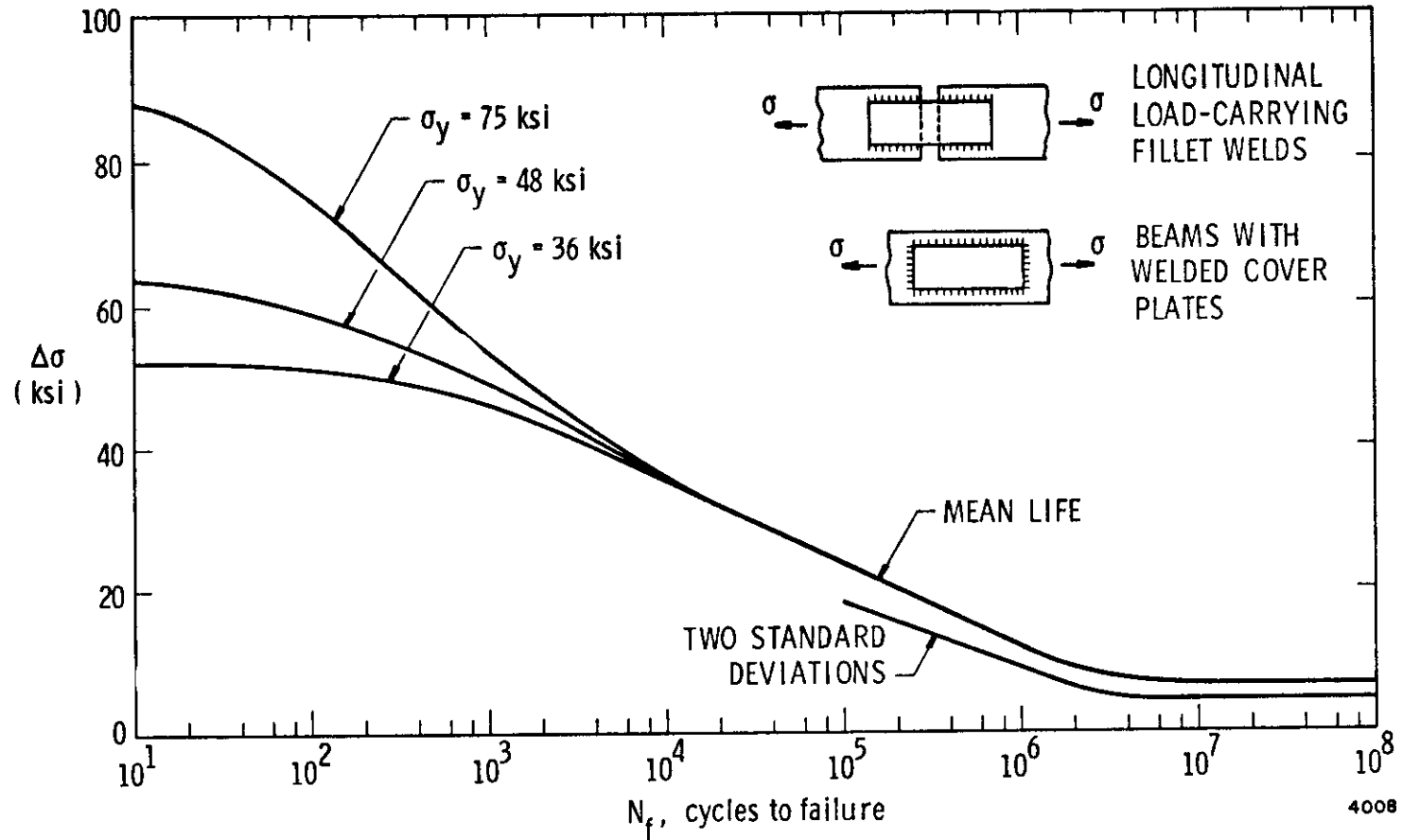


Figure 59.  $\Delta\sigma$ - $N_f$  curves for Type 6 weldments

With this purpose in mind the following spectrum has been derived based upon stress measurements taken on 10 voyages of the S.S. Wolverine State during 1964-65.<sup>(109)</sup> These voyages encountered a variety of sea states, and the data acquired reflected Beaufort Nos. 1 to 10 inclusive. These Beaufort Nos. were grouped into five Weather Groups (WG's) for purposes of describing the spectrum in five discrete blocks. The spectrum derived from the Wolverine State data, while not necessarily representing actual current ship data, does serve as a guide and as a tentative spectral criterion for estimating fatigue life.

TABLE 7. WOLVERINE STATE LOAD SPECTRAL DATA USED IN CRITERION

<u>Weather Group</u>	<u>Beaufort Numbers</u>	<u>% Total Load Cycles</u>	<u>Fraction of <math>\sigma_{rms}</math> in WG II</u>	<u><math>\Delta\sigma/\sigma_{rms}</math></u>
I	1 & 2	40	0.700	2.355
II	3 & 4	40	1.000	3.364
III	5 & 6	15	1.536	5.166
IV	7 & 8	4	1.964	6.607
V	9 & 10	1	2.343	7.881
		100		

The relationship between  $\Delta\sigma$  and  $\sigma_{rms}$ , given as the last column above, was computed from the relation  $\Delta\sigma = 2\sqrt{2} \left[ \Gamma(1 + b/2) \right]^{1/b} \sigma_{rms}$  presented in Section II. E. 5 of this report. The parameter b was chosen as 4.0 for calculations.

## 2. Implications

The technical discussion just presented leads to the following state-of-the-art summary regarding crack initiation and subcritical crack growth in ship steels:

- (a) SCC is not a factor in the fatigue resistance of ship steels having yield strengths up to 100 ksi.
- (b) Fatigue problems develop first at structural weldments,

for there fatigue damage resistance is much less than in the base steel plate.

- (c) The fatigue strength of typical weldments is independent of yield strength in the region  $N_f > 10^5$  cycles, wherein nearly all of the fatigue life resides. Also, crack growth rates  $da/dN$  are indifferent to  $\sigma_Y$  for yield strengths at least up to 100 ksi. From these observations, it is concluded that the crack initiation process in critical weldments is essentially independent of the yield strength of the base material.

These conclusions, in turn, lead to the implication that HSLA steels are no worse than mild steels from a crack initiation and subcritical crack growth standpoint. In fact, they emerge as somewhat better considering the relatively few high level stress cycles which can be expected, on statistical grounds, to occur within the spectral distribution of loads. It is impossible, however, without some specific knowledge of the expected fatigue loads envelope for a given ship, to associate a numerical index of the improved spectral fatigue resistance of HSLA steels. HSLA steels are most apt to be integrated into primary ship structure from static design and other factors. Their resistance to fatigue will depend principally upon the endurance limit (and its scatter, or dispersion) of the weldment in question, and not upon the yield strength.

Typically, during its lifetime a cargo ship may be expected to experience between  $10^7$  and  $10^8$  cycles of load in its primary structure. The strength levels at these cyclic lives (see Figures 54-59) are relatively high compared to the stresses in conventional ship structure deployed today. (107) Thus, contemporary ship design is doubly conservative with respect to fatigue resistance: the operating stresses are low compared with the weldment endurance strengths, beyond which design based on endurance strength (infinite life) is a conservative design philosophy.

If one considers, as here, the crack initiation period to be that number of cycles needed to "make-up" the difference between total life and propagation life, the criterion forecasts that  $N_i$  is generally much greater than  $N_p$ . In ship primary structures the operating stresses are low in keeping with the large number of load cycles expected. At these stresses nearly all the life is consumed in initiating a crack, and the lower the cyclic stresses, the more so. The implication in terms of NDI is clear: NDI systems should be concerned primarily with initial flaw detection. Once a crack has initiated, its growth rate may be very high (regardless of yield strength level) and short inspection intervals are then required to prevent sudden failures.

All of the remarks just made must be tempered with one fact: the data base upon which this criterion has been built is, in certain respects,

incomplete. There are a number of areas in which enough or the right kind of experimental results simply do not exist to enable the confident, orderly pyramiding of knowledge which characterizes sound engineering practice. In these situations, assumptions have had to be made concerning fatigue life and subcritical crack growth, assumptions which if later proven to be poor could undermine the conclusions drawn from this study. Section V.B of this report discusses these areas in some detail.

#### D. Tentative Criterion for Fatigue Resistant Design of Ships

Two simple procedures are set forth here to provide design guidance for fatigue resistant ship design. The rationale which underlies these procedures was given earlier in Section IV.C.1. For the reasons explained therein, the yield strength of the material does not enter as a direct parameter in applying this criterion. Following this section, in Section IV.E there is given an example to illustrate the use of these procedures in a typical ship structural application.

##### Procedure 1

This procedure enables the designer to design for indefinite fatigue life  $N_f$  of primary ship structural weldments. It is based upon the endurance strengths for welded steel structures presented as Figures 54-59 in Section IV.C.1. Since this procedure is intended to insure indefinite fatigue life, it is a more conservative criterion than that given in Procedure 2 below, which enables finite design life criteria to be accommodated.

The procedure simply involves determining, for a particular weldment configuration, the endurance limit from Table 8. (For illustrations of these joint types, see Figures 54-59, Section IV.C.1) The designer should use the endurance strength corresponding to two standard deviations below the mean endurance strength, for conservative design. (The mean endurance strength is to be used for design only when there is additional justification that such a procedure will still be conservative for a given weldment). The value of the endurance limit thus chosen is the maximum stress range  $\Delta\sigma$  that can be tolerated consistent with indefinite fatigue life. It is to be considered as a fatigue design allowable, not to be exceeded unless justified by cumulative damage calculations. Note that  $\Delta\sigma$  is taken as the algebraic difference between the maximum and minimum extensional stresses, without regard to tension or compression. In order to convert from the stress range  $\Delta\sigma$  to the corresponding rms endurance limit  $\sigma_{rms}$ , the relation

$$\sigma_{rms} = \frac{0.3536\Delta\sigma}{[\Gamma(1 + b/2)]^{1/b}} \quad (39)$$

is to be used (cf Section II. E. 5). The parameter  $b$  is given in Table 8 for each weldment type, and  $\Gamma$  is the gamma function. For convenience in using the above expression this function is plotted in Figure 60.

TABLE 8. DESIGN ENDURANCE LIMITS FOR STRUCTURAL WELDMENTS

Weld Joint Type	Description	$b^*$	Endurance Limit ( $\Delta\sigma$ , ksi)	
			Mean	2 Std. Dev. from Mean
1	Continuous Automatic Longitudinal Butt Weld	4.51	19.0	16.8
2	Continuous Automatic Longitudinal Fillet Weld	3.62	15.3	9.5
3	Continuous Manual Longitudinal Fillet Weld	3.27	12.0	8.0
4	Stiffener-to-Web Joint	2.95	11.0	8.0
5	Transverse (Non-Load-Carrying) Fillet Weld, etc.	2.94	9.8	5.0
6	Longitudinal (Load-Carrying) Fillet Welds; Beams with Welded Cover Plates	3.15	6.5	4.3

\* The constant in  $N_f \sigma^b = \text{constant}$ , which characterizes the mean  $\Delta\sigma - N_f$  relationship in the high cycle region.

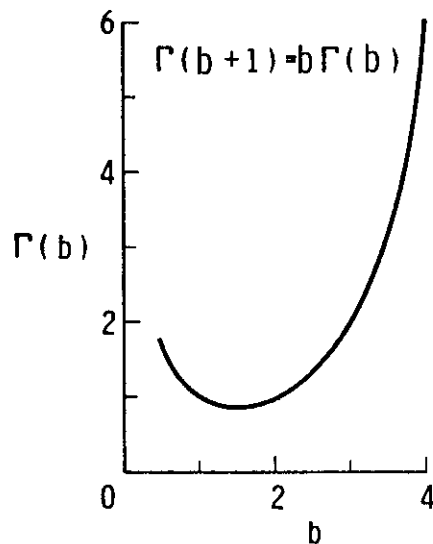


Figure 60. Gamma function

It should be mentioned that the fatigue stress allowables given in Table 8 can be raised by entering Figures 54-59 for a finite number of cycles. Usually, however, the gain in stress allowables is achieved only at the expense of a substantially reduced fatigue life.

### Procedure 2

As a companion to Procedure 1, this procedure enables design estimates to be made of the fatigue stresses for spectral loading. It is less conservative than the preceding procedure, as it is intended to apply to finite life designs. This procedure should be regarded as a guide only, for its applicability depends upon the spectra similarity between the ship in question and the Wolverine State, on which this procedure is based (cf Section IV.C.1).

The procedure makes use of two curves which have been prepared on the basis of the fatigue spectrum discussed in Section IV.C.1. Figure 61 gives the fatigue crack initiation period,  $N_i$ , in ship service years, for the same six weldment types discussed in the preceding procedure. For purposes of Figures 61 and 62 a ship service year is defined as  $1.728 \times 10^6$  cycles of load, which may accrue, e.g., from 200 operational days per calendar year, with a fundamental hog-sag bending frequency of 6 cpm. The total crack initiation period was determined by subtracting  $N_p$  from  $N_f$  for each Weather Group in the spectrum, and then summing the incremental values.

Figure 62 describes the dependence of the crack propagation life,  $N_p$  in service years, on the stress range (or  $\sigma_{rms}$ ).  $N_p$  has been determined from the expressions discussed in Section IV.C.1 for three values of  $a_o$  and for a terminal crack length (regarded as a failure condition) of 10 inches. The parameter  $a_o$  is taken to be one half the thickness of the thinnest plate in the weldment considered. Thus, for a 1 in. butt welded plate,  $a_o = 0.5$  inch. The curves in Figure 62 have been adjusted so that the  $N_p$  due to the spectral loading is the same as the  $N_p$  calculated using the constant value of  $\Delta\sigma$  corresponding to Weather Group II (Beaufort Nos. 3 & 4).

Figures 61 and 62, it should be pointed out, are based upon the parameter value  $b = 4$ , which is an average value typical of ship structural weldments (see Table 8.). While specific weldments have values of  $b$  somewhat different than 4.0 (typical values range from about 3.0 to about 4.5), the curves are not sensitive to these values. Also, the curves were established on the basis of the mean  $\Delta\sigma - N_f$  curves in Figures 54-59.

Through the use of Figures 61 and 62 it is possible to estimate the permissible value of  $\Delta\sigma$  (or  $\sigma_{rms}$ ) in WG II which corresponds to a chosen period  $N_i$  or  $N_p$ . By adding the  $N_i$  and  $N_p$ , any finite life can be accounted for in this procedure. Once the permissible fatigue stress level for WG II has been determined from these curves, the corresponding stress levels for

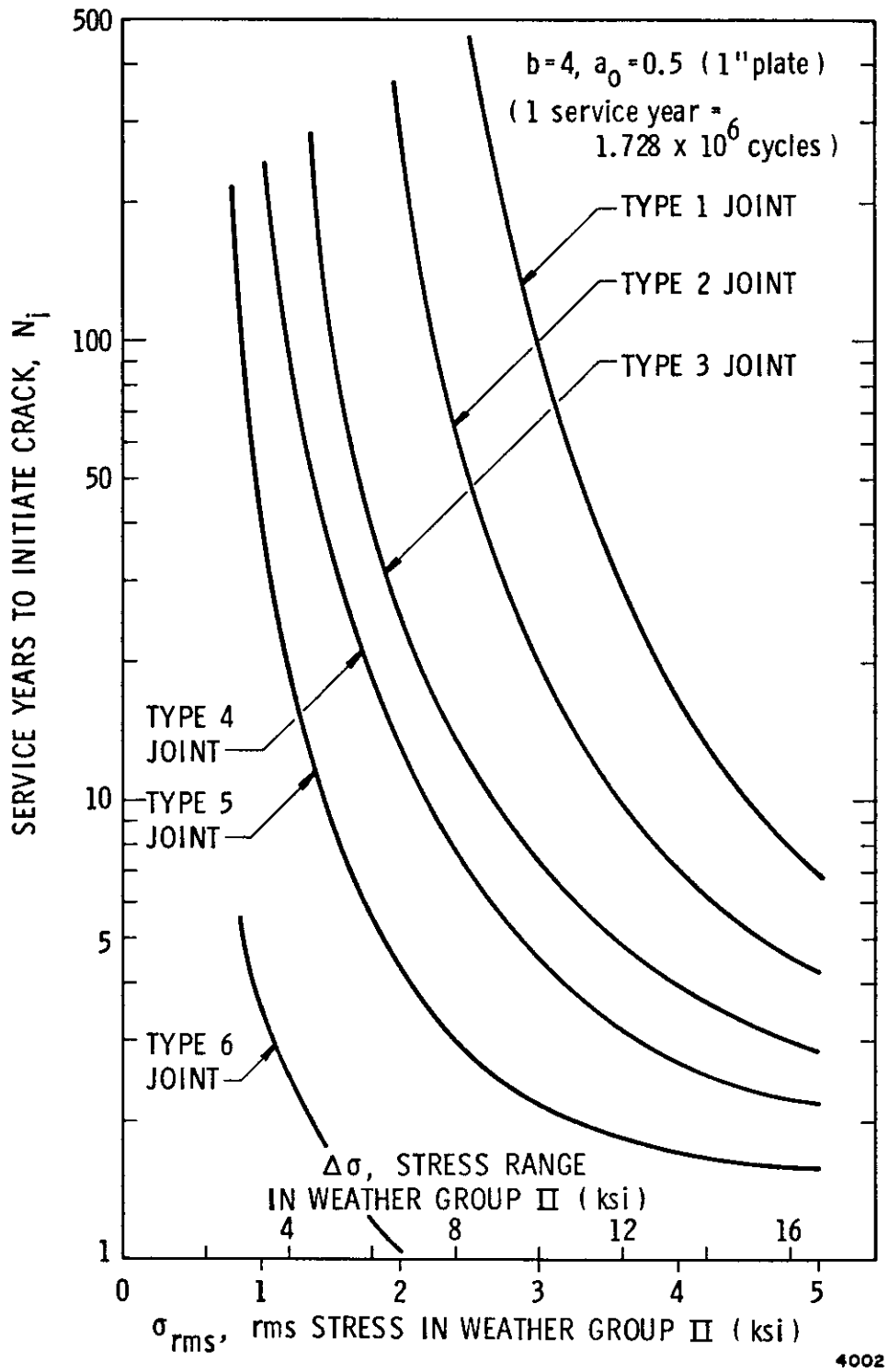


Figure 61. Crack initiation period, in service years, for typical weldments

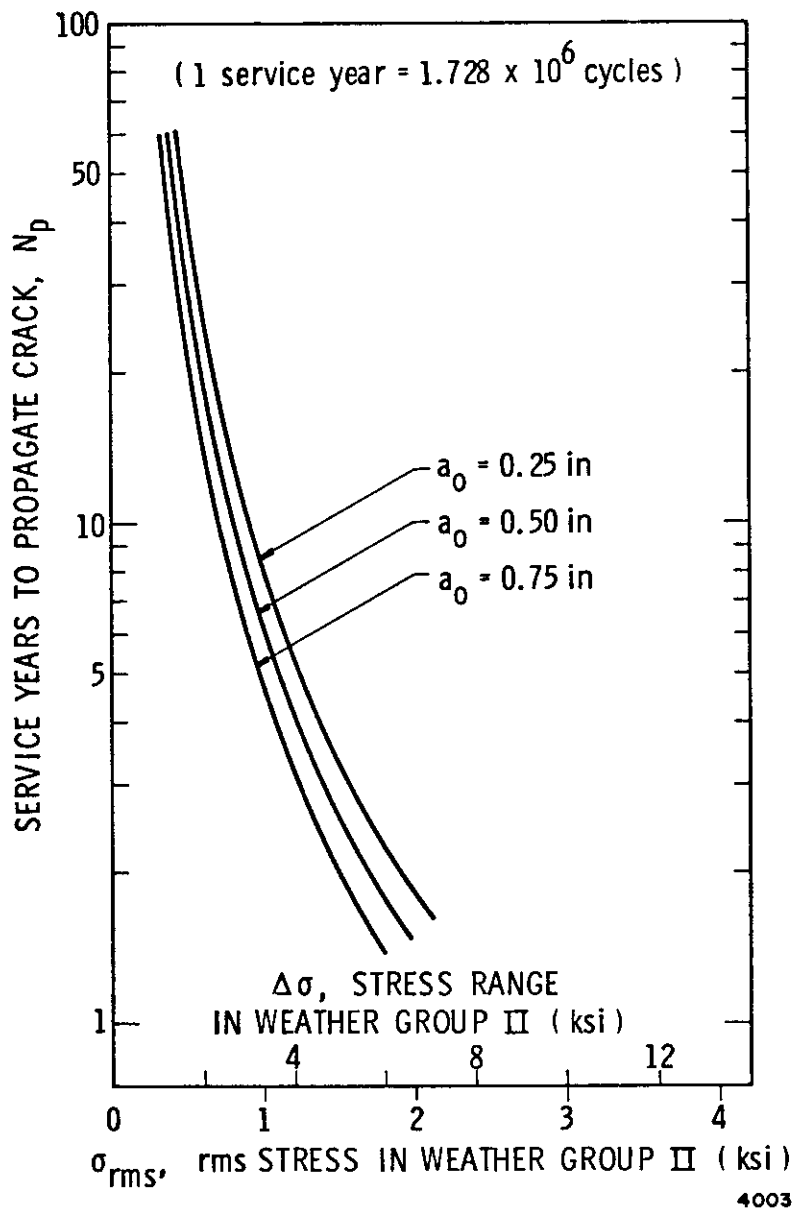


Figure 62. Crack propagation period, in service years, for various initial flaw sizes

the other Weather Groups can be found by apportioning the stresses in the following manner.

<u>Weather Group</u>	<u>Fraction of WG II <math>\sigma_{rms}</math></u>
I	0.700
II	1.000
III	1.536
IV	1.964
V	2.343

The stress levels so obtained constitute the design spectral loads envelope. The higher stresses found by this Procedure, those in WG IV and V, will normally be found to exceed the permissible  $\Delta\sigma$  (or  $\sigma_{rms}$ ) value established via Procedure I.

In the following Section an example is given to illustrate the use of these two procedures.

E. Example

As an example to illustrate the use of the criterion, consider the problem of estimating the fatigue life of welded steel deck plating. Assume the plating is joined by a continuous automatic longitudinal fillet welding process (Type 2, Figure 55). The ship under consideration, which has been designed initially from static loads criteria, has a fundamental bending frequency (hog/sag mode) of 6 cpm. The problem is to estimate the maximum permissible stress amplitudes in the plate consistent with a design life of at least 25 years (180 days/year operations).

As one approach to this problem, and the more conservative of the two to be discussed, the deck plating can be designed to insure that the peak stress amplitude in service never exceeds the endurance strength. From Table 8 in Section IV.D, the lower limit endurance strength for this type of weldment is  $\Delta\sigma = 9.5$  ksi. To obtain the correspondence between  $\Delta\sigma$  and  $\sigma_{rms}$ , the relation given as Equation (39) is to be used.\* Here,  $b = 3.62$  Table 8, Section IV.D, and  $\Gamma$  is the Gamma function. From this relationship it follows that  $\sigma_{rms} = 0.306 \Delta\sigma = 2.91$  ksi.

---

\* Assuming, as here, that in the case of zero mean stress  $\sigma_{max} = \Delta\sigma/2$ .

These equivalent stress values,  $\Delta\sigma = 9.5$  ksi and  $\sigma_{\text{rms}} = 2.91$  ksi, represent the highest admissible levels that the deck plating can be expected to tolerate with indefinite life. Higher stress levels, of course, could be sustained for finite design lives.

To appreciate the tradeoff between stress level and fatigue life, suppose that the peak stress envelope was raised from  $\sigma_{\text{rms}} = 2.91$  ksi to  $\sigma_{\text{rms}} = 3.20$  ksi, an increase of 10%. The corresponding sinusoidal stress level is  $\Delta\sigma = 3.20/0.306 = 10.5$  ksi. From Figure 55, Section IV.C.1, the expected life now becomes  $N_f = 4.5 \times 10^6$  cycles, or, at 6 cpm and 180 operational days per year, 2.89 calendar years. Thus, for this example, a reduction in life from indefinite to 2.89 years is a heavy price to pay for a 10% increase in cyclic stress allowables.

It should be noticed that in this constant-amplitude stress calculation, material strength effects do not enter in for design lives  $N_f > 10^5$  cycles.  $10^5$  cycles, incidentally, is operationally equivalent to 11.6 days. In view of this, it can safely be said that yield strength effects will have no influence on constant-amplitude cyclic stress allowables.

As an alternative approach, it will be interesting to examine this design problem from the standpoint of spectral analysis. To do this it is necessary first to define the expected root-mean-square stress level  $\sigma_{\text{rms}}$  for the sea state corresponding to Weather Group II. From this parameter the values of  $N_i$  and  $N_p$ , and hence  $N_f = N_i + N_p$ , can be obtained from Figures 61 and 62, Section IV.D. Notice that in using these figures an adjustment must be made from the 200 operational days per year on which the figures are based to the 180 operational days per year for the problem at hand. The results of such calculations may be summarized as follows:

$\sigma_{\text{rms}}$ in WG II (ksi)	$N_i$ (years)	$N_p$ (years)	$N_f$ (years)
0.5	$\infty$	34.5	$\infty$
1.0	$\infty$	7.0	$\infty$
2.0	310	1.8	311.8
3.0	24	negligible	24
4.0	7.9	"	7.9
5.0	4.7	"	4.7

In calculating  $N_p$  a value of  $a_o = 0.5$  in. (1-in. plate) was assumed. Corresponding values for differing plate thicknesses can be calculated directly from Figure 62, Section IV.D. These figures serve to show that  $N_p$  is negligible at moderate-to-high values of  $\sigma_{rms}$ , and that  $N_i$  is always in excess of  $N_p$  in the high-cycle fatigue regime of interest to ship design. For the problem at hand, it is possible to establish a maximum permissible Weather Group II cyclic stress environment for a specified design life, say 25 calendar years. By plotting  $\sigma_{rms}$  as a function of  $N_f$ , both of which are found in the foregoing calculation summary, it is found that  $\sigma_{rms} = 2.95$  ksi for WG II for the stated design life. In fact, from this the permissible stress levels for each Weather Group may be found as follows:

W.G.	% $\sigma_{rms}$	% cycles	$\Delta\sigma/\sigma_{rms}$	$\Delta\sigma$ (ksi)	$\sigma_{rms}$ (= .306 $\Delta\sigma$ , ksi)
I	0.7000	40	2.3545	6.95	2.12
II	1.000	40	3.3636	9.92	3.04
III	1.5357	15	5.1655	15.2	4.66
IV	1.9643	4	6.6071	19.5	5.96
V	2.3429	<u>1</u>	7.8806	23.2	7.11

100

These calculated values of  $\sigma_{rms}$  for each Weather Group for a 25 calendar year design life may be compared with the more conservative constant  $\sigma_{rms}$  value of 2.91 ksi found according to Procedure 1.

To summarize, in neither of the two approaches (constant-amplitude cyclic load or spectral loads distribution) did the yield strength of the material affect the calculated fatigue stress allowables or lifetimes. For the example at hand, if the stresses are maintained always below  $\sigma_{rms} = 2.91$  ksi ( $\Delta\sigma = 9.5$  ksi) the ship decking under consideration should have an indefinite life. Increasing this level by about 10% to  $\sigma_{rms} = 3.2$  ksi, however, brings the expected life down to 2.89 calendar years. It is possible, however, to operate at somewhat higher stress levels based on the more realistic spectral load estimates. For realistic ship design lives the crack propagation period  $N_p$  is very small when compared with  $N_i$ . The calculations made for purposes of this example used the mean  $\Delta\sigma - N_f$  relationship, not accounting for scatter. Estimates of the scatter effect may, however, be made on the basis of Figures 54-59. Finally, it should be clear that if the designer has some particular knowledge of the expected stress spectrum for the particular ship under consideration, these can be used in a conventional linear cumulative damage analysis (cf Section II. E. 1) to derive more reliable ship life estimates.

## V. CONCLUSIONS AND RECOMMENDATIONS

### A. Significance of Crack Initiation and Growth in HSLA Ship Steels

This study has been concerned with the factors which influence crack initiation and subcritical crack growth in conventional mild steel and in high-strength low-alloy (HSLA) primary and secondary cargo ship structure exposed to typical sea environments. Under normal operating conditions the structural components of interest experience a low-frequency, narrow-band random dynamic response to the sea. Under conventional fabrication techniques, the potential for crack initiation and subsequent propagation exists almost exclusively in welded regions and their associated heat-affected zones. This potential, in addition, is very sensitive to the quality of the welding procedures and technique used during shipyard fabrication and only by scrupulous adherence to the strictest quality control measures can one hope to avoid problems of crack initiation and propagation during in-service operations.

For purposes of discussing the mechanics of the process, the total number of load cycles-to-failure,  $N_f$ , has been assumed to be composed of  $N_i$ , the number of cycles required to initiate a crack, plus  $N_p$ , the number of cycles needed to propagate the crack to some critical length. It was found that under conditions typical of service, cracks will usually initiate (if at all) in the weld or HAZ, and that by far the greatest portion of life is spent in crack initiation:  $N_i/N_p \gg 1$ . It is, however, impossible at the present time to determine  $N_i$  directly for structural weldments, and recourse must be made to the indirect determination  $N_i = N_f - N_p$ , since both  $N_f$  and  $N_p$  can be measured to an acceptable level of confidence. It was found that  $N_i$  is not sensibly affected by the strength level of the weldment under consideration, but is more strongly influenced by the geometry of the detail (i. e., stress concentrations), by the nature and distribution of the flaws introduced during the weld process, and by the operating stress levels.

The crack propagation rate likewise appears to be insensitive to the strength level, although the role of residual and constraint stresses is not entirely clear.  $N_p$ , the number of cycles required to carry an existing crack from an initial length  $a_0$  to a critical length  $a_{CR}$ , depends only upon the applied stress range, and upon  $a_0$  and  $a_{CR}$  themselves. Experience has also shown that the crack propagation rate,  $da/dN$ , is greater in the parent material than in either the weld or HAZ, and hence conservative design practice requires that values of  $da/dN$  that are characteristic of the base metal should be used.

In assessing the combined effects of  $N_i$  and  $N_p$ , the number of cycles to failure,  $N_f$ , is found to be independent of yield strength at stresses corresponding to lifetimes  $N_f \geq 5 \times 10^5$  cycles. Virtually all cyclic life is expended within this high-cycle regime. Thus, insofar as crack initiation and

subcritical crack propagation in ship steels are concerned, there is no important benefit or penalty associated with yield strength. Indeed, HSLA steels emerge as having no less fatigue resistance than mild steels, and the benefits that accrue from using HSLA steels to withstand the static design loads with reduced structural section may be enjoyed without sacrifice. HSLA steels may also be expected to possess enhanced fatigue resistance due to greater ability to withstand the overload cycles which, while few in number, do inflict increased fatigue damage on the structure.

The marine environment can, in some cases, severely restrict the ability of welded structure to serve faithfully its intended purpose. For example, it appears as though mild and HSLA ship steels (including Q & T steels) are immune to stress corrosion cracking in marine environments, although the critical weld and heat-affected zones at this time can not be declared sufficiently resistant to SCC to be ignored. A survey of the literature concerned with corrosion fatigue suggests that below the threshold SCC level,  $K_{I_{SCC}}$ , aggressive marine environments may have little or no effect on the rate of subcritical crack propagation. In this regime the mechanical variables, especially  $\Delta K$ , frequency, and wave form, dominate. At working stresses which place the crack tip above the  $K_{I_{SCC}}$  level, the environmental factors (temperature, humidity, thermochemistry) share the same role of importance as the mechanical variables. Insufficient data are available at present to include in the criterion provision for estimating the extent of the deleterious environmental effects. Great care must therefore be exercised in using data from specimens tested in relatively inert environments for design of structures exposed to aggressive marine environments, especially where corrosion fatigue at high-stress levels may be of concern.

Cathodic protection systems can be effective in minimizing corrosion, and can also be helpful in minimizing SCC and corrosion fatigue. The one potential danger in cathodic protection systems, however, is that there is a potential for hydrogen-induced SCC in HSLA Q & T steels. Coatings, in a variety of available types, are the most widely used protective systems to prevent general corrosion, and can be effective against SCC and corrosion fatigue if properly applied.

Using the proposed criterion, safe-life quality assurance can be provided by either of two approaches. In the first approach, and the more conservative of the two, weldment stresses are maintained below the endurance strength, leading to indefinite lifetimes. A somewhat less conservative design philosophy emerges from the alternative procedure given, in which a spectral loading distribution is assumed, and stress levels are determined in accordance with the desired service lifetime. It does appear, in general, that the stress level/lifetime tradeoff is an unrewarding one: substantial sacrifices in design lifetime may be the price to be paid for modest gains in operating stresses.

## B. Priority Problem Areas

Several areas warranting investigation in order to improve the utility of, and confidence in, the proposed criterion are outlined below, in descending order of importance to the criterion:

1. Expand Data Base of Fatigue Life of Welded Joints. A program to improve and expand on the inventory of data presented in Figures 54-59 needs to be undertaken, to include the effects of marine environments, more joint types common to ship primary structure, and U. S. steel types (the data in the criterion are all based on British specification steels). This would mean gathering existing information from British Welding Institute, and American organizations known to be working in this area currently, where such data are not in the literature. Then, an experimental program would be undertaken to fill in gaps.

2. SCC Properties of Ship Steels. There presently are no published data on the SCC properties of the low- and high-strength alloy steels and HAZs of interest to the purposes served by this report. An experimental program needs to be undertaken to confirm or qualify the assumption of the criterion that SCC can be ignored.

3. Effects of Residual Stresses Due to Welding on Subcritical Crack Growth. The residual stresses which exist in welded coupon specimens are generally not as high as those found in actual structure due to the lack of external (structural) constraint. Fatigue life tests should be made on coupons in which realistic residual stresses are present, to determine whether the design data of Figures 54-59 are realistic. This experimental work would also serve to test the assumption that crack growth rate is independent of  $R$  and depends only on  $\Delta\sigma$ ; this assumption may be invalid under the wide range of minimum stresses present in actual welded structures. This effort would also include ancillary studies to determine whether the observed difference in crack growth rate in parent vis-a-vis weld material is due to the difference in microstructure or to residual stresses.

4. Environmental Effects on Crack Growth Rate. Crack growth data for low- and high-alloy steels need to be generated for  $R \neq 0$  in aggressive marine environments to test validity of current theories (such as Equation (6)), which do not account for  $R$ . This needs to be done so that this work can be included in the criterion. Also, the effect of frequency on environmentally conditioned crack growth needs to be established for sinusoidal and random loading. These effects are known to be important in higher strength steels (such as the maraging steels).

5. Validation of Criterion. An experimental program should be organized to "exercise" the criterion, to ensure that it is capable of producing correct prediction differentials between various ship steels. This must be done to validate the general framework and to gain confidence in it.

6. Improved Design Loads Spectra. The spectral loading data presented in Table 7 and carried on into Procedure 2 of the criterion are drawn from incomplete records of a single ship. A research program should be undertaken in which ship response data are generated for other cargo vessels, and these results then condensed into design spectral loading data as a function of ship length, loading condition, and seas traveled. As a part of this study, the desirability and feasibility of generating "standardized" random crack growth data, to replace the sinusoidally-based data of the criterion, should be made. The purpose of this undertaking would be to eliminate the step of calculating a "damage equivalence" between  $\Delta\sigma$  and  $\sigma_{rms}$ , and simply reference both the loading and the weldment fatigue properties to the random sea/structural environment.

7. Generation of  $\Delta K_{th}$  and  $\Delta K_T$  Data.  $\Delta K_{th}$  and  $\Delta K_T$  data are not available for relevant low- and high-strength steels, and this information is needed in the criterion. An experimental program should be undertaken to provide this information under a standard benign atmosphere, and under various corrosive environments. Data thus obtained would also be used to test the validity of the crack growth relation  $da/dN \approx (\Delta K)^{2.25}$ , used in the criterion, under various environments.

8. Cathodic Protection Effects. An experimental research program needs to be conducted to determine the effects of various cathodic protection systems on crack initiation and subcritical growth. Are either or both regimes affected by cathodic protection? Ancillary to this investigation is the importance of determining whether or not SCC cracks are in fact a source of initiation.

The areas of investigation outlined above are considered to be of primary importance to qualifying the criterion, herein proposed tentatively. In addition to these areas which are directly linked to the criterion, these are also ancillary technical questions that arise in connection with implementing the criterion. Two of these are mentioned here.

The first question concerns the current practice and technology of weldment NDI as related to ship structures. The criterion brought out the fact that the crack initiation process heavily dominates the propagation process in ship loading environments. Inasmuch as the criterion allows for some increase in working stresses over present practice, the early detection of subcritically propagating cracks assumes even greater importance. It should be determined whether current NDI technology and procedures as applied to ship structure are adequate to enable full implementation of the criterion for HSLA steels.

The second area of related interest concerns the development of data and design guidelines for introducing crack arrest devices in critical ship structural areas. These devices, in actual fact, consist of structural design principles such as structural reinforcement techniques which will serve to retard or arrest dangerous subcritically-propagating cracks.

## VI. REFERENCES

1. Schijve, J., "Significance of Fatigue Cracks in Micro-Range and Macro-Range," FATIGUE CRACK PROPAGATION, ASTM STP 415, 415-459, 1967.
2. Forman, R. G., "Study of Fatigue Crack Initiation from Flaws Using Fracture Mechanics Theory," Engineering Fracture Mechanics, Vol. 4, No. 2, 333-345 (June 1972).
3. Barsom, J. M., and McNicol, R. C., "Effect of Stress Concentration on Fatigue-Crack Initiation in HY-130 Steel," ASTM STP 559, American Society for Testing and Materials, August, 1974.
4. Clark, W. G., Jr., "An Evaluation of the Fatigue Crack Initiation Properties of Type 403 Stainless Steel in Air and Stream Environments," ASTM STP 559, American Society for Testing and Materials, August, 1974.
5. Topper, T. H., Wetzel, R. M., and Morrow, J., "Neuber's Rule Applied to Fatigue of Notched Specimens," Journal of Materials, Vol. 4, 200-209 (1969).
6. Gowda, C. V. B., Topper, T. H., and Leis, B. N., "Crack Initiation and Propagation in Notched Plates Subjected to Cyclic Inelastic Strains," MECHANICAL BEHAVIOR OF MATERIALS: VOL. II - FATIGUE OF METALS, Proceedings, International Conference on the Mechanical Behavior of Metals, Kyoto, 187-198, 1971.
7. Manson, S. S., and Hirschberg, N. H., "Crack Initiation and Propagation in Notched Fatigue Specimens," PROCEEDINGS OF THE FIRST INTERNATIONAL CONFERENCE ON FRACTURE, Sendai, Vol. 1, 479-498, 1966.
8. Barsom, J. M., "Fatigue Behavior of Pressure-Vessels," WRC Bulletin No. 194, Pressure Vessel Research Committee, May 1974.

9. Barsom, J. M., "Fatigue-Crack Propagation in Steels of Various Yield Strengths," Transactions of the ASME, Journal of Engineering for Industry, Vol. 93, 1190-1196 (1971).
10. Gurney, T. R., "The Effect of Mean Stress and Material Yield Stress on Fatigue Crack Propagation in Steels," Metal Construction and British Welding Journal, Vol. 1, 91-96 (1969).
11. Crooker, T. W., "The Role of Fracture Toughness in Low-Cycle Fatigue Crack Propagation for High-Strength Alloys," NRL Report 7422 (1972).
12. Tomkins, B., "Fatigue Crack Propagation - An Analysis," Philosophical Magazine, Vol. 18, 1041-1065 (1968).
13. Crooker, T. W., "Basic Concepts for Design Against Structural Failure by Fatigue Crack Propagation," NRL Report 7347 (1972).
14. Miller, G. A., "The Dependence of Fatigue Crack Growth Rate on the Stress Intensity Factor and the Mechanical Properties of Some High Strength Steels," ASM Transactions Quarterly, Vol. 61, 442-448 (1968).
15. Plumbridge, W. J., "Review: Fatigue Crack Propagation in Metallic and Polymeric Materials," Journal of Materials Science, Vol. 7, 939-962 (1972).
16. Heiser, F. A., and Hertzberg, R. W., "Anisotropy of Fatigue Crack Propagation," Transactions of the ASME, Journal of Basic Engineering, Vol. 93, 211-217 (1971).
17. Crooker, T. W., "Effect of Tension-Compression Cycling on Fatigue Crack Growth in High-Strength Alloys," NRL Report 7220 (1971).
18. Donahue, R. J., Clark, McI. H., Atanmo, P., Kumble, R., and McEvily, A. J., "Crack Opening Displacement and the Rate of Fatigue Crack Growth," International Journal of Fracture Mechanics, Vol. 8, 209-219 (1972).
19. Hickerson, J. P., and Hertzberg, R. W., "The Role of Mechanical Properties in Low-Stress Fatigue Crack Propagation," Metallurgical Transactions, Vol. 3, 179-189 (1972).

20. Gurney, T. R., FATIGUE OF WELDED STRUCTURES, Cambridge University Press, Cambridge, U.K. (1968).
21. Lawrence, F. V. and Munse, W. H., "Fatigue Crack Propagation in Steel Weldments," SAE Paper 720267, January 10-14 (1972).
22. Burdekin, F. M., Harrison, J. D., and Young, J. G., "The Effect of Weld Defects with Special Reference to B.W.R.A. Research," Institute of Welding Non-Destructive Testing Conference, London, February, (1967).
23. Savage, W. F. and Szekeres, E. S., "Technical Note: A Mechanism for Crack Formation in HY-80 Steel Weldments," Welding Research Supplement, 94-96 (1967).
24. Warren, W. G., "Fatigue Tests on Defective Butt Welds," Welding Research Supplement, Vol. 6, (1952).
25. Newman, R. P., "The Influence of Weld Faults on Fatigue Strength with Reference to Butt Joints in Pipe Lines," Transactions of the Institute for Marine Engineering, Vol. 68, 153-172 (1956).
26. Newman, R. P. and Gurney, T. R., "Fatigue Tests on Plain Plate Specimens and Transverse Butt Welds," British Welding Journal, Vol. 6, 569-594 (1959).
27. Yamaguchi, I., Tereda, Y., and Nitta, A., "On the Fatigue Strength of Steels for Ship Structures," International Institute of Welding Documentation, No. XIII, 425 ff (1966).
28. Sanders, W. W., Derecho, A. T., and Munse, W. H., "Effect of External Geometry on Fatigue Behavior of Welded Joints," Welding Research Supplement, Vol. 30, (1965).
29. Signes, E. G., Baker, R. G., Harrison, J. D., and Burdekin, F. M., "Factors Affecting the Fatigue Strength of Welded High Strength Steel," British Welding Journal, Vol. 14, 108-116 (1967).
30. Lawrence, F. V. and Radziminski, J. B., "Fatigue Crack Initiation and Propagation in High-Yield-Strength Weld Metal," Welding Research Supplement, Vol. 35, 445-452 (1970).

31. Maddox, S. J., "Fatigue Crack Propagation in Weld Metal and HAZ," Metal Construction and British Welding Journal, Vol. 2 , 285-289 (1970).
32. Watanabe, M., Nagai, K., Otsuka, A., and Nagata, Y., "A Study of Fatigue Strength in Weld Metal and H.A.Z. of Mild Steel Weld," Journal of the Japanese Welding Society, Vol. 36, 55-63 (1967).
33. Ohta, S., "Fatigue Properties in Notched Steel Plates and the Effect of Welding on Them," Quarterly Report of the Railway Technical Research Institute, Vol. 11, 79-83 (1970).
34. Watanabe, M., Yoshino, Y., Watanabe, I., and Aoki, H., "Variation in the Positions Where the Welded Joints of HT 80 Failed in the Fatigue Test," Transactions of the Japanese Welding Society, Vol. 39, 98-104 (1970).
35. Dowse, K. R., and Richards, C. E., "Fatigue Crack Propagation Through Weld Heat Affected Zones," Metallurgical Transactions, Vol. 2, 599-603 (1971).
36. Akaike, H., and Swanson, S. R., "Load History Effects in Structural Fatigue," Proceedings of the 15th Annual Meeting of the Institute of Environmental Sciences, Anaheim, April 20-24, 1969, pp 66-77.
37. Palmgreen, A., "Die Lebensdauer von Kvgellagern," Verein Deutscher Ingenieure Zeitschrift, Vol. 68, 339 ff (1924).
38. Miner, M. A., "Cumulative Damage in Fatigue," Transactions of the ASME, Journal Applied Mechanics, Vol. 67, pp A159-A164, (1945).
39. Saunders, S. C., "A Review of Miner's Rule and Subsequent Generalizations for Calculating Expected Fatigue Life," M.I.S. Report No. 45, Boeing Company, December, (1970)
40. Miner, M. A., "Estimation of Fatigue Life with Particular Emphasis on Cumulative Damage," in: METAL FATIGUE, Edited by G. Sines and J. L. Waisman, McGraw-Hill Book Company, Inc., pp 278-289 (1959).
41. O'Neill, M. J., "A Review of Some cumulative Damage Theories," Aeronautical Research Laboratory, Structures & Materials Report 326, Melbourne, June 1970.

42. Gucer, D. E. and Capa, M., "Frequency Effects in Low-Cycle Fatigue," Metallurgical Transactions, Vol. 1, 3075-3081, November, 1970.
43. Carden, A. E., "Bibliography of the Literature on Multiaxial Stress Fatigue," Report No. MH-67-AEC-2, College of Engineering, University of Alabama.
44. Marin, J., MECHANICAL BEHAVIOR OF ENGINEERING MATERIALS, Prentice-Hall, Englewood Cliffs, 204-214 (1962).
45. Blatherwick, A. A., and Viste, N. D., "Cumulative Damage Under Biaxial Fatigue Stress," Materials Research and Standards, Vol. 7, No. 8, 331-336, August 1967.
46. Havard, D. G., and Topper, T. H., "Biaxial Fatigue of 1018 Mild Steel at Low Endurance," Proceedings of the First International Conference on Pressure Vessel Technology, Delft, ASME, 1267-1277, 1969.
47. Miles, J. W., "On Structural Fatigue Under Random Loading," Journal of Aeronautical Sciences. Vol. 21, 753-762 (1954).
48. Crandall, S. H., and Mark, W. D., RANDOM VIBRATION IN MECHANICAL SYSTEMS, Academic Press, New York, 112-125, 1963.
49. Madayag, A. F., (Ed.), METAL FATIGUE: THEORY AND DESIGN, John Wiley & Sons, Inc., New York, Chapter 8, (1969).
50. Judy, R. W., Jr., and Goode, R. J., "Stress Corrosion Cracking of High Strength Steels and Titanium Alloys," Welding Research Supplement, September, 1972, pp 437S-445S.
51. Reinoehl, J. E. and Boyd, W. K., "The Use of Slow Strain Rate Experiments in Evaluating Resistance to Environmental Cracking," Specialist Meeting on Stress Corrosion Testing Methods, AGARD Conference Proceedings No. 98, January, 1972, pp 299-302.
52. Phelps, E. H., "A Review of the Stress Corrosion Behavior of Steels with High Yield Strength," Proceedings of Conference on Fundamental Aspects of Stress Corrosion Cracking, pp 398-410, National Association of Corrosion Engineers, Houston, 1969.

53. Brown, W. F., Jr., and Srawley, J. E., Plane-Strain Crack Toughness Testing of High-Strength Metallic Materials, ASTM STP 410, 1966.
54. Brown, W. F., Jr., ed., Fracture Toughness Testing and Its Applications, ASTM STP 381, 1965.
55. "Tentative Method of Test for Plane-Strain Fracture Toughness of Metallic Materials," ASTM Designation E399-70T.
56. Brown, F. G., "Metals and Corrosion," Machine Design, January 18, 1968, pp 165-173.
57. Logan, H. L., "SCC in Low-Carbon Steel," Physical Metallurgy of Stress Corrosion Cracking, AIME, Interscience, 1959, pp 341-372.
58. Sutcliffe, J. M., Fessler, R.R., Boyd, W. K., and Parkins, R. N., Stress Corrosion of Carbon Steel in Carbonate Solutions," Corrosion, Vol. 28, No. 8, October, 1972, pp 313-320.
59. Mazille, H., and Uhlig, H. H., "Effect of Temperature and Some Inhibitors on SCC of Carbon Steels in Nitrate and Alkaline Solutions," Corrosion, Vol. 28, No. 11, November 1972, pp 427-433.
60. Engell, H. J., and Baumel, A., "The Electrochemical Mechanism of Stress Corrosion Cracking of Mild Steel," Physical Metallurgy of Stress Corrosion Cracking, AIME Interscience, 1959, pp 341-372.
61. Sandoz, G., "The Effects of Alloying Elements on the Susceptibility to Stress Corrosion Cracking of Martensitic Steels in Salt Water," Metallurgical Transactions, Vol. 2, April 1971, pp 1055-1063.
62. Schmitt, R. J., and Phelps, E. H., "Corrosion Performance of Constructional Steels in Marine Applications," Journal of Metals, Vol. 22, 47-55 (1970).
63. Novak, S. R., "Effect of Plastic Strain on  $K_{ISCC}$  of HY-80, HY-130(T) and 12 Ni - 5 Cr - 3 Mo Steels," U. S. Steel Applied Research Laboratory Report No. 39.018-007(20), January 1, 1968.

64. Leckie, H. P., and Loginow, A. W., "A Comparison of the Stress Corrosion Behavior of Some High-Strength Steels," U. S. Steel Applied Research Laboratory Report No. 39.001-001(2), July 15, 1968.
65. Smith J. H., and Davis, J. A., "Stress-Corrosion and Hydrogen Embrittlement Cracking Behavior of HY-80 and HY-130 Weld Metals," U. S. Steel Applied Research Laboratory Report No. 89.021-024(4) (B-63304), 40.001-021(8), January 8, 1971.
66. Townsend, H. E., Jr., "Resistance of High Strength Structural Steel to Environmental Stress Corrosion Cracking," Stress Corrosion Cracking - A State of the Art, ASTM STP 518, American Society for Testing and Materials, 1972, pp 155-166.
67. Smith, J. H., and Rolfe, S. T., "Effects of Welding Position on the  $K_{ISCC}$  of HY-130(T) Weld Metals," U.S. Steel Applied Research Laboratory Report No. 39.018-016(7) (a-ORD-NP-3) (B-23204), January 1, 1968.
68. Lowenberg, A. L., et al, "High-Strength, Low-Alloy Steel Weldments," First Technical Report, SSC-199, NAVSEC Contract N00024-67-C5416, Ship Structure Committee, August 1969, p 25.
69. Duquette, D. J., "A Review of Aqueous Corrosion Fatigue," Corrosion Fatigue: Chemistry, Mechanics, and Microstructure, Proceedings of Conference held at the University of Connecticut, June 14-18, 1971; National Association of Corrosion Engineers, 1972, pp 12-24.
70. McEvily, A. J., and Wei, R. P., "Fracture Mechanics and Corrosion Fatigue," Corrosion Fatigue: Chemistry, Mechanics, and Microstructure, Proceedings of Conference held at the University of Connecticut, June 14-18, 1971; National Association of Corrosion Engineers, 1972, pp 12-24.
71. Gallagher, J. P., and Sinclair, G. M., "Environmentally Assisted Fatigue Crack Growth Rates in SAE 4340 Steel," Journal of Basic Engineering, Transactions of the ASME, Vol. 91, 1969, p 598.

72. Wei, R. P., and Landes, J. D., "Correlation Between Sustained Load and Fatigue Crack Growth in High Strength Steels," Materials Research and Standards, ASTM, Vol. 9, July, 1969, p 25.
73. Gallagher, J. P., "Corrosion Fatigue Crack Growth Rate Behavior Above and Below  $K_{I_{SCC}}$  in Steels," Journal of Materials, Vol. 6, 1971, p 941.
74. Crooker, T. W., and Lange, E. A., "The Influence of Salt Water on Fatigue Crack Growth In High Strength Structural Steels," Effects of Environment and Complex Loading History on Fatigue Life, ASTM STP 462, 1970, p 258.
75. Crooker, T. W., and Lange, E. A., "Corrosion Fatigue Crack Propagation of Some New High Strength Structural Steels," Journal of Basic Engineering, Transactions of the ASME, Vol. 91, 1969, p 570.
76. Gallagher, J. P., "Corrosion Fatigue Crack Growth Behavior Above and Below  $K_{I_{SCC}}$ ," NRL Report 7064, Naval Research Laboratory, Washington, D.C., May 1970.
77. Barsom, J. M., "Effect of Cyclic Stress Form on Corrosion Fatigue Crack Propagation Below  $K_{I_{SCC}}$  in a High Yield Strength Steel," *Ibid.*, pp 424-436.
78. Barsom, J. M., Sovak, J. F., and Imhof, E. J., Jr., "Corrosion Fatigue Crack Propagation Below  $K_{I_{SCC}}$  in Four High-Yield Strength Steels," Technical Report 89.021-024(3), United States Steel Applied Research Laboratory, Monroeville, Pennsylvania, December 14, 1970.
79. Gould, A. J., "Influence of Temperature on Severity of Corrosion Fatigue", Engineering, Vol. 141, 1936, p 495.
80. Cornet, I., and Golan, S., "Influence of Temperature on Corrosion Fatigue", Corrosion, Vol. 15, 1959, p 262 t.
81. Sopwith, D. G., and Gough, H. J., "Some Comparative Corrosion-Fatigue Tests Employing Two Types of Stressing Action," Journal of the Iron and Steel Institute, Vol. 127, No. 1, pp 301-335, 1933.
82. Gould, A. J., "Corrosion Fatigue of Steel Under Assymmetric Stress in Sea Water," Journal of the Iron and Steel Institute, Vol. 161, Part 1, pp 11-16, January 1947.

83. Duquette, D. J., and Uhlig, H. H., "The Critical Reaction Rate for Corrosion Fatigue of 0.18% Carbon Steel and the Effect of pH," Transactions of the ASM, Vol. 62, 1969, pp 839-845.
84. Brown, B. F., "Concept of the Occluded Corrosion Cell," Corrosion, Vol. 26, August 1970, pp 249-250.
85. Duquette, D. J., and Uhlig, H. H., "Effect of Dissolved Oxygen and NaCl on Corrosion Fatigue of 0.18% Carbon Steel," Transactions of the ASM, Vol. 61, 1968, pp 449-456.
86. Lee, H. H., and Uhlig, H. H., "Corrosion Fatigue of Type 4140 High Strength Steel," Metallurgical Transactions, Vol. 3, November 1972, pp 2949-2957.
87. Evans, U. R. and Simnad, M. T., "The Mechanism of Corrosion Fatigue of Mild Steel," Proceedings of the Royal Society, Vol. 188, 1947, p 372.
88. Brown, B. F., "Stress Corrosion and Corrosion Fatigue of High Strength Steels," (Source not identified on document), pp 91-102.
89. Brown, B. F., Corrosion Fatigue in Naval Structures," Corrosion Fatigue: Chemistry, Mechanics, and Microstructure, Proceedings of Conference held at the University of Connecticut, June 14-18, 1971; National Association of Corrosion Engineers, 1972, pp 25-29.
90. Endo, K., and Komai, K., "Corrosion Fatigue Strength of a Steel Under Controlled Potential and pH Values," Proceedings of the 13th Japanese Congress on Materials Research, Tokyo, Japan, September, 1969, pp 162-166.
91. Hudgins, C. M., Jr., et al, "The Effect of Cathodic Protection on the Corrosion Fatigue Behavior of Carbon Steel in Synthetic Seawater," Journal of Petroleum Technology, March, 1971, pp 283-293.
92. Crooker, T. W., and Lange, E. A., "Fatigue Crack Propagation in a High-Strength Steel Under Constant Cyclic Load with Variable Mean Loads," NRL Report 6805, November 29, 1968.
93. Kline, R. G., "Application of Higher Strength Steels to Great Lakes Vessels," Marine Technology, pp 273-287, July 1966.

94. Phelps, E. H., and Loginow, A. W., "Stress Corrosion of Steel for Aircraft and Missiles," Corrosion, Vol. 16, p 325, July, 1960.
95. Robinson, R. B., and Uzdarwin, R. J., "Investigation of Stress-Corrosion Cracking of High-Strength Alloys, Aerojet General Report 2092, Contract DA-04-495-ORD-3069, August, 1961.
96. Gurney, T. R., and Maddox, S. J., "Determination of Fatigue Design Stresses for Welded Structures from an Analysis of Data," Metal Construction and British Welding Journal, Vol. 4, No. 11, 418-422, November 1972.
97. Frost, N. E., and Denton, K., "The Fatigue Strength of Butt-Welded Joints in Low-Alloy Structural Steels," British Welding Journal, Vol. 14, No. 4, 157-163, April 1967.
98. Pook, L. P., "Fatigue Crack Growth Data for Various Materials Deduced From the Fatigue Lives of Precracked Plates," in: STRESS ANALYSIS AND GROWTH OF CRACKS, ASTM STP 513, American Society for Testing and Materials, Philadelphia, 106-124 (1972).
99. Bucci, R. J., Clark, W. G., and Paris, P. C., "Fatigue Crack Propagation Growth Rates Under a Wide Variation of  $\Delta K$  for an ASTM a517 Grade F(T-1) Steel," in: STRESS ANALYSIS AND GROWTH OF CRACKS, ASTM STP 513, American Society for Testing and Materials, Philadelphia, 177-195 (1972)
100. Parry, M., Nordberg, H., and Hertzberg, R. W., "Fatigue Crack Propagation in A514 Base Plate and Welded Joints," Welding Research Supplement, Vol. 51, 485s-490s, October 1972.
101. Lawrence, F. V., "Estimation of Fatigue-Crack Propagation Life in Butt Welds," Welding Research Supplement, Vol. 52, No. 5, 212s-220s, May 1973.
102. Imhof, E. J., and Barsom, J. M., "Fatigue and Corrosion-Fatigue Crack Growth of 4340 Steel at Various Yield Strengths," in: PROGRESS IN FLAW GROWTH AND FRACTURE TOUGHNESS TESTING, ASTM STP 536, American Society for Testing and Materials, Philadelphia, 182-205 (1973).
103. Paris, P. C., and Sih, G. C., "Stress Analysis of Cracks," in: FRACTURE TOUGHNESS TESTING AND ITS APPLICATIONS, ASTM STP 381, American Society for Testing and Materials, Philadelphia, 30-83 (1965).

104. "Guide for Interpretation of Non-Destructive Tests for Welds in Ship Hull Structures," SSC Report SSC-177, 1966.
105. Youshaw, R. A., "A Guide for Ultrasonic Testing and Evaluation of Weld Flaws," SSC Report SSC-213, 1970.
106. Lewis, E. V., et al., "Load Criteria for Ship Structural Design," SSC Report SSC-240, 1973.
107. Walters, I. J., and Bailey, F. C., "Results From Full-Scale Measurements of Midship Bending Stresses on Three Dry Cargo Ships," SSC Report SSC-209, 1970.
108. Hoffman, D., Williamson, J., and Lewis, E. V., "Correlation of Model and Full-Scale Results in Predicting Wave Bending Moment Trends," SSC Report SSC-233, 1972.
109. Hoffman, D., van Hooff, R., and Lewis, E. V., "Evaluation of Methods for Extrapolation of Ship Bending Stress Data," SSC Report SSC-234, 1972.

## APPENDIX

This Appendix consists of basic background information in support of the main report text. This Appendix should be consulted as a reference to the reader who needs a more introductory exposition in able to study the main report effectively.

	<u>Page</u>
A. METALLURGY OF SHIP STEELS AND WELDMENTS	A-1
B. SHIP ENVIRONMENT	A-10
1. Loads Acting on Ships	A-10
2. Corrosion and Corrosion Protection of Steels in Marine Environments	A-16
C. BASIC STRUCTURAL, FABRICATION AND NDT ASPECTS	A-20
D. ELEMENTS OF FRACTURE MECHANICS	A-23
REFERENCES	A-31

## A. METALLURGY OF SHIP STEELS AND WELDMENTS

The most common structural materials for shipbuilding are the carbon steels having 0.2% offset yield strengths in the neighborhood of 32,000 psi. However, there are many higher strength steels currently in use, and others under consideration, by shipbuilders desirous of producing lighter, stronger, and more economical ships. The higher strength steels of current interest possess yield strengths as high as 100 KSI, and many have been classified, along with the more familiar medium steels, by the several classifying organizations (American Bureau of Shipping (ABS), Lloyd's Register of Shipping, and Det Norske Veritas). As can be seen in the following Classification Tables, requirements for ship steels generally have been based upon considerations related to strength and brittle fracture resistance.

It is useful here to discuss the most common shipbuilding steels, ABS (1973) classes A, B, and C.<sup>(1)</sup> The class distinction is based primarily on plate thickness, all plates of 1/2 in. and below being in Class A. Thinner steel plates have greater notch toughness and lower nil ductility transition temperatures than do thicker plates rolled from the same melt. Class B includes plates over 1/2 in. and up to 1 in., inclusive. Class C contains plates over 1 in. and up to 2-in. thickness. Since both decreased carbon and increased manganese lower the brittle-ductile transition temperature, Classes B and C are restricted regarding the carbon and manganese content, as noted in Table I. The other steels in the Table are used in somewhat smaller quantities, although it should be pointed out that grades CS and E are intended primarily for applications where superior notch toughness is required in certain specially designed strakes. It can be seen from the Tables that most of the ship steels are killed or semi-killed, in order to promote grain refinement and to minimize microcracks caused by blowholes, through the addition of deoxidizing elements such as silicon and aluminum. Again, this is a procedure designed to improve notch toughness, strength, and workability.

The use of higher strength steels for major structural components in large merchant ships is increasing, especially for the more highly stressed members of the hull girders. This serves primarily to keep the extreme-fiber stress within permissible limits without resorting to extremely thick plates, which often are excessively heavy and difficult to fabricate. In Tables II and III, ABS (1973) higher strength steels are summarized with regard to chemical and mechanical specifications. As in the case of the ordinary medium steels, the ABS higher-strength classification is based on thickness. Special heat-treatment requirements for higher strength steels are listed in Table IV. At this point, it may be appropriate to describe the normalizing process. Normalizing consists of heating iron base alloys above the upper critical temperature range,

TABLE I. REQUIREMENTS FOR ORDINARY-STRENGTH HULL STRUCTURAL STEEL

PROCESS OF MANUFACTURE		FOR ALL GRADES: OPEN-HEARTH, BASIC-OXYGEN OR ELECTRIC-FURNACE				
GRADES	A	B	C	CS	D	E
DEOXIDATION	any method <sup>1</sup>	semi-killed or killed	fully-killed, fine-grain practice	fully-killed, fine-grain practice	semi-killed or killed	fully-killed, fine-grain practice
CHEMICAL COMPOSITION (Ladle analysis)						
Carbon, %		0.21 max.	0.23 max. <sup>4</sup>	0.16 max.	0.21 max. <sup>5</sup>	0.18 max. <sup>5</sup>
Manganese, %	1	0.80-1.10 <sup>2,6</sup>	0.60-0.90 <sup>2</sup>	1.00-1.35	0.60-1.40 <sup>5</sup>	0.70-1.50 <sup>5</sup>
Phosphorus, %	0.05 max.	0.05 max.	0.05 max.	0.05 max.	0.05 max.	0.05 max.
Sulphur, %	0.05 max.	0.05 max.	0.05 max.	0.05 max.	0.05 max.	0.05 max.
Silicon, %		3	0.10-0.35	0.10-0.35	0.35 max.	0.10-0.35
HEAT TREATMENT			normalized over 35.0 mm (1.375 in.) thick <sup>8</sup>	normalized		normalized
TENSILE TEST						
Tensile strength	For All Grades: 41-50 kgs per sq. mm <sup>7,9</sup> or 58,000-71,000 lb/in <sup>2</sup> or 26-32 tons/in <sup>2</sup>					
Elongation, min	For All Grades: 21% in 200 mm (8 in.) <sup>7</sup> or 24% in 50 mm (2 in.) or 22% in 5.65/A (A equals area of test specimen)					
IMPACT TEST						
CHARPY STANDARD V-NOTCH						
Temperature, Energy, avg., min.					0C (32F)	-10C (14F)
Longitudinal specimens					4.8 kgm (35 ft-lb)	6.2 kgm (45 ft-lb)
or Transverse specimens					3.2 kgm (23 ft-lb)	4.1 kgm (30 ft-lb)
No. of specimens					3 from each 40 tons	3 from each plate
STAMPING						
	$\frac{AB}{A}$	$\frac{AB}{B}$	$\frac{AB}{C}$ (as rolled) $\frac{AB}{CN}$ (normalized)	$\frac{AB}{CS}$	$\frac{AB}{D}$	$\frac{AB}{E}$

NOTES:

- Unless otherwise specially approved, Grade A steel over 12.5 mm (0.50 in.) in thickness is to be semi-killed or killed with a minimum manganese/carbon ratio of 2.5. Grade A shapes and bars are not subject to the manganese/carbon ratio of 2.5.
- Upper limit of manganese may be exceeded, provided carbon content plus 1/6 manganese content does not exceed 0.40%.
- When the silicon content is 0.10% or more (killed steel), the minimum manganese content may be 0.60%.
- For normalized Grade C plates, the maximum carbon content may be 0.24%.
- Carbon content plus 1/6 manganese content shall not exceed 0.40%.
- Where the use of cold-flanging quality has been specially approved, the manganese content may be reduced to 0.60-0.90%.
- The tensile strength of cold-flanging steel shall be 39-46 kg/mm<sup>2</sup> (55,000-65,000 psi) and the elongation 23% min. in 200 mm (8 in.).
- Grade C plates over 35.0 mm (1.375 in.) in thickness are to be ordered and produced in the normalized condition when intended for important structural parts.
- A tensile strength range of 41-56 kg/mm<sup>2</sup> (58,000-80,000 psi) may be applied to Grade A shapes provided the carbon content does not exceed 0.26% by ladle analysis.

**TABLE II. REQUIREMENTS FOR HIGHER STRENGTH  
HULL STRUCTURAL STEEL**

GRADES<sup>1</sup> — AH32, DH32, EH32

PROCESS OF MANUFACTURE — Open Hearth, Basic Oxygen or Electric Furnace

CHEMICAL COMPOSITION (Ladle Analysis)

Carbon, % 0.18 max.	Manganese, % <sup>2</sup> 0.90-1.60	Phosphorus, % 0.04 max.	Sulfur, % 0.04 max.	Silicon, % <sup>3</sup> 0.10-0.40
Nickel, % 0.40 max.	Chromium, % 0.25 max.	Molybdenum, % 0.08 max.	Copper, % 0.35 max.	
Aluminum, % <sup>4</sup> (acid-soluble) 0.060 max.	Aluminum, % <sup>4</sup> (total) 0.065 max.			

TENSILE TEST

Tensile strength	48-60 kg/mm <sup>2</sup> ; 68,000-85,000 psi; 30.5-38 tons per sq. in.
Yield point, min.	32 kg/mm <sup>2</sup> ; 45,500 psi; 20.5 tons per sq. in.
Elongation, min.	19% in 200 mm (8 in.) or 22% in 50 mm (2 in.) or 20% in 5.65 √A (A equals area of test specimen)

HEAT TREATMENT — See Table IV.

	AH32	DH32	EH32
DEOXIDATION	semi-killed or killed <sup>3</sup>	killed, fine grain practice <sup>6</sup>	killed, fine grain practice <sup>6</sup>
IMPACT TEST STANDARD CHARPY V-NOTCH			
Temperature	none required	-20C (-4F)	-40C (-40F)
Energy, min. avg. Longitudinal specimens or Transverse specimens		3.5 kgm (25 ft-lb) <sup>6</sup> 2.4 kgm (17 ft-lb) <sup>6</sup>	3.5 kgm (25 ft-lb) 2.4 kgm (17 ft-lb)
No. of specimens		3 from each 40 tons	3 from each plate
STAMPING	AB/AH 32	AB/DH32 or AB/DHN32 <sup>7</sup>	AB/EH32

**NOTES:**

- 1 The numbers following the Grade designation indicate the yield point to which the steel is ordered and produced in kg/mm<sup>2</sup>. A yield point of 32 kg/mm<sup>2</sup> is equivalent to 45,500 psi and a yield point of 36 kg/mm<sup>2</sup> is equivalent to 51,000 psi.
- 2 Grade AH 12.5 mm (0.50 in.) and under in thickness may have a minimum manganese content of 0.70%.
- 3 Grade AH to 12.5 mm (0.50 in.) inclusive may be semi-killed, in which case the 0.10% minimum Silicon does not apply. Unless otherwise specially approved, Grade AH over 12.5 mm (0.50 in.) is to be killed with 0.10 to 0.40 percent Silicon.
- 4 Aluminum may be either partially or totally replaced by Columbium (Niobium) (0.05% maximum) or Vanadium (0.10% maximum) in which case the heat treating requirements of Table IV for Columbium (Niobium)-treated or Vanadium-treated steel apply.
- 5 Grades DH and EH are to contain at least one of the grain refining elements in sufficient amount to meet the fine grain practice requirement.
- 6 Impact tests are not required for normalized Grade DH.
- 7 The marking AB/DHN is to be used to denote Grade DH plates which have either been normalized or control rolled in accordance with an approved procedure.

**TABLE III. REQUIREMENTS FOR HIGHER STRENGTH  
HULL STRUCTURAL STEEL**

GRADES — AH36, DH36, EH36

PROCESS OF MANUFACTURE — Open Hearth, Basic Oxygen or Electric Furnace

CHEMICAL COMPOSITION (Ladle Analysis)

Carbon, % 0.18 max.	Manganese, % <sup>2</sup> 0.90-1.60	Phosphorus, % 0.04 max.	Sulfur, % 0.04 max.	Silicon, % <sup>3</sup> 0.10-0.40
Nickel, % 0.40 max.	Chromium, % 0.25 max.	Molybdenum, % 0.08 max.	Copper, % 0.35 max.	
Columbium, % (Niobium) 0.05 max.	Vanadium, % 0.10 max.	Aluminum, % <sup>4</sup> (acid-soluble) 0.060 max.	Aluminum, % <sup>4</sup> (total) 0.065 max.	

TENSILE TEST

Tensile strength	50-63 kg/mm <sup>2</sup> ; 71,000-90,000 psi; 32-41 tons per sq. in.
Yield point, min.	36 kg/mm <sup>2</sup> ; 51,000 psi; 23 tons per sq. in.
Elongation, min.	19% in 200 mm (8 in.) or 22% in 50 mm (2 in.) or 20% in 5.65 √A (A equals area of test specimen)

HEAT TREATMENT — See Table IV.

	AH36	DH36	EH36
DEOXIDATION	semi-killed or killed <sup>3</sup>	killed, fine grain practice <sup>5</sup>	killed, fine grain practice <sup>5</sup>
IMPACT TEST STANDARD CHARPY V-NOTCH			
Temperature	none required	-20C (-4F)	-40C (-40F)
Energy, min. avg. Longitudinal specimens or Transverse specimens		3.5 kgm (25 ft-lb) <sup>6</sup> 2.4 kgm (17 ft-lb) <sup>6</sup>	3.5 kgm (25 ft-lb) 2.4 kgm (17 ft-lb)
No. of specimens		3 from each 40 tons	3 from each plate
STAMPING	AB/AH36	AB/DH36 or AB/DHN36 <sup>7</sup>	AB/EH36

NOTES:

- 1 The numbers following the Grade designation indicate the yield point to which the steel is ordered and produced in kg/mm<sup>2</sup>. A yield point of 32 kg/mm<sup>2</sup> is equivalent to 45,500 psi and a yield point of 36 kg/mm<sup>2</sup> is equivalent to 51,000 psi.
- 2 Grade AH 12.5 mm (0.50 in.) and under in thickness may have a minimum manganese content of 0.70%.
- 3 Grade AH to 12.5 mm (0.05 in.) inclusive may be semi-killed, in which case the 0.10% minimum Silicon does not apply. Unless otherwise specially approved, Grade AH over 12.5 mm (0.50 in.) is to be killed with 0.10 to 0.40 percent Silicon.
- 4 Aluminum may be either partially or totally replaced by Columbium (Niobium) (0.05% maximum) or Vanadium (0.10% maximum), in which case the heat treating requirements of Table IV for Columbium (Niobium)-treated or Vanadium-treated steel apply.
- 5 Grades DH and EH are to contain at least one of the grain refining elements in sufficient amount to meet the fine grain practice requirement.
- 6 Impact tests are not required for normalized Grade DH.
- 7 The marking AB/DHN is to be used to denote Grade DH plates which have either been normalized or control rolled in accordance with an approved procedure.

TABLE IV. HEAT TREATMENT<sup>1</sup> REQUIREMENTS FOR  
HIGHER STRENGTH HULL STRUCTURAL STEELS

Aluminum-Treated Steels

AH - Normalizing not required

DH - Normalizing required over 25.5 mm (1.0 in.)<sup>2</sup>

EH - Normalized

Columbium (Niobium)-Treated Steels

AH - Normalizing required over 12.5 mm (0.50 in.)

DH - Normalizing required over 12.5 mm (0.50 in.)

EH - Normalized

Vanadium-Treated Steels

AH - Normalizing not required

DH - Normalizing required over 19.0 mm (0.75 in.)

EH - Normalized

NOTES:

1. Control rolling of Grades AH and DH may be specially considered as a substitute for normalizing in which case impact tests are required on each plate.
2. Aluminum-treated DH steel over 19.0 mm (0.75 in.), intended for special applications, is to be ordered and produced in the normalized condition.

followed by cooling below that range in still air at ordinary temperature. The process resembles full annealing in a general way, but the temperatures are higher (1650-1700°F) and the cooling is somewhat faster than that encountered in annealing. The principal objectives of normalizing are (1) to promote a homogeneous structure by breaking down masses of ferrite or eliminating network carbides, and (2) to impart moderate hardness and strength, since the accelerated cooling results in less ferrite separation and a finer pearlite spacing, and (3) to promote grain refinement. The "mass" effect is of importance here, since the cooling rate varies inversely with the section thickness, and therefore the strengthening effect of normalizing is limited by the section thickness.

On the other hand, the steels described in Table V represent a fundamental metallurgical departure with respect to the normalized steels mentioned above. HY-80 (high yield - 80 KSI) and HY-100 derive their superior strength and toughness from two sources, namely, their higher

TABLE V. MIL-S-16216G (SHIPS)  
February 27, 1963

	HY-80		HY-100	
	To 5/8 in., excl	5/8-8 in., incl	To 5/8 in., excl	5/8-3 in., incl
Carbon .....	0.18	0.18	0.20	0.20
Manganese .....	0.10-0.40	0.10-0.40	0.10-0.40	0.10-0.40
Phosphorus .....	0.025	0.025	0.025	0.025
Sulfur .....	0.025	0.025	0.025	0.025
Silicon .....	0.15-0.35	0.15-0.35	0.15-0.35	0.15-0.35
Nickel .....	2.00-3.25	2.00-3.25	2.25-3.50	2.25-3.50
Chromium .....	1.00-1.80	1.00-1.80	1.00-1.80	1.00-1.80
Molybdenum .....	0.20-0.60	0.20-0.60	0.20-0.60	0.20-0.60
Residual elements .....				
Titanium, max percent .....	0.02	0.02	0.02	0.02
Vanadium, max percent .....	0.03	0.03	0.03	0.03
Copper, max percent .....	0.25	0.25	0.25	0.25
Tensile strength, psi .....	--	--	--	--
Yield strength, 0.2% offset, psi	80,000-100,000	80,000-100,000	100,000-120,000	100,000-120,000
Elongation in 2 in., min percent	19	20	18	18

NOTES:

1. HY-80 plates over 6 in. add 0.02 percent carbon.
2. The percentage of phosphorus and sulfur for HY-80 and 100 shall not be more than 0.045.
3. Charpy V-notch impact tests are required.
4. Elongation specimens shall be type F2 for plates 5/8 in. and over and type R1 under 5/8 in.

percentages of nickel and chromium, and the fact that the HY steels are quenched-and-tempered martensite, rather than normalized. In the former process, the material is heated (austenitized) within a temperature range of 1550-1650°F and quenched into water. The resulting structure is strong, brittle martensite. Tempering consists of reheating and holding for a period of time at about 1150°F (HY-100) or about 1250°F (HY-80). This treatment relieves the highly strained martensitic microstructure through the precipitation of complex carbide platelets, which impart toughness to the matrix, while lowering the yield strength of the metastable martensite.

Increasing the carbon content increases the strength and hardness of HY steels, but impairs weldability, since the brittleness of as-quenched martensites in the weld heat-affected zone increases with carbon. To improve weldability, carbon content generally is restricted to 0.18% maximum.<sup>(1)</sup> Nevertheless, HY steels present special welding problems, and their use in merchant ships, subject to repairs under unfavorable conditions, in place of normalized steels, requires careful consideration. The lower distortion attendant upon normalizing, as compared to quenching and tempering, also is a prime consideration in deciding between two possible steels of similar yield strengths, but differing heat treatments. Moreover, the mass effect mentioned earlier is even more evident during the

extremely rapid water quench required to attain martensite, than during the relatively leisurely air quench typical of normalizing.

The basic higher strength steels (of which over 125 different commercial varieties are manufactured in the U. S. , Europe, Canada, and Japan) have been reviewed. It is useful to consider their regions of applicability in ship structures, before discussing briefly the related problems of fatigue and welding.

A typical application of high-strength steel to a merchant hull is shown in Figure A-1.<sup>(1)</sup> The stress  $MY/I$  resulting from a tentative section modulus  $I/Y$  is indicated by the line A-A. Through most of the depth of the hull girder, this stress lies within the acceptable limit for medium steel, but exceeds it for the two upper decks, the innerbottom and bottom shell, and the top and bottom side shell. If these members were to be made of a special high-strength steel with the acceptable stress shown in Figure A-1, the tentative section modulus could be accepted; otherwise, heavier top and bottom members would be required in order to bring the extreme-fiber stress within design limits. It is obvious that all of the upper decks, etc. , should be made of the special steel, and that there would be no justification for using it only on some of the highly stressed members. Conversely, there is no advantage to using the special steel for components of the hull girder near the neutral axis, insofar as primary bending stresses are concerned.

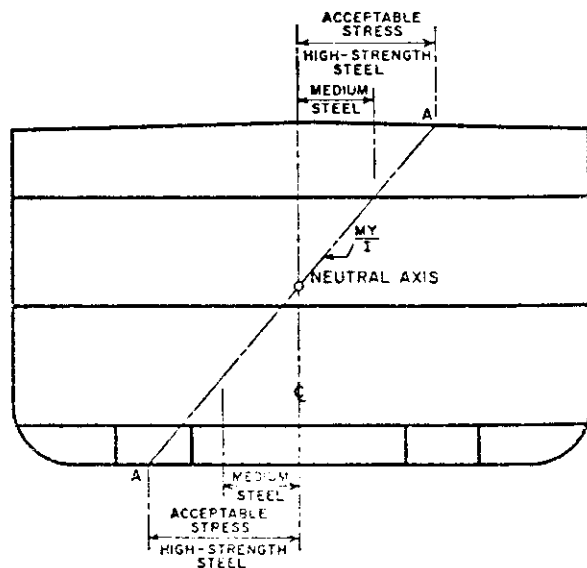


FIGURE A-1. APPLICATION OF HIGH-STRENGTH STEEL

The relevancy of the foregoing is as follows. The primary reason for using high-strength materials is to save weight by reducing section thickness, taking advantage of the higher strength of the special steels. However, higher strength may not necessarily permit a proportionate increase in the design allowable stress level if either elastic stability or fatigue is a consideration. In the stability problem nothing is gained by increasing strength, since the elastic modulus for both medium and high strength steels is nearly the same. Concerning fatigue, not only are the fatigue characteristics of the basic materials important, but even more crucial are the fatigue properties of the welded structure composed of these materials. There is overwhelming evidence to indicate that the fatigue strength of welded joints, at least at long life, is completely independent of the static strength of the parent material. One must therefore examine very carefully the low-life (hence high stress) fatigue characteristics of higher strength steels and their weldments, as well as the anticipated cyclic loading during service, in determining the extent to which it is possible to capitalize on the inherently greater static strength and notch toughness of higher strength parent steel.

Welds in the lower-strength ship steels are usually as strong as the parent metal, and special electrodes and procedures have been developed for use on these higher strength steels, in which welds can be produced with a static strength approximately that of the parent steel. On the other hand, a geometric discontinuity frequently is associated with a welded joint, which may introduce adverse effects such as surface irregularities (especially at the toe of the weld), residual welding stresses, weld porosities and cracks, undercutting, slag inclusions, and incomplete fusion of the material joined by the weld. Such metallurgical faults and geometric discontinuities at the welded joint are prime sources of fatigue cracks.

Most weld metals for joining low-carbon structural steels and low-alloy higher strength steels are low-carbon, low-alloy ferritic steels.<sup>(2)</sup> They contain less than 0.2% carbon and minor alloying elements such as manganese, nickel, chromium, vanadium, and molybdenum. Some work has been performed to study the effect of alloy additions upon notch toughness, but almost nothing is known regarding the effects of weld metal alloying upon fatigue strength.

Weld regions are basically and unavoidably cast structures. Since the rather low-heat input of welding produces a high-cooling rate, grains in the weld metal turn out to be quite fine, for what may be considered a casting.<sup>(2)</sup> During multipass welding, those structures in areas adjacent to subsequent weld passes are recrystallized to form finer, equiaxed grains. The fine-grained recrystallized structures exhibit notch toughness exceeding that of coarse-grained as-cast structures. Many research efforts have

been aimed at establishing welding procedures which would produce weld metals having a favorable microstructure. However, there has been little information published concerning quantitative relations between weld microstructures and notch toughness, and again almost nothing regarding control of fatigue crack initiation and growth by weld-region microstructural variation.

Of the some 40 welding processes which are employed commercially, only the following are the most important in fabricating hull structures:(3)

- (1) Shielded metal-arc process,
- (2) Submerged-arc process,
- (3) Gas metal-arc process,
- (4) Vertical welding process (electroslag and electrogas).

The shielded metal-arc and submerged-arc processes are far and away the most commonly used for ship hull fabrication. However, the other two have been used increasingly in recent years. Although any of the above procedures can be used in joining higher-strength steels, it is important that the process be of the low-hydrogen type, in order to avoid underbead cracking caused by hydrogen embrittlement. Further, the high rates of heat input associated with the electroslag or electrogas processes sometimes cause excessive degradation in the heat-affected zone of the base metal, to the extent that reheat treatment of the weldment may be required for quenched-and-tempered steels. The guidelines for welding high-strength steels are extremely stringent, and have previously been reviewed exhaustively(4) and summarized excellently(3) regarding crucial points. Proper electrode selection and welding procedures cannot be overemphasized. The handling of low-hydrogen electrodes and flux deserves special mention, since hydrogen-induced cracking is a possible consequence of less than extreme care according to specified practices, and avoiding the problem demands high competence on the part of the welder. Satisfactory welding requires a compromise between (1) a sufficiently high preheat and interpass temperature to remove moisture and relieve weld-shrinkage stresses, and (2) a sufficiently low preheat, weld heat input, and interpass temperature to provide a high weldment quench rate and thereby maintain strength and toughness.

Finally, it should be pointed out that the ABS has not yet adopted requirements for specifications for weld metals. The American Welding Society has proposed specifications in terms of notch toughness,(2) but again this does not bear on the question of fatigue resistance.

## B. SHIP ENVIRONMENT

Ship design is largely dependent upon the environment the ship will experience in service. Strength requirements differ for various service conditions. For example, a ship structure designed for smooth-water service may be inadequate to withstand wave-induced stresses the ship would encounter in the ocean. Ship design also may be significantly influenced by the corrosivity of the water in which the ship will operate. Criteria established for design of a Great Lakes vessel would likely be unsuitable for design of an ocean-going vessel because of the higher corrosivity of salt water and salt water atmospheres.

A short discussion of the various types of loadings experienced by ships and of the corrosion and corrosion protection of steels in marine environments is given below. These discussions are brief and general in nature. For detailed treatments, the reader is referred to authoritative references on these subjects. (5-7)

### 1. Loads Acting on Ships

Longitudinal Loading. A ship is a deformable body that floats on the surface of the sea. In still water, a ship is subject to upward buoyancy forces and downward gravity forces, e. g., hull weight, payload, machinery and equipment, fuel, etc. Figure B-1 illustrates these forces acting on a ship which is divided into five sections by water-tight bulkheads. Within each section the forces may be considered to be evenly distributed; weight forces are indicated by downward arrows on the deck and buoyancy forces are indicated by upward arrows on the bottom. The difference between weight and buoyancy forces on each section is represented by the heavy central arrows; a plus sign indicates an excess buoyancy force and a negative sign indicates excess weight. The buoyancy and weight forces balance each other for the ship as a whole, but a point-to-point balance, as would be the case for a uniformly loaded, homogeneous floating body, does not exist. If the ship were cut at the four bulkheads, each of the sections would float at a different draft, as indicated in Figure B-2. These upward and downward shearing forces tend to change the shape of the ship's hull. If the hull is represented as a beam with a plane of vertical symmetry, bending moments and longitudinal stress produced by the shearing forces may be calculated by the principles of structural mechanics.

When a ship is at sea, waves will produce greater and varying differences between weight and buoyance and, as a result, generally greater bending moments and correspondingly greater bending stresses will be generated. A ship centered on the crest of a wave produces tensile stresses in the deck and compressive stresses in the bottom; under such loading the ship is said to be "hogging." A ship centered on the trough of a wave produces

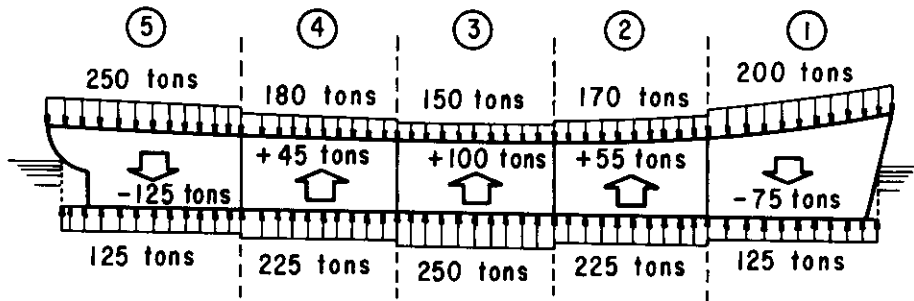


FIGURE B-1. FORCES ACTING ON A SHIP IN STILL WATER

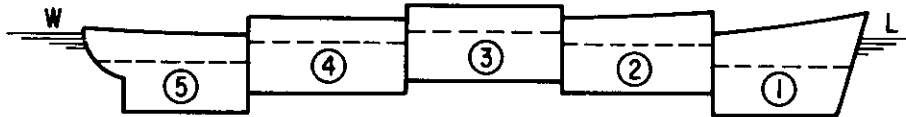


FIGURE B-2. RELATIVE DRAFT OF FIVE SHIP'S SLICES IN STILL WATER

compressive stresses in the deck and tensile stresses in the bottom; under this loading the ship is said to be "sagging." These modes of bending are shown in Figure B-3. Buoyant sea forces acting on the ship are continuously changing, subjecting the deck and bottom to successive stress reversals as the ship passes from wave crest to wave trough. At any given time, assuming that the ship remains upright in the water, stresses across the deck and bottom are fairly uniform, while stresses in the side shells vary uniformly from zero at the neutral axis to the maximum values existing at the deck and bottom, as indicated in Figure B-4. When a ship is heeled, the position of the neutral axis may change, and the maximum stresses may occur at the intersections of the side shells and the deck and bottom; i. e., at the greatest distance from the neutral axis. For this reason the sheer strake and bilge plating on the deck and bottom must either be thicker or made of higher strength material than the plating used in the side shells. Figure B-3 illustrates the hogging and sagging conditions when bending moments are likely to reach maximum values. In either case, the bending stresses will be greatest at the mid-length, and thicker or stronger strake plating is therefore required amidships.

Because wave spectra are largely random and ships at sea encounter combinations of many sizes of waves, bending moments can only be estimated. The usual basis for calculating the required strength of the ship's hull girder for standard loading is to assume that the ship is statically balanced on a stationary standard wave with the crest amidships for the hogging bending moment and the trough amidships for the sagging bending moment. The buoyancy curve is predicted on the following assumptions: (1) the wave is trochoidal in form; (2) the wave length is equal to the ship length,  $L$ ; (3) the wave height is equal to  $1.1\sqrt{L}$ ,  $L/20$ , or some other standard height; (4) the ship is perpendicular to the wave. The inadequacies of this static model are compensated for by supplementary empirical rules and safety factors developed by classification societies and governmental regulating agencies.

Several attempts have been made to supplement the standard static model by introducing concepts based on the fundamental laws of structural dynamics. The most important is the "Smith Effect." One of the basic assumptions in calculation of the bending moment on a ship is that pressure in a trochoidal wave, and therefore buoyancy, is directly proportional to the depth of the ship below the wave surface. The Smith effect calls attention to the fact that centrifugal forces caused by the orbital motion of water in waves modify hydrostatic pressure gradients. As a result of the acceleration of water particles, and consequent changes in apparent mass/weight, the water appears less dense than normal at wave crests and more dense than normal at wave troughs. A more even distribution of wave buoyancy results and both hogging and sagging moments are decreased. Neglect of the Smith effect will lead to overestimation of bending moments. Similar effects occur in the weight distribution curve

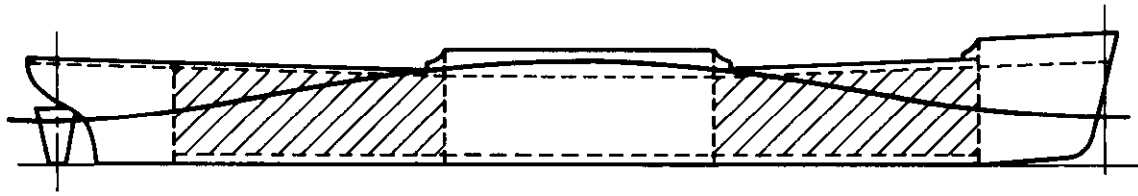


FIGURE B-3a. VESSEL IN HOGGING CONDITION

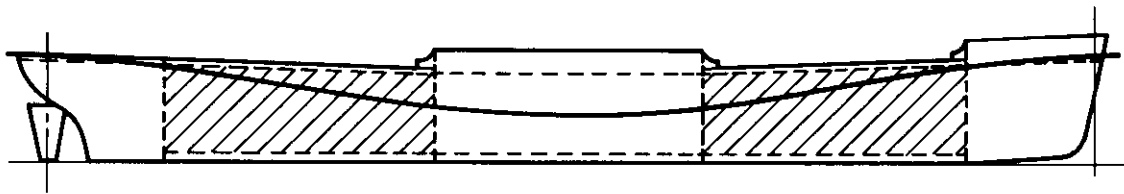


FIGURE B-3b. VESSEL IN SAGGING CONDITION

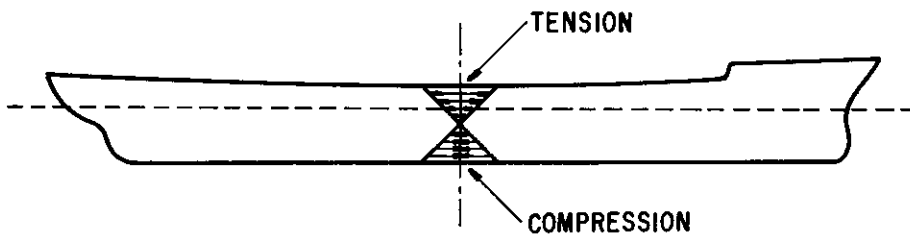


FIGURE B-4. SHIP-GIRDER BENDING STRESS DISTRIBUTION IN THE SIDE SHELL

required for moment calculation. A ship in waves experiences rolling, pitching, and heaving motions, and the weight of every part of the ship, its payload, fuel, etc., is affected by acceleration forces resulting from these motions. These forces cause a reduction in apparent weight at the top of an upward heave which tends to reduce the hogging moment. The increase in apparent weight at the bottom of a downward heave tends to increase the sagging moment. Pitching forces are smallest amidships and largest near the bow and stern.

Another dynamic effect on hull bending moments results from forward motion which causes a change in waterline and in the distribution of buoyancy forces. As speed increases, wave crests form at the bow and stern and a wave trough forms amidships, resulting in a sagging moment. If, simultaneously, the ship is propelled into a head sea, the upward impact of the sea on the bow ("bow slamming") results in an additional sagging moment and compression of the forebody. Such combinations are reported to have buckled the upper deck forward of ships moving at too high a speed into head seas.<sup>(5)</sup>

A third dynamic effect is the vibratory bending moment resulting from slamming, i. e., the impact of the bow on the water during a severe downward pitch. This effect is commonly known as "whipping." The magnitude of the slamming force is primarily dependent upon the descending velocity of the bow and the area subjected to impact. The resulting vibrations have the second vibration mode frequency of the ship, and last for some 30 to 60 cycles. The slamming stresses produced can be additive to wave-bending stresses. The additive stress is a maximum during the first sagging cycle after impact and is reduced after the second hogging cycle. For normal merchant ships the increase in stress may be 20 to 30 percent or more of the primary sagging stress, but long, slender ships of the destroyer type may experience significantly greater increases; slamming stresses as high as 1.6 times the primary stress have been recorded in destroyers.<sup>(5)</sup> The most severe slamming occurs when the ship's pitching period is approximately the same as the period of the wave encountered. Slamming forces increase with increasing wave height and speed. Increasing the draft results in a decrease in the slamming stress and in the speed range in which slamming occurs, but may increase bow-flare slamming.

In addition to slamming, vibratory forces may be excited in a ship hull by its propellers. The interaction of propellers with an irregular wake and with adjacent hull surfaces generates periodic forces which may induce vibration in the hull and in adjacent machinery. These forces contain simple harmonic components of the propeller blade frequency. Bending stresses produced in the hull girder by propeller vibration are negligible. But near the propellers where the basic vibration of the hull may be

magnified by local resonance, localized structural damage, most commonly fatigue, may occur in plating, frames, and internal structures.

Transverse Loading. Transverse loads tend to change the shape of a ship's cross section and thereby introduce transverse stresses. Transverse stresses may also result indirectly from longitudinal loads. Transverse loads are imposed on bottoms and sides of a ship as a result of hydrostatic and hydrodynamic pressure. Vertical loads result from structural and cargo weight. In addition, transverse loads result from slamming, racking, and torsion. Slamming was discussed earlier. Racking is the tendency of the deck to move laterally relative to the bottom of the shell on one side, and to move vertically with respect to the shell on the other side when the ship is rolling or is subjected to slamming. Racking stresses caused by rolling reach a maximum each time the ship completes an oscillation in one direction and is about to return. Torsional loads are the result of the ship twisting about its longitudinal axis as it heads obliquely into waves. Maximum twisting occurs when the angle between the ship's heading and the wave crest is about  $45^\circ$  (or  $135^\circ$ ). Torsional loads generally have negligible effect except at hatch corners in ships with very long and wide hatches.

Residual Stresses. In stress calculations it is usually assumed that the structure is stress-free prior to being subjected to the various types of loading described above. This is, of course, far from the actual condition. Residual stresses are present in the structures from a variety of sources such as heat treatment of metal plates, machining, and most importantly, welding operations. Residual tensile stresses reduce the load-carrying capacity of a structural component and are instrumental in producing sub-critical crack growth by fatigue, corrosion fatigue, and stress corrosion cracking. Compressive residual stresses, on the other hand, increase load-carrying capacity and are generally considered to be beneficial.

Stress Concentrations. A stress concentration is a localized magnification of stress produced by a structural discontinuity. Discontinuities range from the gross mismatch formed by the ends of superstructures to minute crack-like defects in welds. The most prevalent type of discontinuity in ships is the many openings required for cargo handling, service access, etc. The ratio of the maximum stress at a discontinuity to the average stress that would be present in the absence of the discontinuity is termed the stress concentration factor,  $K$ . Stress concentration factors of openings increase with the sharpness of the corners of the opening.

Thermal Stresses. Thermal stresses are developed in ship structures as a result of restraint and temperature gradients. Stress increases from solar heating of 5,000 to 11,000 psi have been measured.

A wider temperature range is experienced in ships carrying liquid sulfur, heated oil, and refrigerated products. Stresses produced are often comparable in magnitude to those produced by cargo. It has been reported that lowering the temperature of a refrigerated ship from 100 to 20°F resulted in stresses in the second and third decks of 10,000 psi and 8,000 psi, respectively. It is extremely difficult to predict the magnitude of thermal stresses because of complex heat transfer conditions. Temperature effects of interest to ship designers are the shape and magnitude of temperature gradients in the hull, deflection of the hull girder by thermal expansion, thermal stresses in the hull girder, buckling of hull plating as a result of thermal expansion, and changes in material fracture toughness in refrigerated areas.

Fatigue. Fatigue is the progressive cracking of a metal under cyclic stressing at stress levels well below the ultimate strength of the metal. Three basic factors are necessary for fatigue failure to occur: (1) a maximum tensile stress of sufficiently high value, (2) a sufficiently large variation in the applied stress, and (3) a sufficiently large number of cycles of applied stress. Two key design parameters are fatigue strength, the value of stress at which a metal will fail after a specified number of stress cycles, and the fatigue limit, the stress level below which the metal can be stressed for an infinite number of cycles without failure. Steel has a definite fatigue limit in air, but under the corrosive conditions present in sea water, this fatigue limit no longer exists. All ship's hulls are subject to fatigue loading during service. In the past, there has been little evidence to indicate that fatigue is an important consideration in the design of the primary hull-girder structure. Fatigue has not been identified as the cause of sudden, catastrophic cracking of hull girders, but, rather, has been associated with fracture of secondary structures. However, design for fatigue resistance may well become much more important in the future as more and more higher strength steels are employed in ship structures. This is because, in general, stable fatigue crack growth rates go up and critical crack sizes required for initiation of unstable crack growth go down as the yield strength is increased.

## 2. Corrosion and Corrosion Protection of Steels in Marine Environments

Steel is the most widely used metal in marine environments, but it is chosen for its cost and structural properties rather than its resistance to corrosion. In the atmosphere, a nonprotective coat of rust forms. At the "splash zone," or "wind and water line," where the material is intermittently sprayed with sea water, the attack is significantly higher than in the case of complete immersion. Steels typically corrode at the rate of 3 to 5 mils (0.003-0.005 in.) per year (mpy) in quiescent seawater, with higher rates usually being observed as flow velocity is increased. At the

wind and water line, rates as high as 50 mpy are not uncommon. Pitting, galvanic attack, crevice corrosion, and other forms of localized corrosion frequently occur. Under submerged conditions, corrosion of steel is governed by the chemical reaction at cathodic sites on the metal surface. In neutral or alkaline seawater the reaction at cathodic sites is governed by the amount of oxygen arriving at the surface; the corrosion rate increases with the increased concentration of oxygen. At cathodic sites, hydroxyl ions may be formed which increase the alkalinity of these localized sites and promote deposition of protective calcareous scales.

Because seawater is a complicated, delicately balanced mixture of salts containing living matter, silt, dissolved gases, and decaying organic matter, the individual effect of each factor affecting the corrosion behavior is not readily separable. Dissolved oxygen concentration is the major factor governing the corrosivity of seawater. The amount of oxygen present at a steel surface depends upon the concentration of oxygen in the water and the velocity of flow. Water low in oxygen flowing at a high velocity can provide as much oxygen to a steel surface as water high in oxygen moving slowly past the surface. The oxygen level of seawater may range up to 12 parts per million (ppm). Plant life and wave action tend to increase the oxygen level. On the other hand, decaying organic material tends to reduce oxygen consumption.

When steel is first immersed in seawater, a biological slime develops in a matter of a few hours. This film of bacteria and other microorganisms is attractive for embryonic fouling organisms looking for a place to settle. Of most concern from a corrosion viewpoint are the sessile organisms which arrive at slime-covered steel surfaces in embryonic form and become firmly attached in a few hours. They then rapidly transform to a mature form and become immobile. Typical sessile fouling organisms are barnacles, bryzoa, mollusks, corals, and algae. Biofouling, the growth of these organisms, tends to reduce general corrosion because the organisms act as a barrier preventing water from reaching the steel surface. However, they promote formation of localized corrosion cells which leads to pitting and crevice corrosion at the interface between the organisms and the steel surface.

Increasing the ambient temperature of seawater tends to accelerate corrosion of steel. Increasing salinity also tends to increase corrosion rate by decreasing the electrical resistance of the water, thereby making it possible for localized anodes and cathodes to operate over longer distances than would be the case in a less conductive liquid such as fresh water. The pH of seawater varies slightly depending on plant life present. Plants consume carbon dioxide and this affects the pH. This slight shift in pH has little direct effect on corrosion behavior; however, it can affect calcareous scale deposition which, in turn, will influence corrosivity. As water depth increases the corrosion rate generally decreases. This is attributed to such factors as

lower oxygen concentration, lower temperature, and less water movement at the greater depths. Corrosion of steel in polluted seawater may be quite different from that in normal seawater. Depending upon the pollutant, the effects of oxygen concentration, salinity, biofouling, and pH may change. Acidic pollutants will be much more corrosive. Sulfides, which normally are present in polluted seawater, greatly accelerate corrosion of steel.

The problem of providing protection against corrosion in seawater is aggravated by its high conductivity, which favors local-action cell formation, a high content of sodium ions to promote the development of alkalinity at cathodic sites, and a high total ion content which facilitates establishment of ion concentration gradients and osmotic transfer of water through protective films. The principal method for mitigating corrosion of ship's hulls is use of protective coatings supplemented with cathodic protection.

Protective coatings normally are intended to form a continuous film of electrically insulating material over the steel surface to be protected. The function of a coating is to isolate the metal from direct contact with the surrounding environment, and to impose a high electrical resistance in the anode-cathode circuit so that there can be no significant corrosion current flowing from anodic sites to cathodic sites. The ideal protective coating would have an electrical resistance in the multi-megohm range and would completely and permanently separate the metal from the surrounding environment. This condition is never realized in practice. On a typical well-coated ship hull, approximately 1% of the total surface area will remain uncoated. This exposed area usually will be under small coating defects, commonly called "holidays." Holidays result from skips by the coating machine, pinholes in the film, cracks from mechanical or thermal stresses, action of solvents, action of bacteria, and penetration or mechanical damage by organisms. Some of this damage can be prevented by rigid quality control and careful systematic inspection of coated hull. The ability of coating to resist development of holidays after its initial construction is governed basically by its chemical and mechanical properties in the service environment.

In general, any effective coating for marine use must have certain characteristics. The coating

- (1) Must be highly water resistant. This means that the coating must be able to withstand continuous immersion in water and should have a very low water absorption and moisture vapor transfer rate. It should also be able to resist cycles of wetting and drying as occur in the splash zone.
- (2) Must resist passage of ions, such as chloride, sulfate, and carbonate, that on penetration could start corrosion under the coating.

- (3) should be highly dielectric in order to resist any electron passage caused by anodes set up at breaks in the coating.
- (4) must be highly weather resistant.
- (5) must be chemically resistant.
- (6) should be highly adherent.
- (7) should also be abrasion resistant since any material lacking toughness, hardness, and shock resistance could soon be eroded away.
- (8) should not be susceptible to undercutting in areas that become damaged.
- (9) should be inhibitive. Should damage occur, the coating itself should tend to minimize and restrict corrosion of the bare metal thus exposed.
- (10) should be easily applied and easy to repair.
- (11) should be resistant to biofouling.

Cathodic protection is the use of a direct electric current from an external source to oppose the discharge of corrosion current from anodic areas. When a cathodic protection system is installed for maximum effect, all exposed portions of the metal surfaces become cathodic. The function of cathodic protection used with coatings is to protect metal exposed at holidays. The direct current required is usually obtained from sacrificial anodes, the most common which are zinc, magnesium, and aluminum.

### C. BASIC STRUCTURAL, FABRICATION AND NDI ASPECTS

This report concerns subcritical crack growth in conventional structure associated with commercial surface ships. It is appropriate to review here a few of the most basic structural aspects of such vessels, and to highlight the typical nondestructive test and inspection procedures used today to qualify the structure.

We are considering conventional surface cargo and passenger ships, generally in the over 400-ft class. In such ships, the primary structure, i. e., the main load-carrying elements, may be considered to act as a box

girder. While the structure varies in detail in the vicinity of the bow and stern, a typical cross section through the ship hull is shown in a simplified form in Figure C-1. The main components of the primary structure are the deck and bottom plating and the side shell. Together, these elements form a continuous structure which serves both to carry the primary ship loads and to support the internal structure.

During its service, the ship is exposed to hydrodynamic forces which tend to bend and twist the structure. As the ship hogs and sags (the fundamental bending mode) the bending stresses generally are greatest on the stringer plate and on the sheer and bilge strakes, since these critical primary elements are farthest from the neutral axis. Torsional forces add shear stresses to these direct stress components due to bending. Additional shear stresses arise in the side shell due to the behavior of the ship structure as a thick beam. These shear stresses in the primary structure are greatest near the plane containing the neutral axis, at the quarter points (i. e., one-fourth of the ship length in from the bow and the stern). The "strength envelope," or primary structure as discussed thus far, is assisted somewhat by the secondary support offered internally in the form of transverse and/or longitudinal frames.

Most of the potentially dangerous cracks that develop in a ship may either be associated with welding seams or with corners and other structural discontinuities in the primary and secondary structural assemblies. With regard to the former, arc welding is used today almost exclusively as the means of joining principal ship structural components. The most common weld joints are the double welded "V" joint, intermittent fillet joint, double fillet "T" joint, double bevel "T" joint, and the double bevel corner joint (fillet reinforced). These weld joint configurations are standard for all types of stiffened plate and structural construction. While welding enjoys a number of advantages over earlier riveting practice, slag inclusions, residual stresses and steep property gradients associated with weld regions offer convenient sites for the initiation of cracks.

Structural regions where load discontinuities occur are inevitable in ship structures, and often are the sites of cracks and fractures. Major openings in the structure may occur in the strength decks for cargo hatches, and in stairway and elevator wells. These openings can be especially dangerous when large tensile stress concentrations occur on the main deck. For example, the Liberty ships had square corners on the main hatch openings; these corners were the sources of hundreds of reported fractures. Large side openings, such as cargo ports, may be another potential source of failure, particularly when the opening includes the sheer strake or is located close to the quarter points of the ship. When the side openings involving the sheer strake are in the same transverse plane as large deck

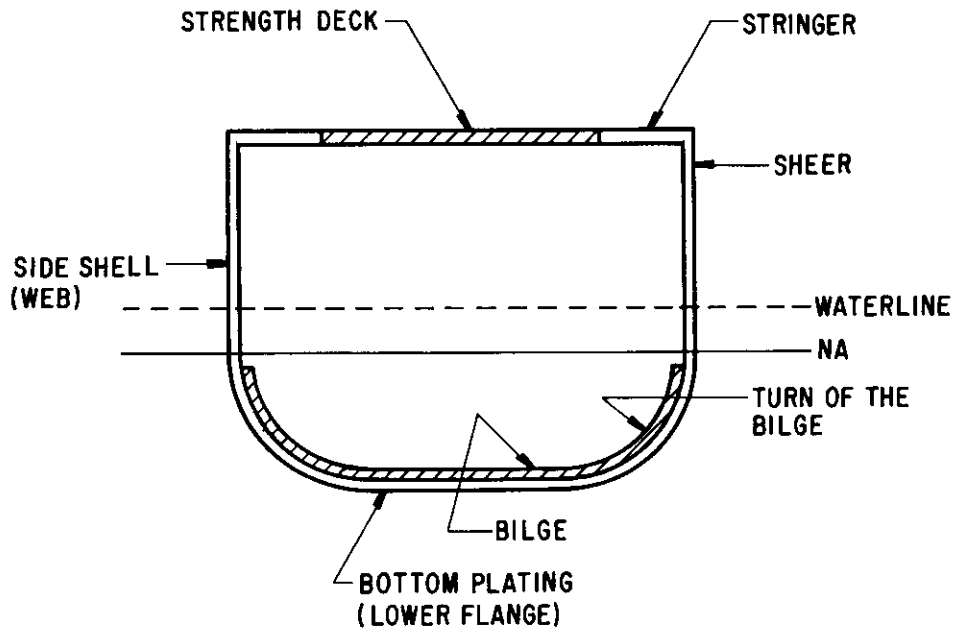


FIGURE C-1. CROSS SECTION OF IDEALIZED SURFACE SHIP HULL

openings, the failure potential is increased. In addition to the major openings, a large number of minor openings must usually be introduced to accommodate access, cargo handling, drainage, air escape, piping systems and other needs. These openings may also present potential fracture hazards. Critical areas can also be present where structural members intersect, with abrupt changes in load transfer and consequent stress concentrations.

Nondestructive inspection of joint details is an essential part of ship structure qualification. Several years ago the Weld Flaw Evaluation Committee reviewed the most common NDT techniques used in shipbuilding.<sup>(8)</sup> The purpose of this review was implied in the opening statement of Ship Structure Committee Report SSC-177: "At the present time (1966) the shipbuilding industry, as concerned with general cargo tanker and passenger ship construction, does not have a uniformly accepted procedure for examining and comparing the quality of welds in such ships." This report outlines the following five most commonly used NDT techniques:

- Visual
- Radiographic (x-ray or gamma-ray)
- Magnetic particle
- Liquid dye penetrant
- Ultrasonic

One or more of these methods may be applied to nearly any welded joint configuration, depending on the geometry, metallurgy, and type of cracking of interest (e. g. , surface heat check cracks, deep slag inclusions, etc. ). A major problem which exists today, and which in part motivated the present study, is the lack of adequate criteria for positive acceptance/rejection of joint details in structural qualification. The reader is referred to Reference 9, which presents a detailed NDT guide for the inspection of steel weldments.

#### D. ELEMENTS OF FRACTURE MECHANICS

The subject of subcritical crack growth in ship steels is intimately related to the discipline of fracture mechanics. It is difficult to imagine any thorough contemporary discussion of this subject without occasional recourse to its terminology and nomenclature. Therefore, it is appropriate to present in this subsection a brief account of some of the most important results and methods of fracture mechanics.

Our discussion of fracture mechanics will concern fracture processes in metals which are both homogeneous and isotropic on the macro-scale. It is customary to imagine the fracture process in such metals as consisting of three successive stages: crack initiation, subcritical crack growth, and fast fracture. Crack initiation refers to the creation, by various physical mechanisms occurring at the crystalline or subcrystalline level, of a small microcrack. Thus, even though the mechanism for crack initiation may be activated on the microscale, the description of the process is frequently presented in terms of macroscopic quantities such as, e.g., the formation of an isolated crack of specified size.

The second stage of the fracture process, subcritical crack growth, is that period wherein the crack increases its size in a stable manner. Subcritical crack growth may take place as a result of constant loads, variable amplitude (fatigue) loads, environmental forces such as corrosive environments, or combinations of these. During this stage the crack grows into structural regions in which the local stress state may change; accordingly, the crack may change its shape, direction of propagation, or it may accelerate its growth or self-arrest. Finally, the third stage of the fracture process is fast fracture, or unstable crack growth. This terminal stage develops when a large slowly-growing crack in a structure experiences an overload condition which can not be carried by the net uncracked structure remaining.

The field of fracture mechanics is not presently developed to the point where it can supply all the needed information in connection with the three above-mentioned stages. It can, however, be very useful in describing subcritical crack growth and the conditions under which fast fracture will occur. Thus, fracture mechanics concerns the behavior of a pre-existing crack in a structure under load.

In our brief discussion of fracture mechanics we will consider the state of stress and deformation near the tip of a sharp crack. Since there are three different modes of displacement of one crack surface with respect to the adjacent surface, it is customary to treat these three basic cases separately. Figure D-1 illustrates these three basic modes of crack tip displacement. Figure D-1a represents the crack opening mode (which is, in fact, one of the most common concerns in application); D-1b is the so-called edge-sliding mode, and D-1c is the tearing mode. These three modes are almost universally designated as Mode I, Mode II, and Mode III, respectively. It is quite common for a crack tip to experience a combination of two or all three of these modes simultaneously. However, by breaking the general problem down into its three fundamental elements, such cases can often be treated by superposition techniques.

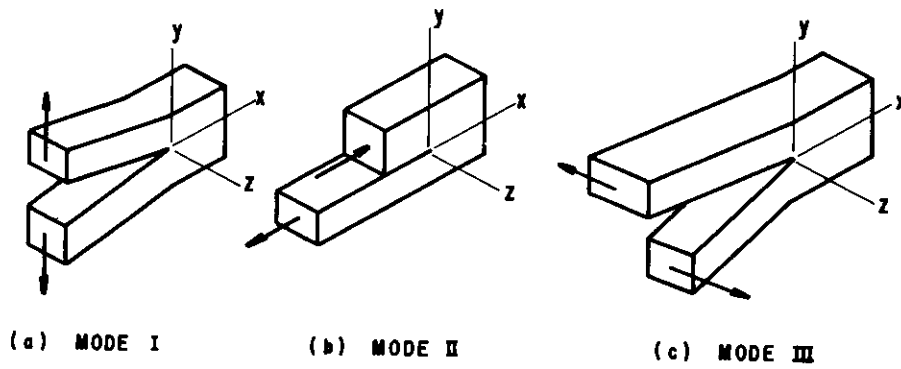


FIGURE D-1. THREE MODES OF CRACK SURFACE DISPLACEMENT

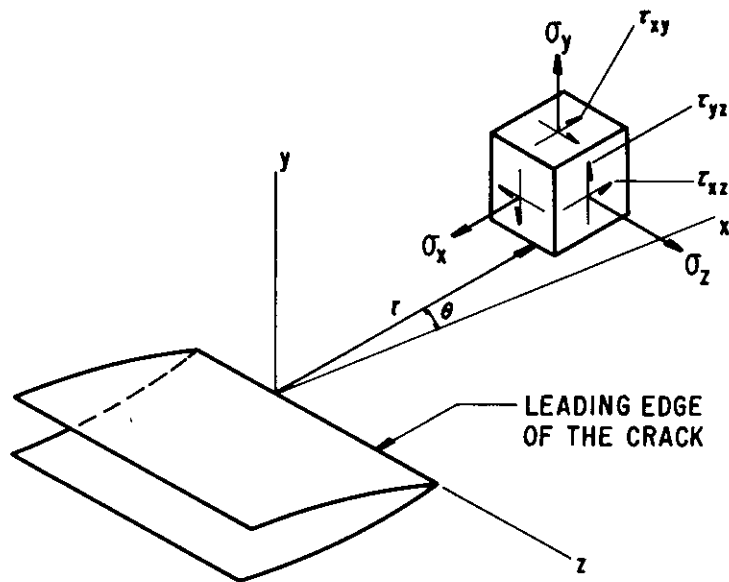


FIGURE D-2. NOMENCLATURE OF STRESS COMPONENTS NEAR THE CRACK TIP

It is of particular interest in fracture mechanics to calculate the stresses and displacements at the crack tip. This has been done for crack tips subjected to the three modes of surface displacement under the assumption that the material is homogeneous, isotropic and linearly elastic. The results for the Mode I configuration are given below (cf Figure D-2 for nomenclature):

$$\sigma_x = \frac{K_I}{(2\pi r)^{1/2}} \cos \frac{\theta}{2} \left[ 1 - \sin \frac{\theta}{2} \sin \frac{3\theta}{2} \right]$$

$$\sigma_y = \frac{K_I}{(2\pi r)^{1/2}} \cos \frac{\theta}{2} \left[ 1 + \sin \frac{\theta}{2} \sin \frac{3\theta}{2} \right]$$

$$\tau_{xy} = \frac{K_I}{(2\pi r)^{1/2}} \sin \frac{\theta}{2} \cos \frac{\theta}{2} \cos \frac{3\theta}{2}$$

$$\sigma_z = \nu (\sigma_x + \sigma_y), \quad \tau_{xz} = \tau_{yz} = 0$$

$$u = \frac{K_I}{G} \left[ r/(2\pi) \right]^{1/2} \cos \frac{\theta}{2} \left[ 1 - 2\nu + \sin^2 \frac{\theta}{2} \right]$$

$$v = \frac{K_I}{G} \left[ r/(2\pi) \right]^{1/2} \sin \frac{\theta}{2} \left[ 2 - 2\nu - \cos^2 \frac{\theta}{2} \right]$$

$$w = 0$$

Here,  $r$  is the coordinate to the point in question measured perpendicular to the crack tip,  $\theta$  is the angle from the crack plane to the point, and  $u$ ,  $v$  and  $w$  are, respectively, the displacement components in the  $x$ ,  $y$  and  $z$  directions.  $K_I$  is the Mode I stress-intensity factor, a scalar parameter which depends only on the crack shape and the magnitude of the stress field in which the crack resides. For example, for a centrally located through-crack of length  $2a$  in a large plate under tension normal to the crack,

$K_I = \sigma \sqrt{\pi a}$ . Equations (1) above are written for the case of plane strain.<sup>\*</sup> For the case of plane stress, the stresses are unchanged and the displacements are found simply by replacing the Poisson ratio  $\nu$  in these formulae by  $\nu/(1 + \nu)$ ; the shear modulus remains unchanged. The corresponding equations for Mode II (involving  $K_{II}$ ) and Mode III (involving  $K_{III}$ ) are not written here, but are available in the literature.

The stress-intensity factors,  $K_I$ ,  $K_{II}$ ,  $K_{III}$  characterize the size and shape of a crack, and the intensity of the stress field in which the crack resides. It is measured in terms of (Force)(Length)<sup>-3/2</sup>, or psi  $\sqrt{\text{in.}}$  in conventional engineering units. It can always be expressed as  $K = \sigma \sqrt{\alpha \pi c}$  where  $K$  is generic for  $K_I$ ,  $K_{II}$  or  $K_{III}$ ,  $c$  is a length characteristic of the crack,  $\sigma$  the applied stress and  $\alpha$  is a scalar parameter of order-of-magnitude unity which depends on the crack shape (and possibly upon the ratio  $\sigma/\sigma_Y$ , where  $\sigma_Y$  is the uniaxial yield strength). Closely associated with the stress-intensity factor is the strain-energy-release rate, or crack-extension force,  $G$  :

$$\left. \begin{aligned} G &= K^2 (1 - \nu^2)/E && \text{(plane strain)} \\ G &= K^2/E && \text{(plane stress)} \end{aligned} \right\} \begin{array}{l} \text{Modes} \\ \text{I and II} \end{array} \quad (2)$$

Physically,  $G$  (again, taken generically for  $G_I$ ,  $G_{II}$  or  $G_{III}$ ) is interpreted as the rate of strain-energy-release per unit crack area.

All of the above considerations have concerned cracks in linearly elastic media. In real structures, however, the stresses near the tip of sharp cracks are in excess of the proportional limit, and hence some plastic yielding always takes place. The exact size and shape of the plastic zone is exceedingly difficult to calculate, and depends on a number of material properties, the way in which the loads have been applied, and the detailed configuration of the crack. However, for engineering purposes the size of the plastic zone can be estimated simply by inserting a yield criterion into the equations for the elastic stresses at the crack tip, e. g., Eqs. (1). For example, by introducing the von Mises ( $J_2$ ) yield criterion, we find that  $R$ , the maximum dimension of the plastic zone, is approximately

---

\*Plane strain and plane stress represent limiting cases in which, respectively, the strain and the stress are assumed to be zero in the direction normal to the plane of loading. A thick plate loaded in its plane is considered to be in a state of plane strain, while a thin plate will approximate a state of plane stress.

$$R = \frac{3}{8\pi} \left( \frac{K_I}{\sigma_Y} \right)^2 \quad (\text{plane strain})$$

$$R = \frac{2}{3\pi} \left( \frac{K_I}{\sigma_Y} \right)^2 \quad (\text{plane stress})$$
(3)

It should be borne in mind that the stress-intensity factor, and hence the size of the plastic zone, will, in general, vary from point-to-point along the leading edge of the crack tip. Only for ideal cases, involving ideal through-notches in plates under in-plane forces, and a few other such examples, is  $K$  the same for all points on the crack tip.

The methods of fracture mechanics have been developed primarily for conditions of small-scale yielding, where the size of the plastic zone  $R$  is quite small with respect to the crack length  $c$  :  $R/c \ll 1$ . In such cases the stresses in the vicinity of the crack tip are very nearly the same as computed under the assumptions of elasticity theory. As a practical matter, what is commonly done is to assume that the crack has an effective length equal to the actual length plus the dimensions of the plastic zones, and this effective length is then used to calculate the stress-intensity factor. However, when the crack tip experiences large-scale yielding, the procedures of linearly elastic fracture mechanics fail to be valid. Such conditions are usually reached in connection with cracks in thin section sheet prior to fast fracture, but can also occur in thick sections, depending upon the yield strength and toughness.

The concepts introduced above may, under appropriate conditions, be applied to predict the onset of fast fracture. From Eqs. (1) it can be seen that the distribution of stresses near the tips of two dissimilar cracks is identical, provided the stress-intensity factors are the same. If we assume that crack extension is controlled by the conditions at the crack tip, then it follows that unstable crack extension will take place when the stress-intensity factor  $K_I$  achieves some critical level.\* This critical value is denoted as  $K_{Ic}$ , the plane-strain fracture toughness. Its significance is that  $K_{Ic}$  may be regarded as a material property, independent of the crack shape or size that triggers fracture, or the type of specimen used to determine  $K_{Ic}$ . The distinction between  $K_I$  and  $K_{Ic}$  is of essential importance:  $K_I$  is analogous to stress, while  $K_{Ic}$  is analogous to strength. Also, since  $K_I$

---

\*From this point the discussion concerns only the Mode I crack configuration, since it is by far the most important encountered in the field. The same general statements will apply, however, to both Mode II and Mode III.

and  $G_I$  are related in a simple way through the elastic constants (Eqs. (2)), for every property  $K_{IC}$  there is its counterpart,  $G_{IC}$ , called the critical strain-energy-release rate.

There are certain restrictions that must be placed on the crack configuration for the concept of a critical value of  $K_I$ , independent of the specimen, to exist.\* These restrictions have to do primarily with the plastic zone that forms at the crack tips. First of all, the size of the plastic zone must be small with respect to the crack length, so that the stress distribution near the tip may accurately be approximated by the elastic stress field. Secondly, the crack tip must be primarily in a state of plane strain, which means that the specimen must be thick enough so that little, if any, strain develops in the direction of the leading edge of the crack. This thickness effect is illustrated in Figure D-3. For relatively thin specimens the critical stress intensity factor, called  $K_C$ , is high, owing to the large stabilizing crack tip plasticity zone. This critical value, however, decreases with increasing specimen thickness until a thickness is reached such that the critical value is independent of thickness. This critical value is called the plane-strain stress-intensity factor,  $K_{IC}$ . It, unlike  $K_C$ , which is thickness-dependent, is considered a material property and always represents a conservative value of the critical stress-intensity factor for design purposes. One might expect that the critical specimen thickness necessary to achieve plane-strain conditions is related to the plastic zone size. It was seen earlier (Eq. (3)) that the zone size is proportional to  $(K_I/\sigma_Y)^2$ . ASTM has set standards for "valid" plane-strain fracture toughness testing based on a specimen thickness  $T$  such that  $T \geq 2.5 (K_{IC}/\sigma_Y)^2$ .\*\* For  $T$  less than these values, the crack tip is substantially or entirely in a state of plane stress.

The subject of fracture mechanics, as described to this point, provides a framework for answering the following general questions:

- (1) Within the resolution capabilities of the pertinent nondestructive inspection equipment, is the largest detectable flaw well within the subcritical region for its stress state?
- (2) Can it be assured that a known flaw will be non-propagating within the expected operational loads of the structure?

However, recent developments in fracture mechanics permit one to address such problems when more complex environmental factors are involved. Perhaps the most important of these is the problem of metal fatigue, or subcritical

---

\*The plane-strain fracture toughness,  $K_{IC}$ , like other thermo-mechanical material properties, does depend upon temperature and strain rate to some extent.

\*\*Section 6 of ASTM E399-70T.

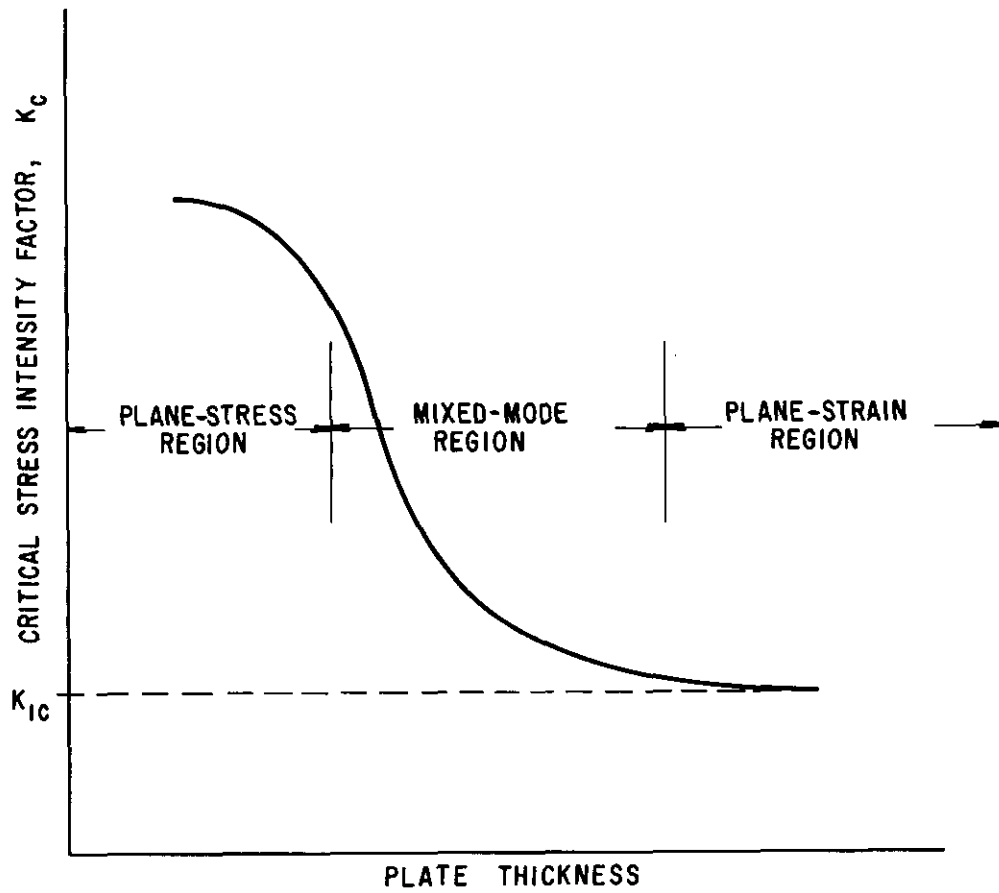


FIGURE D-3. THICKNESS EFFECT ON CRITICAL STRESS-INTENSITY FACTOR

growth of a crack under cyclic stresses. It has been reliably demonstrated that the growth of a crack of length  $c$ , as a function of the number of applied load cycles  $N$ , can be expressed in terms of the variation in stress-intensity factor at the crack tip,  $\Delta K_I$ . A number of analytical expressions have been proposed, but the most widely accepted perhaps is that proposed by Forman, et al. (11)

$$\frac{dc}{dN} = \frac{C (\Delta K_I)^n}{(1 - R) K_c - \Delta K_I} \quad (4)$$

where  $C$  and  $n$  are constants, and  $R$  is the ratio of the minimum to the maximum stress in a loading cycle. This equation can be integrated over the anticipated loading spectrum to produce an estimate of the number of cycles to fast fracture, which develops when  $\Delta K_I \rightarrow (1 - R) K_c$ . It has been noted by some that the above expression has particular limitations when applied to steels having low-yield strengths. This area is discussed in detail in Chapter II, Section B.

A further application of fracture mechanics has been in the area of predicting the life of statically loaded structures in an aggressive environment. The problem of stress corrosion cracking (cf. Chapter III, Section A) involves the slow growth of a crack, under conditions of constant load, to critical proportions. It has been established that the time-to-failure is a function of the crack tip stress-intensity factor. The critical stress-intensity factor, below which the life is indefinite and above which the life is finite, is called  $K_{Isc}$ , for Stress Corrosion Cracking.  $K_{Isc}$ , which is determined under static conditions, plays a role analogous to the endurance limit in cyclic metal fatigue, inasmuch as both quantities are upper limits on the region of indefinite life. This subject is discussed comprehensively in Chapter III, Section A.

## REFERENCES

1. MacNaught, D. F., "Strength of Ships," Principles of Naval Architecture, Ed. J. P. Comstock, Rev. Ed., 1967, 167.
2. Masubuchi, K., Monroe, R. E., and Martin, D. C., "Interpretative Report on Weld-Metal Toughness," SSC-169, July 1965.
3. "Higher Strength Steels in Hull Structures," Technical and Research Bulletin 2-19, SNAME, New York, N.Y., Dec. 1971.
4. Welding High Strength Steels, American Society for Metals, Metals Park, Ohio, 1969.
5. Comstock, J. P., Ed., PRINCIPLES OF NAVAL ARCHITECTURE, Soc. of Naval Arch. & Marine Engrs., New York, N.Y., 1967.
6. D'arcangelo, A. M., SHIP DESIGN AND CONSTRUCTION, Cornell Maritime Press, Inc., Cambridge, Md., 1964.
7. Fink, F. W., and Boyd, W. K., THE CORROSION OF METALS IN MARINE ENVIRONMENTS, D.M.I.C. Report No. 245, Bayer & Co., Inc., Columbus, Ohio, 1970.
8. \_\_\_\_\_, "Guide for Interpretation of Non-Destructive Tests of Welds in Ship Hull Structures," SSC-177, Prepared for the Ship Structure Committee by the Weld Flaw Evaluation Committee, Sept. 1966.
9. \_\_\_\_\_, "Guide for Interpretation of Non-Destructive Tests of High-Strength Low-Alloy Steel Weldments in Ship Hull Structures," SSC-245, Prepared for the Ship Structure Committee by the Weld Flaw Evaluation Committee, 1973.
10. Paris, P. C., and Sih, G., "Stress Analysis of Cracks," in SYMPOSIUM ON FRACTURE TOUGHNESS TESTING AND ITS APPLICATIONS, ASTM STP 381, pp 30-82, ASTM, Philadelphia.
11. Forman, R. G., Kearney, V. E., and Engle, R. M., "Numerical Analysis of Crack Propagation in Cyclic-Loading Structures," Trans. ASME, Journal of Basic Engineering, Vol. 89, No. 3, 1967, pp 459-464.

DOCUMENT CONTROL DATA - R & D

(Security classification of title, body of abstract and indexing annotation must be entered when the overall report is classified)

1. ORIGINATING ACTIVITY (Corporate author) Southwest Research Institute P. O. Drawer 28510 San Antonio, Texas 78284		2a. REPORT SECURITY CLASSIFICATION Unclassified	
		2b. GROUP	
3. REPORT TITLE A STUDY OF SUBCRITICAL CRACK GROWTH IN SHIP STEELS			
4. DESCRIPTIVE NOTES (Type of report and inclusive dates) Final Technical Report			
5. AUTHOR(S) (First name, middle initial, last name) Philip H. Francis James Lankford, Jr. Fred F. Lyle, Jr.			
6. REPORT DATE June 1974	7a. TOTAL NO. OF PAGES 172	7b. NO. OF REFS 109	
8a. CONTRACT OR GRANT NO. N00024-73-C-5199	9a. ORIGINATOR'S REPORT NUMBER(S) 02-3568		
b. PROJECT NO. SR-209	9b. OTHER REPORT NO(S) (Any other numbers that may be assigned this report) SSC-251		
c.			
d.			
10. DISTRIBUTION STATEMENT This document has been approved for public release and sale; its distribution is unlimited.			
11. SUPPLEMENTARY NOTES		12. SPONSORING MILITARY ACTIVITY Naval Ship Systems Command	
13. ABSTRACT This report presents an evaluation of the potential problems associated with crack initiation and subcritical crack growth in high strength, low alloy steels used in welded ship structure. An interpretive review of the state-of-the-art is given, emphasizing design tools that are available and their potential for use in fail safe or safe crack growth ship design philosophy. A crack initiation and crack growth Criterion is presented, which permits welded ship structure to be designed with confidence that serious failures can be avoided, while at the same time full use of the attractive static properties of HSLA steels can be exploited. The report also includes a list of problem areas in need of further clarification in order to enhance confidence in the proposed Criterion.			

14 KEY WORDS	LINK A		LINK B		LINK C	
	ROLE	WT	ROLE	WT	ROLE	WT
Design Criterion Fatigue Ships Subcritical Crack Growth Crack Initiation High Strength, Low Alloy Steels Welded Structures						

SHIP RESEARCH COMMITTEE  
Maritime Transportation Research Board  
National Academy of Sciences-National Research Council

The Ship Research Committee has technical cognizance of the inter-agency Ship Structure Committee's research program:

PROF. J. E. GOLDBERG, Chairman, *School of Civil Engineering, Purdue University*  
PROF. R. W. CLOUGH, *Prof. of Civil Engineering, University of California*  
DR. S. R. HELLER, Jr., *C'man, Civil & Mech. Eng. Dept., The Catholic Univ. of America*  
MR. G. E. KAMPSCHAEFER, Jr., *Manager, Technical Services, ARMCO Steel Corporation*  
MR. W. W. OFFNER, *Consulting Engineer, San Francisco*  
MR. D. P. ROSEMAN, *Chief Naval Architect, Hydronautics, Inc.*  
MR. H. S. TOWNSEND, *Vice President, U.S. Salvage Association, Inc.*  
DR. S. YUKAWA, *Consulting Engineer, General Electric Company*  
MR. R. W. RUMKE, *Executive Secretary, Ship Research Committee*

Advisory Group III, "Materials, Fabrication, and Inspection", prepared the project prospectus and evaluated the proposals for this project:

MR. G. E. KAMPSCHAEFER, Jr., Chairman, *Manager, Tech. Services, ARMCO Steel Corp.*  
DR. J. M. BARSOM, *Research Consultant, U.S. Steel Corporation*  
PROF. J. R. FREDERICK, *Dept. of Mech. Engineering, The University of Michigan*  
MR. S. GOLDSPIEL, *Mechanical Engineer, Board of Water Supply, New York*  
MR. T. E. KOSTER, *Naval Architect, AMOCO International Oil Company*  
DR. J. M. KRAFFT, *Head, Ocean Materials Criteria Branch, Naval Research Lab.*  
MR. G. E. LINNERT, *North American Representative, The Welding Institute*  
PROF. H. W. LIU, *Professor of Materials Science, Syracuse University*  
PROF. W. H. MUNSE, *Dept. of Civil Engineering, University of Illinois*  
MR. W. W. OFFNER, *Consulting Engineer, San Francisco*  
PROF. H. C. ROGERS, *College of Engineering, Drexel University*  
DR. W. F. SAVAGE, *Professor of Metallurgy, Rensselaer Polytechnic Institute*  
DR. W. K. WILSON, *Analytical Mechanics, Westinghouse Electric Corporation*

The SR-209 Project Advisory Committee provided the liaison technical guidance, and reviewed the project reports with the investigator:

DR. S. YUKAWA, Chairman, *Consulting Engineer, General Electric Company*  
DR. J. M. BARSOM, *Research Consultant, U.S. Steel Corporation*  
MR. R. L. GRAY, *Vice President, States Steamship Company*

## SHIP STRUCTURE COMMITTEE PUBLICATIONS

*These documents are distributed by the National Technical Information Service, Springfield, Va. 22151. These documents have been announced in the Clearinghouse journal U.S. Government Research & Development Reports (USGRDR) under the indicated AD numbers.*

- SSC-242, *Fast Fracture Resistance and Crack Arrest in Structural Steels* by G. T. Hahn, R. G. Hoagland, M. F. Kanninen, A. R. Rosenfield and R. Sejnoha. 1973. AD 775018.
- SSC-243, *Structural Analysis of SL-7 Containership Under Combined Loading of Vertical, Lateral and Torsional Moments Using Finite Element Techniques* by A. M. Elbatouti, D. Liu and H. Y. Jan. 1974. AD-A 002620.
- SSC-244, *Fracture-Control Guidelines for Welded Steel Ship Hulls* by S. T. Rolfe, D. M. Rhea and B. O. Kuzmanovic. 1974. AD-A 004553.
- SSC-245, *A Guide for Inspection of High-Strength Steel Weldments* by The Weld Flaw Evaluation Committee. (To be published).
- SSC-246, *Theoretical Estimates of Wave Loads On the SL-7 Containership In Regular and Irregular Seas* by P. Kaplan, T. P. Sargent and J. Cilmi. 1974. AD-A 004554.
- SSC-247, *Flame Straightening Quenched-And-Tempered Steels in Ship Construction* by R. L. Rothman. 1974. AD-A 002621.
- SSC-248, *Fracture Toughness Characterization of Shipbuilding Steels* by J. R. Hawthorne and F. J. Loss. 1974.
- SSC-249, *Ship-Vibration Prediction Methods and Evaluation of Influence of Hull Stiffness Variation on Vibratory Response* by R. G. Kline and J. C. Daidola. 1975.
- SSC-250, *Bibliography to Ship-Vibration Prediction Methods and Evaluation of Influence of Hull Stiffness Variation on Vibratory Response* by R. G. Kline and J. C. Daidola. 1975.

### SL-7 PUBLICATIONS TO DATE

- SL-7-1, (SSC 238) - *Design and Installation of a Ship Response Instrumentation System Aboard the SL-7 Class Containership S.S. SEA-LAND McLEAN* by R. A. Fain. 1974. AD 780090.
- SL-7-2, (SSC 239) - *Wave Loads in a Model of the SL-7 Containership Running at Oblique Headings in Regular Waves* by J. F. Dalzell and M. J. Chiocco. 1974. AD 780065.
- SL-7-3, (SSC-243) - *Structural Analysis of SL-7 Containership Under Combined Loading of Vertical, Lateral and Torsional Moments Using Finite Element Techniques* by A. M. Elbatouti, D. Liu and H. Y. Jan. 1974. AD-A 002620.
- SL-7-4 (SSC-246), *Theoretical Estimates of Wave Loads On the SL-7 Container Ship in Regular and Irregular Seas* by P. Kaplan, T. P. Sargent and J. Cilmi. 1974. AD-A 004554.